Environmental Chamber and Fixture Design for Hydrodynamic Thermal Aging of Coupons and Fibers

by

Jerome C. L. Wong

A thesis submitted in partial fulfillment of the requirements for the degree
of
Master of Science

Department of Mechanical Engineering
University of Alberta

Abstract

Accelerated aging of test specimens has always been the staple method for determining long term compatibility for any material in a given range of process conditions. The application of accelerated aging is to simulate real time conditions in an accelerated manner utilizing more severe conditions while maintaining consistency between the test specimens to minimize any unintended deviations of these parameters from target conditions. This thesis explores various designs for holding tensile test coupons and loose fibers along with their advantages and disadvantages. A brief discussion of the fiber aging fixtures are explored and compared. The tensile test coupon aging setup is investigated and described in detail with the use of temperature logging, visual dye tests, and computational fluid dynamics to quantify its effectiveness at maintaining fluid homogeneity and the aging conditions. Initial trials of both the fiber fixtures and tensile test coupon aging setups are discussed along with their initial issues and solutions. As the experiments are ongoing as of writing this thesis, the finalized results are not available for discussion and are also not in the scope of this thesis.

Preface

This thesis is an original work by Jerome Wong. No part of this thesis has been previously published.

Dedication

To my grandmother, 周瑞心,

my aunt, Melina, 陳小芬,

my sister, Fiona, 黃卓羚, and

my brother, Cedric, 黃卓俊,

for their unfailing support and encouragement throughout this journey that has made the completion of this thesis a reality.

and

In memory of my grandfather, 陳錦芳,

my uncle, 陳伯昌, and

my mother, 陳小芳.

Acknowledgements

I would like to take this opportunity to acknowledge those who have assisted me to finish this thesis project during my master's study at the University of Alberta. My first thanks go to my supervisor, Dr. Pierre Mertiny, for his tutelage and support throughout the entire duration of my study and thesis. A big thanks to my friend, Christer Thor, for his aid in proofreading my thesis. Thanks to my auntie Helen who provided guidance in helping me navigate the work processes of the university. I would also like to thank Dr. Carlos Lange for his help with the CFD model review. Lastly, I would like to thank a fellow student, John Sunny, for his help in the lab and for continuing with my experiments when my work commitments prevent me from doing so. Thanks to everyone very much for their help.

Table of Contents

List of Tables

List of Figures

Nomenclature

A_s	=	Surface area [m^2]
AAF	=	Accelerated aging factor [-]
h	=	Heat transfer coefficient [$W/m^2 \cdot {}^oC$]
h_{rad}	=	Radiation heat transfer coefficient [$W/m^2 \cdot {}^oC$]
k	=	Thermal conductivity [$W/m \cdot {}^oC$]
L	=	Length [m]
L_{height}	=	Height [m]
Q_{cond}	=	Heat flux from conduction [W]
Q_{conv}	=	Heat flux from convection [W]
Q_{Loss}	=	Total heat flux [W]
Q_{rad}	=	Heat flux from radiation [W]
Q_{10}	=	Aging factor for 10°C change [-]
r	=	Radius [m]
r_{inner}	=	Inner radius [m]
r_{outer}	=	Outer radius [m]
R_{cond}	=	Resistance to heat transfer from conduction [°C/W]
R_{cond_radial}	=	Radial resistance to heat transfer from conduction [°C/W]
R_{conv}	=	Resistance to heat transfer from convection [°C/W]
R_{conv_radial}	=	Radial resistance to heat transfer from convection [°C/W]

R_{rad}	=	Resistance to heat transfer from radiation [°C/W]
R_{total}	=	Total resistance to heat transfer [°C/W]
T_{∞}	=	Ambient temperature or average temperature [°C]
T	=	Temperature [°C]
T_{AA}	=	Accelerated aging temperature [°C]
T_{RT}	=	Ambient temperature [°C]
T_{surface}	=	Surface temperature [°C]

Greek Letters

ε	=	Emissivity [-]
σ	=	Stefan-Boltzmann constant [5.670 x 10^{-8} W/m²·K⁴]
π	=	Pi [3.14159]

Abbreviations

ABSA	-	Alberta Boilers Safety Association
API	-	American Petroleum Institute
ASME	-	American Society of Mechanical Engineers
CFD	-	computational fluid dynamics
DCM	-	dichloromethane
HDPE	-	high density polyethylene
PP	-	polypropylene
PREN	-	pitting resistance equivalent number
PSV	-	pressure relief valve
PTFE	-	polytetrafluoroethylene
RTD	-	resistance temperature detector
RTP	-	reinforced thermoplastic pipe

1 Introduction

The introduction of materials into actual applications requires knowledge about their degradation mechanisms when exposed to a given environment. This is especially true for composite materials, such as fiber reinforced polymers, since different and interacting degradation mechanisms need to be discerned. The goal of this research was to improve upon existing aging cell setups for tensile test coupons and fiber reinforcements, and provide a more expedient and effective aging apparatus. It is hypothesized that by investing time and innovation into a design, improved testing processes and thus comprehensive insights into material degradation mechanisms can be achieved. This study is broken down into two main parts, one for a fiber fixture and another for a tensile test coupon aging setup. Coupons are considered in this context to be rigid material samples of suitable shape such as flat dogbone [1], rounded dogbone [2], rectangular [3], or circular [4].

Aging of the uncoated bare fibers are rarely done as they are typically impregnated or coated with thermoset or thermoplastic polymers during fabrication into structural elements. As such, the challenges and methods for bare fiber aging will be briefly covered in this study. Beginning with the synthesis of different conceptual designs for loose fiber fixtures and a comparison of their associated advantages and disadvantages, initial prototyping and testing was performed with the most promising concept.

Tensile test coupons are often aged to assess the degradation of mechanical properties with exposure to water and temperature. This study began with researching and comparing existing methods of tensile test coupon aging and their possible fixtures and aging apparatus setups. Improvements were made to existing design solutions based on the research and the testing conditions provided by the industrial research partner. Testing was performed to qualify the improvements of a newly developed setup; including visual dye testing, computational fluid dynamics, and thermal characterization.

Our industry partner is utilizing the material aging research for improving their reinforced thermoplastic pipe (RTP) products [5]. Figure 1 shows the different layers comprising the thermoplastic pipe [6]. The inner most layer is called the liner and should ideally only be exposed to the inside process conditions. In the middle is the fiber reinforcement layer; this layer provides the bulk of the structural integrity of the pipe and consists of bare fibers wound around the liner. This is major difference compared to typical fiber reinforced piping (FRP) [7] where the fibers are in resin or a polymer matrix. On the outside of this fiber reinforced liner is the jacket; this jacket provides protection for the bare fibers from the external environment. In ideal situations the outer jacket would only see the outer environmental conditions, however, if the inner liner is damaged then the process fluids can seep out into the fiber layer and therefore expose the inner surface of the outer jacket to the process fluids. The reverse can also occur where the outer jacket is compromised leading to the inner liner being exposed to the external environment fluids. When either layer (outer jacket or inner liner) is compromised then the bare fibers in the middle will be exposed to liquid. Thus this provides the driver for testing the bare fibers independently of the plastic coupons.

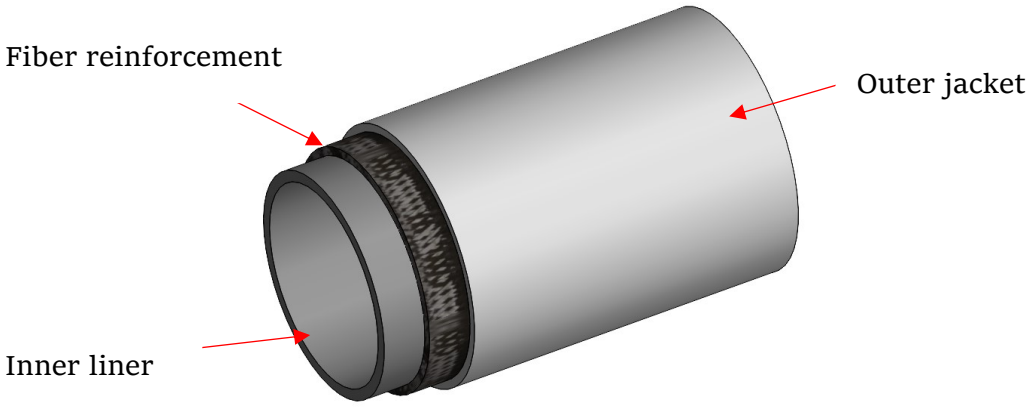

Figure 1: Schematic of reinforced thermoplastic pipe (RTP)

The main goal of this research is to determine the impacts of prolonged fluid exposure on both the coupons and fibers. Due to the nature of the RTP having both the fibers and polymer layers separated, different materials can be selected for each layer to provide the optimal solution in terms of cost and reliability. For example, the inner liner may consist of a material that is best suited for the long term exposure to the process conditions while the fiber and outer jacket layers can be rated for short term exposure only. This means for more aggressive process solvents, such as hydrocarbon service, a more expensive and resilient liner material can be chosen for the inner liner while more cost-effective materials can be chosen for the outer jacket layer [8].

Accelerated aging in the context of this thesis is the artificial aging by hydrothermal means subjecting samples to elevated temperatures relative to the design temperatures of those polymers and fibers being tested. The use of elevated temperatures allows the aging to be completed faster than natural aging would occur by utilizing the Arrhenius Law [9, 10, 11]. The Arrhenius Law describes the temperature dependence of chemical reactions, therefore the same naturally occurring aging can be artificially simulated on a reduced time scale and allow the impacts of natural aging to be predicted. The effects of flow related to the accelerated aging process is to provide a non-stagnant environment and prevent gradients from establishing, which could have an impact on the aging process.

This research will span multiple years and will be transitioned to future researchers. For the current scope within this thesis, the aspect of aging being focused on is primarily the reduction in tensile yield strength of the specimens with prolonged exposure to water at elevated temperatures, called hydrothermal aging. The secondary aspects would be the physical observations of the specimens and changes in the aging fluid. For physical observations, this focuses on but not limited to: shrinkage, swelling, discoloration, opacity, weight and deformation. For changes in the aging fluid, this focuses on but is not limited to: chemical composition changes

(leaching), color and debris (shedding from samples). For future research the use of hydrocarbon solvents in place of water will be explored.

The previous research chapter will encompass the literature review and the previous aging fixture designs. The literature review will focus on the types of heat sources and the damage mechanisms being studied. Previous aging fixtures will include what was used previously at the University of Alberta and what our industry partner previously and currently uses.

The fiber fixtures chapter will be brief as the design focus was reprioritized to another researcher after initial brainstorming and prototyping. Brainstorming will include all the designs discussed with the industry partner and the prioritization process. Appendix A – Concept Drawings for Fiber Fixtures will be included to provide the general arrangement drawings for all the concepts discussed in order to give a more detailed view with some dimensions for scale.

The coupon aging chapters will include the initial design of the coupon aging setup with the challenges seen during initial testing and the resulting changes to the apparatus. The expected heat losses of the aging vessel would be calculated and validated with testing in order to confirm that the immersion style heater was sufficiently sized to overcome the heat losses. Dye tests would also be performed to visually inspect the setup for low flow regions and qualitatively gauge how quickly injected dye reaches homogeneity within the vessel. Computational fluid dynamics was also employed to give a more thorough understanding and validation behind the results of the dye testing.

2 Previous Research

2.1 Literature Review – Heat Sources

In the technical literature, little mention is usually given to the design setup for hydrothermal aging of fiber and tensile test coupons in an immersion fluid. Most papers merely mention that a bath was used or simply state that coupons were submerged in fluid, for example [12-22]. This is due to the commercial availability of aging setups and research disseminations being focused toward the results of the aging rather than the design setup itself.

Commercially, several basic types of setups are suitable for accelerated aging tests, namely; immersion heaters, conduction heaters, ovens, indirect heaters, and environmental chambers. The most common setup being the first three mentioned previously. Next is a detailed description of the different types of heaters.

Immersion-style heaters are most commonly used for aging tests as their effectiveness to maintain a target temperature accurately throughout the test duration is one of the best. They are called immersion style due to the heating element being immersed into the fluid it is heating. A method of stirring or circulating the liquid is sometimes provided to minimize thermal and chemical concentration gradients [23]. Screw plug style immersion heaters are most common for commercial applications, and often they come bundled as an element(s) with a thermostat [24]. These heaters without circulation or mixers are often installed at the bottom of a vessel and rely on natural convection currents to perform the stirring of the immersion fluid.

Conduction-style heaters are the next most common class. They are usually seen as either a water bath with heating elements attached to the underside or in the form of heat tracing wrapped around a vessel. These heaters conduct heat through either a heat sink or the vessel wall to heat the immersion fluid [25]. The heating element is therefore not exposed to the fluid, which is

desirable in the case of corrosive or fouling process conditions. A major drawback of these heaters is the possibility of temperature gradients forming within the heated vessel. The simplest analogy would be heating a pot of soup over a stove; the bottom of the pot would see much higher temperatures potentially burning the soup if it was not stirred. The same situation may occur in heated water baths as the heating usually comes from the bottom and the greatest heat loss is from the top surface of the liquid.

Ovens can be utilized for fiber aging using beakers to hold the immersion fluid. The same beaker method can also be applied to tensile test coupons. In short, coupons or fibers to be aged are placed in beakers which are subsequently placed into an oven to maintain a target temperature for a prolonged time period. A considerable drawback of this method is the introduction of temperature excursions that arise from opening the oven to retrieve coupons and/or topping up liquids to correct for evaporative losses. The heating is usually done via a combination of radiative and convective means. As such, coupons or fibers placed nearer to the heating elements may see larger thermal gradients than coupons or fibers further away due to the line of sight from radiative heat. It should also be noted that waiting for longer periods before topping up the liquid levels, in order to minimize thermal gradients from opening the oven, could adversely impact the chemical concentration of the aging fluid and the leached chemicals.

Indirect heating is more complex to use for aging experiments as it requires more equipment and capital cost. Indirect heating is done by heating another fluid and then circulating that fluid into the second fluid to be heated. The beaker method mentioned previously can be considered indirect heating as the hot air within the oven is the medium used to transport the heat to the beakers. A common indirect heating setup would be a bain-marie (also known as a double boiler), used to minimize the local temperature gradients from conduction heating. The main advantage of this setup would be the buffering effect of the additional heat conduction medium to greatly minimize localized

hot spots; an example this method is commonly used in culinary arts for heating of chocolate or sugary confections without the risk of caramelizing or burning the sugary product.

Environmental chambers are the most costly and complex of the setups utilized owing to the specialization of the equipment used. The previous setups mentioned are intended to be used in steady-state process conditions, while environmental chambers are often employed for transient conditions. For example, cycling temperatures to simulate freeze-thaw cycles; simulation of salt spray; ultraviolet aging; cyclic tidal simulation; and cyclic moisture or humidity simulations. Since environmental chambers are highly specific to their application, and in turn, their cost is relatively high, they are often not utilized for steady-state aging experiments. To that end, if the test calls for cyclic or very specific weathering conditions, then environmental chambers are frequently utilized such as described by ASTM G154 when simulating ultraviolet exposure during the light/dark cycles [26].

2.2 Literature Review – Polymer Aging Mechanisms

Polymers are long chains of monomers assembled together; they can be either synthetically created or derived from organic sources [27]. Polymer degradation is a process where the polymer chain is compromised leading to a deterioration of the material properties. There are four main mechanisms by which polymers degrades: photodegradation, chemical degradation, mechanical degradation, and biological degradation [28]. It should be noted that the composition of the polymer can impact how the various damage mechanisms affect the polymer.

Photodegradation of polymers occurs from exposure to sunlight where the ultraviolet rays provides the activation energy to either break the chemical bonds or allow oxygen to become incorporated into the polymers [28]. Photodegradation is usually the first step in polymers naturally degrading in

the environment [28]. Exposure to sunlight will degrade polymers by making them more brittle and eventually break into smaller pieces.

Chemical degradation of polymers occurs with interaction with chemicals, most notably with oxygen and water [28, 29]. Chemical degradation by oxygen is where oxygen is incorporated into the polymer chains and can be combined with exposure temperature called thermal oxidative. Thermal degradation, also known as pyrolysis, can also occur where the heat itself cause the polymer bonds to break. Some authors will group thermal degradation under chemical degradation, while others would separate it as a category on its own [30]. The elevated temperature provides the activation energy to aid in the oxygen attacking the polymer chain. Chemical degradation by water is called hydrolysis and it is where the bonds of the polymer chain are broken or reacts with the water [31].

Mechanical degradation of polymers occurs from repeated mechanical stress [28]. The mechanical stress can usually occur as bending, stretching or erosion and eventually causes the polymer to fragment into smaller pieces [29]. There are concerns with these small polymer fragments then becoming ingested by wildlife as they can have negative impacts on their wellbeing [28, 29].

Biological degradation of polymers occurs by means of a biological metabolic process achieved by microorganisms excreting enzymes which breaks the polymer chains into simpler compounds [31]. Certain bacteria and fungi can initially colonize the surface of the polymer and secrete enzymes to metabolize the polymer chains. Some polymers can biodegrade more easily than others; polymers designed to break down more easily by microorganisms are called biopolymers or biodegradable polymers [29]. The biopolymers created from renewable sources are also not always biodegradable; polylactic acid (PLA) created from corn is considered

biodegradable, while polythene created from bioethanol is not considered biodegradable [29].

2.3 Literature Review – Glass Fiber Aging Mechanisms

Glass fibers are subject to two common degradation mechanism: chemical attack and mechanical damage [32, 33, 34]. In the context of reinforced thermoplastic pipe, the glass fibers are primarily subjected to the chemical attack as the other mechanism is mitigated by the polymer layers shielding the fibers. Nonetheless, understanding the mechanisms of damage for the glass fibers is critical as it helps predict the longevity of the reinforced thermoplastic pipe in the scenario where the fibers are exposed to the process or elements. It should be noted that the composition of the glass can impact how the various damage mechanisms affect the glass.

Chemical attack of glass has a broad range of damage mechanisms ranging from low/high pH to compounds that react with glass [32]. Glass corrosion (also called “glass disease”) is a common mechanism of attack where alkali ions are leached from the surface of the glass forming a hydrated gel layer which results in visible damage and weakening of the glass structure [32, 35]. Glass corrosion is most commonly seen in soda lime glass placed in alkaline solutions containing hydroxides [36]. A common example of this would be sodium hydroxide’s ability to cause glass corrosion [36]. When glass is placed in low pH environments, the acidic conditions can cause dissolution of the glass [37]. This is seen when glass is placed in solutions containing hydrogen fluoride (hydrofluoric acid) where the acid can etch and dissolve the glass over time [37].

Mechanical damage of glass is typically seen as erosion by weathering or abrasive processes [34]. Erosion of bulk glass is seen in rivers and windy areas where abrasive debris, such as sand, is flows/blown across or impacts the surface of the glass causing the abrasive nature of the debris to erode the glass surface. In the context of FTP, the glass fibers will seldom see

mechanical damage due to the inner liner and outer jacket providing isolation from mechanical damage from occurring. However, if the outer or inner layers of the pipe are compromised then it is possible for debris to enter the fiber layer and when combined with fluid leakage providing flow and/or thermal cycling causing the fibers to expand/contract, it is possible for the glass fibers to then be mechanically abraded.

2.4 Literature Review – Accelerated Aging

Accelerated aging in the context of materials is where a material sample is subjected to more severe test conditions (than expected process conditions) on a smaller time scale in order to predict their long-term behavior at process conditions. This thesis focuses on accelerated aging in water at elevated temperatures, also known as hydrothermal aging. In 1889, Arrhenius discovered that small increases in temperature can have a large impact in the reaction rates [38]. The Arrhenius equation provides a quantitative relationship between temperature and reaction rate; it is with this relationship that engineers can utilize more severe test conditions to quantitatively predict the reaction rates in less severe conditions.

For the accelerated aging of coupons, a modified version of the standard "ASTM D3045 – Standard Practice for Heat Aging of Plastics Without Load" was utilized [10]. The modification of this standard is from performing the tests under heated air only to immersion in liquid. This standard discusses the procedure and data interpretation when multiple temperatures are utilized; in short, a minimum of three different temperatures are used and ideally each temperature should reduce the targeted failure criteria by half the duration. In this way the initial (lowest) temperature test is conducted the longest, and each test thereafter should take half the time.

The ASTM D3045 standard does caution against having samples touching one another and selecting a temperature that does not exceed the transition temperature of the polymer [10]. If the samples touch each other, then their

exposure to the aging fluid would be different on the contact area when compared with the rest of the samples, which could result in inconsistencies in aging. If the aging temperature chosen was at or higher than the transition temperature then it may result in large differences in aging behavior per ASTM D3045 section 9.2.4 [10].

The procedural information regarding the tensile test for the coupon specimens and style of coupon chosen as the design basis was from ASTM D638 [1]. The standard calls this type of sample a dumbbell-shaped test specimen. While the Type 1 specimen was chosen as a design basis and is considered preferred by the standard for rigid sheet materials, many other types of specimens are discussed that can be utilized for various thicknesses and shapes of materials, such as small pipes.

For the aging of bare fibers no industry standard was adhered to, however, for the testing of bare fibers the standard "ASTM D2256 – Standard Test Method for Tensile Properties of Yarns by the Single-Strand Method" was utilized [39]. Per section 5.4 of the standard, the clamping method for the yarns was adapted to best suit our materials as various geometries of fibers were tested from monofilament to multifilament fibers. The adaptation involved the addition of tape or thick paper between the grips of the tensile testing machine and the fibers in order to provide more grip and lessen the stress concentrations on the fibers.

The Arrhenius equation used by ASTM F1980 is shown below in (0) [9]. Where Q_{10} represents the rate of degradation over a 10°C change in temperature for the aging conditions. The difference between the aging temperature to the ambient would be represented by T_{AA}-T_{RT}. To then calculate the accelerated aging time required for a degradation equivalent to a desired time (called shelf life by the ASTM standard), one would just divide the desired time by *AFF* to obtain the equivalent accelerated aging time [9]. Therefore if this method is followed the testing occurring at the accelerated aging time would represent an equivalence to testing a similarly aged sample at the ambient condition for the desired time.

$$AFF \equiv Q_{10}^{[(T_{AA}-T_{RT})/10]} \quad (0)$$

The above method can be easily adapted for accelerated aging of materials, where the ambient temperature can instead be set as the maximum design temperature. In this way the reference of any aging done is with respect to the maximum design temperature and can qualify the aging effects in a shortened period of time, called accelerated aging. Care must also be taken to ensure the chosen accelerated aging temperature (T_{AA}) is not so high that it causes the introduction of other damage mechanisms otherwise not seen at the desired temperature (T_{RT}), else the accelerating aging results may be inaccurate [9].

2.5 Previous Designs

2.5.1 Previous Tensile Test Coupon Aging Setup

The tensile test coupon aging cell used previously by the research group [40, 41] (setup A) is shown in Figure 2. The setup consists of three main parts: (i) the aging carousel holding some tensile test coupons; (ii) the aging vessel with a carousel placed inside; and (iii) the heated insulation blanket placed around the vessel (Figure 3). The carousel was made of waterjet-cut aluminum plates with a central post holding the plates. The aging vessel was made of an aluminum plate that has been rolled and welded. A spray welded coating was applied inside for corrosion protection. Gradients were noted by the author as being the issue with the prior design due to the observation of striations [40]. It is hypothesized that due to the lack of stirring that gradients has occurred. Note the non-coated surface of the bottom carousel plate that has a distinct aluminum oxide formation while the inside surface of the aging vessel does not as shown in Figure 2. Chemical gradients can be formed in this setup due to the differences each layer can be exposed to with a lack of stirring; such as the topmost layer being exposed to air while lower layers are not, this can then lead to an oxygen-deficient environment forming in lower layers and potentially cause different aging reactions. The author also noted that a heavy layer of sediment formed in the lower levels of the aging cell due to the coupons shedding [40]. The sediment would increase surface area for leaching of chemicals within the lower layers.

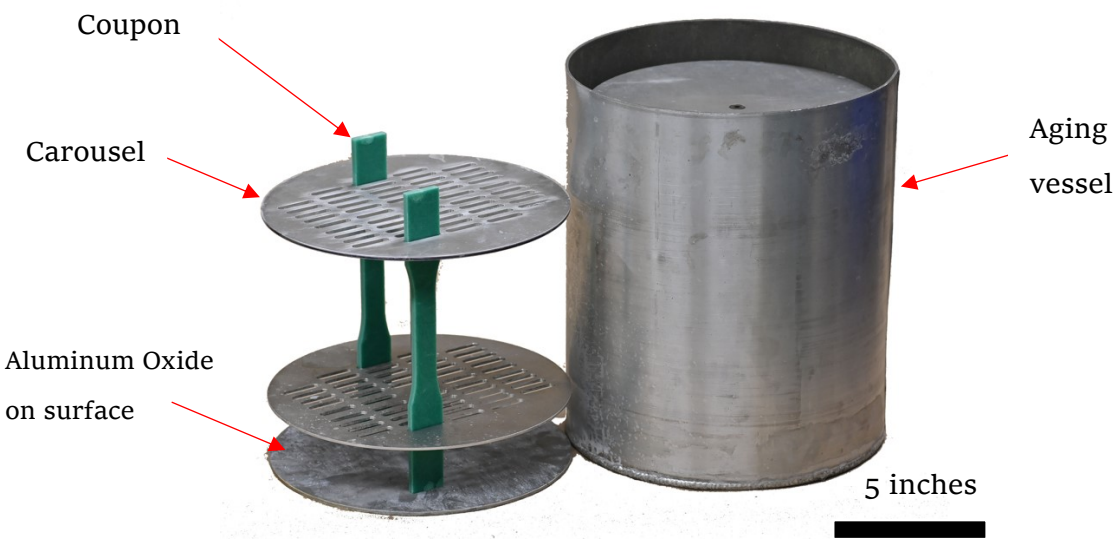

Figure 2: Previous tensile test coupon aging setup A

Figure 3: Previous tensile test coupon aging vessel (setup A) with insulation

Our industry partner is currently supporting a different research group to perform accelerated aging of tensile test coupons (setup B). Their setup consists of a heated blanket wrapped around a central pipe containing the specimens and liquid. The vessel is essentially a straight length of pipe with threaded ends and sealed with pipe caps. A thermocouple is placed in the center of this contraption sandwiched around the tensile test coupons. This thermocouple is used to control the heating to maintain the target

temperature via a controller and the heated blanket. See Figure 4 for a visualization of the test setup.

The largest issue with their setup is it suffers from large thermal gradients as noted by how they melted the industry partner's tensile test coupons during a recent test. The centralized thermocouple also gave a false sense of security as the singular data point would not have shown the gradient or the higher wall temperatures. Previous tests with this setup were slightly more successful owing to the lower packing factor of a partially filled pipe versus a filled pipe; as the space provided room for natural circulation thus reducing the thermal gradients.

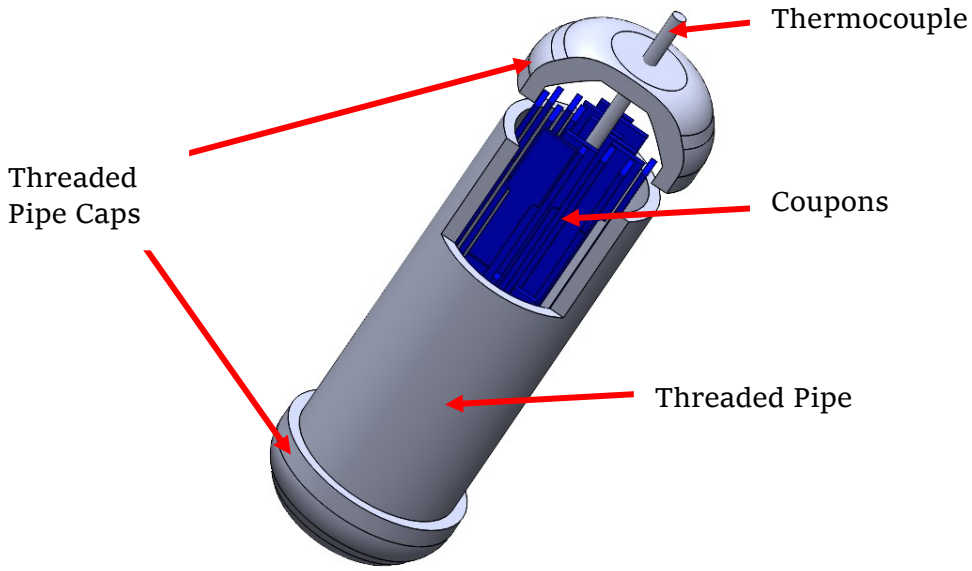

Figure 4: Current coupon aging setup (setup B)

2.5.2 Previous Fiber Aging Setup

Our industry partner also previously performed some fiber aging testing at a different institution. Below is a provided sample of this fixture in Figure 5 (setup C). The fixture is made of inert plastic and intended to be aged and tested with the fibers. The fibers are wound around both shafts and secured with glue. Tension can then be applied to the fiber before tightening the screws that hold the two securing tabs to the backing plate. The whole fixture can then be placed into a vat of liquid for aging. After aging, the fixture can be directly mounted to a tensile test machine and the backing plate removed or loosened before testing to minimize handling of the aged fiber. The fixtures are made of solid polytetrafluoroethylene (PTFE) with stainless steel cotter pins on the shafts. Our industry partner said these fixtures worked well with the main disadvantage being their bulky nature and high manufacturing costs.

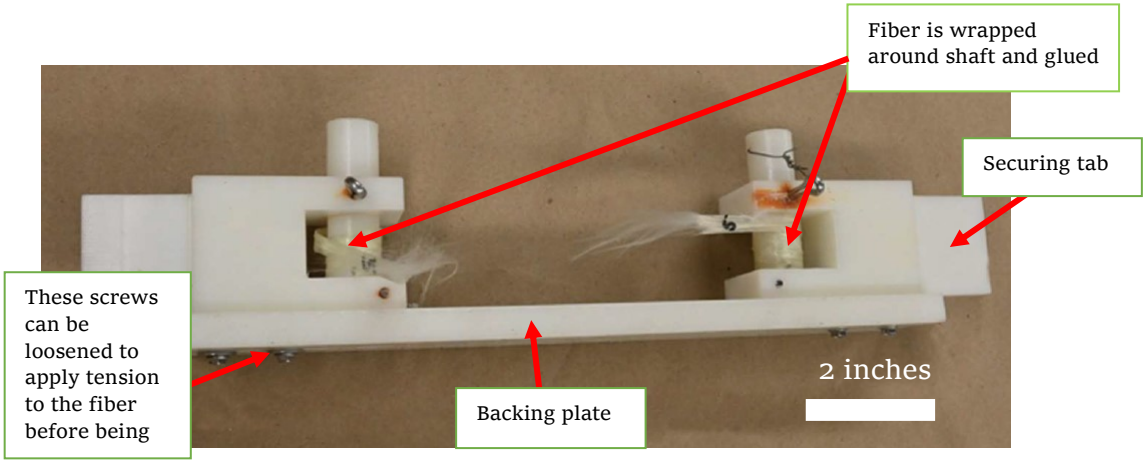

Figure 5: Fiber aging fixture (setup C) from another research group

The current method of aging fibers at the University of Alberta is to place the loose fibers in beakers filled with liquid, which are then placed in an oven shown in Figure 6 (setup D). The tops of the beakers are covered with aluminum foil to minimize evaporative losses, however, every few days the fluids do need topping up. Care must also be taken to pre-heat the fluid before topping up to ensure there isn't a thermogradient or shock introduced. The main advantage of this method is the low cost, with the disadvantages being:

- Varying gauge length for aging as the liquid level fluctuates through the duration
- Concentration of salts and chemicals within the aging fluid fluctuates due to the changes in liquid level
- Labor intensive since refilling the fluid is required at regular intervals; the inability to tension the fibers during aging
- Post aging fiber handling
- Entanglement of the fibers

Testing sodium chloride solutions and their impacts on glass fibers is one of the future works our industry partner expressed interested in exploring after the current experiments are completed. If the same beaker method is utilized then the evaporative losses could have a potential impact on the experiment due to the changing salt concentrations [42].

Figure 6: Fiber aging beaker setup D

Our industry partner has also mentioned details about their existing fiber aging setup. The fixture is made of a welded stainless steel frame with a row of holes drilled into the top and bottom of the frame (setup E). Each fiber is secured to the frame using two fasteners at the opposite ends of the frame utilizing the two rows of holes. A rubber washer is also placed between the fiber and fastener to minimize stress concentrations and provide extra grip in securing the fibers. Tension can also be applied to each fiber individually before tightening the second fastener. The whole fixture is then submerged into a plastic tote of liquid for aging. Their current setup does not contain a heater and aging is done at room temperature.

2.5.3 Shortcomings of Existing Equipment

The motivation behind seeking improvements in creating the new aging setups was driven by the shortcomings in the existing aging setups. A tabulated list of the shortcomings can be found below in Table 1. These shortcomings form a part of the basis for the design criteria in the next section. With each design there are always drawbacks and aiming to eliminate all the shortcomings may in turn introduce a new disadvantage; so it is with innovation we can seek to find a balance between these conditions.

Table 1: Shortcomings of existing aging setups

Shortcomings	Coupon Aging Setup		Fiber Aging Setup		
	Previous setup used at the University of Alberta (Figure 2)	Current setup used by our industry partner	Previous setup used by our industry partner (Figure 5)	Current setup used at the University of Alberta (Figure 6)	Current setup used by our industry partner
Limited number of samples per setup	X	X	X		
Removal of coupons/fibers would disturb experiment		X		X	X
Removal of aging liquid samples would disturb experiment		X			
Stagnant/Gradients	X	X	X	X	X
Uneven spacing of samples		X		X	
High cost			X		
Entanglement risk	N/A	N/A		X	
Extra handling of samples	N/A	N/A		X	X
Inability to tension samples	N/A	N/A		X	

For the fiber aging setup, our industry partner's main concern with our current setup was the risk of fiber entanglement as all the fibers are placed in close proximity with each other within the same beaker. During the aging process the addition of water and movement of the beakers increases the risk of fiber entanglement. We have had experience with fibers becoming entangled during aging and they would become damaged in the process of untangling. Next item of concern was the cost; owing to the industry partner's previous setup being very costly. Followed by ease of use and risk of damaging the delicate fibers due to extra handling to transfer them from the beaker to the machine for testing. All the aforementioned items are therefore ranked highest in the design criteria as they were all considered of equal value and the primary objectives.

For the coupon aging setup, the main design objective was to eliminate gradients (both temperature and chemical) from forming within the aging fluid by fluid motion and increase the number of coupons that can be aged at once. The setup would also need to be able to meet the specified design conditions set by the research partner. Cost and safety were the secondary objectives.

3 Aging Setup Design

3.1 Design Criteria

Our industry partner has expressed interest in building a setup(s) that can be utilized for aging samples of different types; with the primary focus being to evaluate new materials (fibers and polymers) for reinforced thermoplastic pipe construction. It would be optimal if one setup can accommodate aging of both fibers and coupons, but it is not a mandatory requirement. The intended aging medium is either aqueous or hydrocarbon solvent with the duration varying from a few weeks to months.

The most important criteria set forth by our industry partner are: risk of fiber entanglement, cost, ease of use, and minimizing handling of samples (for fibers and other delicate samples). The secondary criteria are as follows: utilizing existing equipment, minimizing stress concentration for the holding fixture, minimizing thermal gradients, active stirring, modular design, ability to take fluid and test samples without impacting the rest of the aging setup, and consideration for adapting the design setup for future expansion into various other test sample sizes and types. Refer to the sections below for a more detailed explanation of the criteria for each setup.

The above criteria set out by our industry partner are many, but the most important requirement of our industry partner is to have a cost-effective setup that shows improvement over the existing methods.

3.1.1 Fiber Aging

The design synthesis of the fiber aging setup began by simply brainstorming to improve upon the existing design setup of the beaker method currently used at the University of Alberta mentioned in the previous section. Care was also taken to meet the design objectives set by the industry partner and improve upon any deficiencies noticed in previous setups.

As for the fiber aging chamber, the preference will be to utilize either the existing environmental chambers, water baths, ovens, or the new tensile test coupon aging tank. Some consideration will be given to a proposal of purchasing or building a new chamber if it is financially feasible and also provides a clear benefit over the existing setups.

Tensile testing of the fibers is preferred to be done in the same fixture as aging without removal of the fibers. This is due to the fragile nature of the aged bare fibers; so consideration is given to the possibility of aging in the same fixture. Minimizing the handling of the fibers would reduce the possibility of damage and the introduction of errors.

One drawback of using the beaker method is the possibility of the fibers being tangled. If the beaker method is used then consideration will need to be taken to minimize this by either tensioning the fibers or holding them in position in some manner.

While mechanical stirring may be desirable for aging of coupons to help minimize striations within the aging medium; it is not recommended for the fibers. Any strong stirring should be avoided with the fibers as they become fragile with aging and mechanical stirring would increase the likelihood of either damage or entanglement. However, low velocity flows would be beneficial to help maintain uniformity of the aging fluid.

Minimizing the disturbance in the event of fiber removal should also be considered but is of low importance here as the testing occurs within a few days to weeks. It would be ideal if the design setup could allow for certain fiber samples to be removed without disturbing the entire setup. The current jar method allows the fibers to sometimes become entangled during aging, so a method to minimize or eliminate this is desired.

3.1.2 Tensile Test Coupon Aging

The criteria for designing the tensile test coupon aging setup was to improve upon the drawbacks of the previous setups and the number of test coupons that can be aged at one time. Our industry partner's existing aging setup is the pipe method mentioned in the previous section. For the University of Alberta, the existing method is the aging setup that was commissioned under a previous industry partner. So the methodology here is to learn from both design setups and improve upon them when designing the new setup.

The biggest flaw of both previous designs was the striation or gradients within the testing vessel. The new design must try to eliminate this with either passive or mechanical circulation. This would help mitigate the issues caused by the localized temperature variations which impact the degree of aging and in some cases cause test coupons to melt. Any localized contamination caused by the coupons' leaching would also need to be uniformly mixed and/or have a region to settle in for debris generated.

Coupon removal for our industry partner's pipe setup requires disturbing the experiment, while our previous setup at the University of Alberta minimizes that disturbance. This is important as the tensile test coupons would be aged for a period of up to 18 months and intermittently coupons would be removed for testing. Another point to consider is the possibility of the aging fluid being sampled throughout the testing period to track the leaching effect and changes in fluid chemistry. The new aging vessel would need to have sufficient fluid levels to minimize this impact and provide for a reasonable buffer due to evaporative losses. A method for topping up the fluid and fluid extraction would also need to be implemented.

The financial feasibility of the setup would also need to be considered as our industry partner's existing setup is very cost-effective when compared with other commercially available environmental chamber setups. Our industry partner has expressed interest in utilizing existing setups such as ovens and beakers due to cost limitations of custom fabrication or purchasing highly specialized equipment. Multiple aging cells would also be required as there is a need to test multiple process conditions simultaneously. The need to have multiple aging cells also compounds with the cost-effectiveness criteria as savings are multiplicative.

The coupon style chosen by the industry partner was based on the Type 1 coupon under ASTM D638 [1]. Not all test samples are of the same size, some are slightly modified compared with the standard ASTM D638 type 1; for example longer grip lengths or thicker/thinner. An adapted drawing of this can be found in Appendix F – Tensile Test Coupon.

3.1.3 Process Conditions

The design process conditions are as follows:

- Fluid: water and hydrocarbon solvents
    - For water, the intent is to test a combination ranging from but not limited to deionized, chlorinated, and salt water.
    - For hydrocarbon solvents, the exact formulations are not explored in this paper. They would be explored in future studies but the general design concepts for hydrocarbons would need to be considered for the current design.
- Water temperature: ranges from 50°C to 95°C
- Hydrocarbon solvent temperature: ranges from 50°C to 140°C
- Both setups cannot be pressurized and thus overpressure protection per AB-525 [43] and CSA B51:19 [44] does not apply. Our industry partner expressed interest in possibly adapting the design for pressurized service in the future, so this path would be explored in the future.

Accommodations would also need to be provided to either keep the same process fluid during the whole test duration or provide intermittent changes of the process fluid with fresh fluids. Our industry partner expressed interest in having both of these options in the design, but will initially start with keeping the same process fluid throughout the test and only adding some warm deionized water to replenish any evaporative and liquid sampling losses.

Due to the large range of process conditions and the intent of having multiple setups, it would be more cost-effective to separate the design into two categories. One design would be optimized for the less aggressive conditions while minimizing the required modifications to adapt the design for the full range of conditions for other setups.

3.1.4 Material Selection

Notable materials such as carbon steel, stainless steel, aluminum alloys, and plastics come to mind at the initial stages of brainstorming due to their common appearance in literature. Consideration was given to each material's compatibility with the process conditions, ease of manufacturing, and financial feasibility.

Carbon steel is used very often in industry due to its ease of manufacturing, relatively good strength-to-weight ratio, and low cost. One of the biggest pitfalls of carbon steel is usually that it can be easily attacked in aqueous solutions [45]. However, this is usually overcome with proper engineering to provide sufficient mitigation in the form of corrosion allowance, preventative maintenance, coatings, and/or cathodic protection. An especially troublesome process condition would be the accelerated aging in salt water, as it would very aggressively attack the exposed carbon steel surfaces [45]. For this design, carbon steel was eliminated early in the design due to the risk of contamination of the process fluid from the corrosion products. It is noted that coatings could have been used to prevent corrosion, but it is not a risk-proof method as coatings can be damaged via abrasion/erosion or consumed like a sacrificial zinc coating.

Stainless steel is a prime candidate for our aging vessel and carousel due to its good corrosion resistance in salty environments. However, the material and manufacturing costs are relatively higher compared to the other materials mentioned in this section. For relative material cost comparison, SA-36 (carbon steel) has a current spot price of $0.45 USD/lb when compared with 304SS at $2.28 USD/lb [46, 47]. In comparison with carbon steel, stainless steel fairs superbly well against attack in aqueous solutions owing to its inert passivation layer. It does not pose the issue of rusting that occurs with carbon steel in water. Although stainless is not without its drawbacks. In particular, its susceptibility to chloride stress corrosion cracking, pitting,

and crevice corrosion would need to be considered. Stainless steel is also one of the higher cost materials being considered.

For these experimental designs, the general stress levels from self-weight and static head pressure would be very low aside from the bolting and specific areas of high-stress concentrations. Therefore, chloride stress corrosion cracking would likely only occur in those regions [45]. To avoid chloride stress corrosion cracking in high-stress concentration areas, care would be taken to reduce the stress concentrations by changing the geometry or thickening the welded areas. For bolted joints, either removing them from the process fluid exposure or having them coated would reduce the likelihood of chloride stress corrosion cracking occurring. Coatings can be done in a variety of ways, with the most common being with a thread sealant or polytetrafluoroethylene (PTFE) coated fasteners. Preference would be given to the thread sealant over the use of PTFE coated fasteners due to the cost. However, the higher cost of PTFE coated fasteners offers superior protection compared to a thread sealant.

The critical factors impacting whether brine pitting or crevice corrosion occurs are chloride concentration of the process fluid, service temperature, stress level, and type of stainless alloy [45]. In particular, 304 stainless steel and 316 stainless steel were considered due to their relatively good availability at a reasonable cost. It should be noted many other types of stainless steel may perform better than the aforementioned, but their scarcity and cost are considered to be prohibitive and therefore not considered in the design. In industry 316 stainless steel is often called “marine grade stainless steel” owing to its superior pitting resistance in saltwater compared to the other common grades of stainless steel. Specifically, the molybdenum content of 316 stainless steel provides a more stable passivation layer to resist attack [45, 48]. A way to gauge the stainless steel resistance to pitting and crevice corrosion would be to use the pitting resistance equivalent number (PREN) [45]. To that end, the American Petroleum Institute (API) recommends a

PREN number of at least 40 for ambient seawater conditions to effectively resist pitting. 304 stainless steel contains 18-20% chromium and up to 0.10% nitrogen, which yields a PREN number of between 18-21.6 [49]. 316 stainless steel contains 16-18% chromium, 2-3% molybdenum, and up to 0.10% nitrogen, which yields a PREN number of 22.6-29.5 [49]. Overall both 304 and 316 stainless steel does not meet the API criteria of at least 40 for the PREN number. A higher grade alloys (Monel and Inconel) that would meet API's criteria were considered but due to the high material cost and difficulty in fabrication, those more costly alloys were not pursued. For this comparison, 316 stainless steel is recommended as it has a higher PREN number when compared with 304 stainless steel and therefore better resistance to pitting and crevice corrosion.

Aluminum alloys were also considered as they were relatively low cost when compared with stainless steel. They also provided better corrosion properties when compared with carbon steel in aqueous solutions in certain scenarios. In particular, 6061 aluminum alloy, also known as A96061 by the Unified Numbering System, was considered due to it being very commonly available and providing excellent mechanical properties. This aluminum alloy is available in various grades, called temper, due to the precipitation hardening; the various tempers it comes in provide a wide range of mechanical properties. For example, the tensile strength can vary between 24-42 ksi depending on the temper [50]. Aluminum alloys are resistant to many acids and solvents aside from halogenated solvents, caustic, and anhydrous alcohols [45, 51]. A major drawback of aluminum alloys would be its susceptibility to corrosion in salty environments.

Acrylic was also considered as it was more cost-effective than stainless steel or aluminum and provided the added advantage of being clear. Acrylic cannot be used at high temperatures or in solvents, unlike the other materials being considered [52]. A service temperature of up to 93°C was cited by the manufacturer which would cover most of the experimental temperature

range required for aqueous solutions [52]. However, initial aging tests with tap water showed that the heat-affected zones of acrylic are prone to developing cracks when aged at 80°C as shown in Figure 7. The crack locations were discovered on the top of the aging cell lid shown in Figure 8 located at the two vents. The vents are shown plugged with custom silicone plugs, which were used to limit the evaporative losses during aging. The cracks were only visible on the top surface of the acrylic and not on the bottom which was exposed to the high moisture and temperature of the aging cell environment. The top surface was also the top surface during laser cutting of the acrylic. The heat affected zone of acrylic after laser cutting can have microcracks [53]. The result is the microcracks provide the stress concentrations needed to grow under the stresses of the aging process, which would explain why noticeable cracks have only formed in the heat affected zone and no where else.

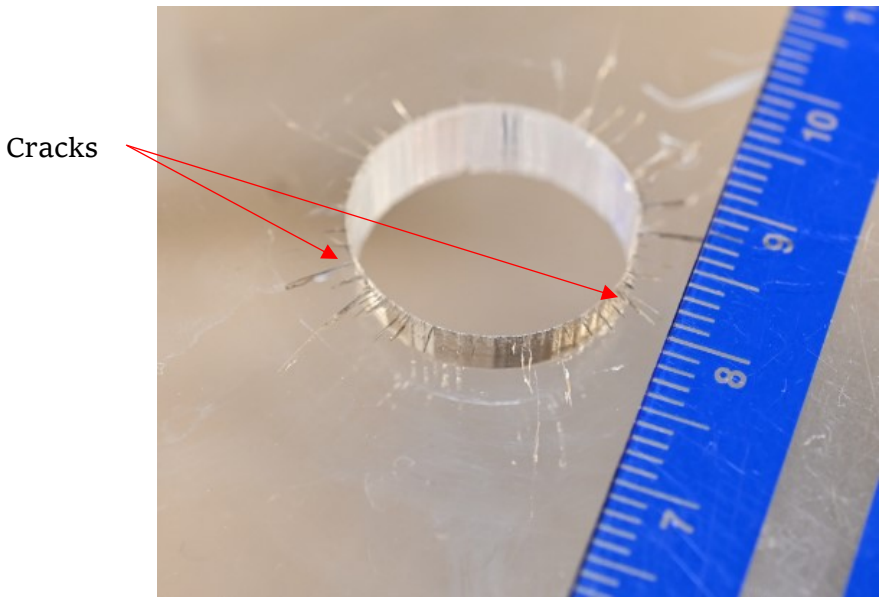

Figure 7: Cracks in acrylic around heat affected zone after exposure high temperatures and water

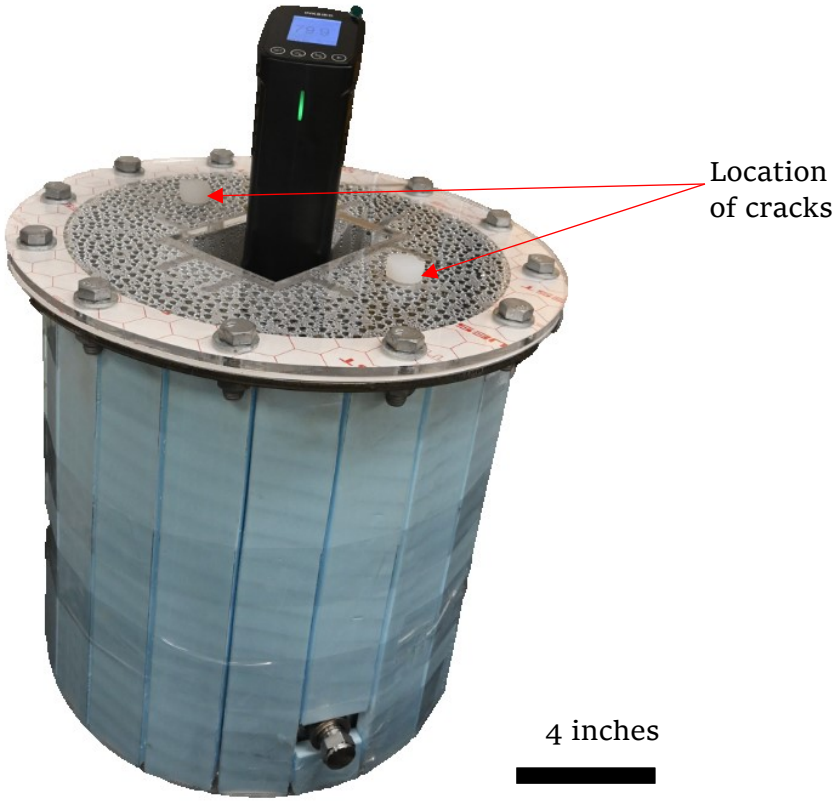

Figure 8: Location of cracks on aging cell from initial testing

This susceptibility to cracking thus limits the upper limit of the operational temperature to less than 80°C to mitigate the risk of cracking resulting in leaks. It should also be noted that some manufacturers state the upper range of the service temperature to be as low as 65°C [54]. Acrylic also has the added advantage of being lightweight compared with metals, with a density of about 43% that of aluminum and 15% of stainless steel.

Fabrication using acrylic is easier than metals with the use of a CO2 laser for cutting and solvent welding with dichloromethane (DCM). Unlike traditional welding where high temperatures are required to fuse the base metal with a filler (welding rod), solvent welding is performed at room temperature with the solvent dissolving the parent material and then evaporating away. This

leaves a bond that is made of the same material as the parent material with no fillers or glues. This would eliminate the possibility of the welded joint being specifically attacked due to differing chemistry in certain cases as seen in the industry where the proper selection of the welding rods is critical [45].

Comparing the four mentioned materials for brine or seawater service, it is clear that stainless steel and acrylic would be the best candidates. For the metals, the following corrosion rates in hot saltwater can shed some light on how they fair: carbon steel 4.2-40.9 mpy, 316 stainless steel 0.0-4.0 mpy, 6061 aluminum alloy 2.1-56.6 mpy [55]. However, it should be noted that the above comparison is for general corrosion only and that the 316 stainless steel did suffer the worse in crevice corrosion [55]. Acrylic on the other hand would fair far better at lower temperatures for saltwater solutions as it is commonly used for saltwater aquariums in commercial settings due to its shatter resistance compared with glass. Acrylic exposed to a 10% brine for 7 days in a 77F solution showed a weight gain of only 0.3-0.5% with no other notable damages [52]. In comparison acrylic submerged in distilled water for the same conditions as above had a water absorption of 0.4-0.6% with no other notable damages [52].

After considering the feasibility of each material it was concluded that both stainless steel and acrylic would be the best materials to construct the aging cells. Stainless steel would be the overall better option if financial considerations were not weighed in. As certain tests would be performed at lower temperatures of approximately 60°C and in aqueous solutions, it would not require the more costly stainless steel material to hold up for these more tame process conditions. Acrylic also has the added benefits of being an insulator to partially limit the heat losses and being optically clear so a visual inspection of the setup during aging could be done. The stainless steel aging cells would therefore be reserved for use in more severe service such as higher temperatures or in solvents where acrylic would be attacked.

3.2 Design Discussion – Fiber Aging Fixture

The design synthesis of the fiber aging fixtures in this section took inspiration from various sources such as: previous design setups with improvements; input from other engineers of the industry partner; and common items in everyday life. Each design would have a brief discussion regarding their pros and cons. As these are conceptual designs, the stages at which they were eliminated from further development varied. For design objectives and process conditions please see details in the previous sections under 3.1 Design Criteria.

3.2.1 Design A

The first fiber aging fixture design is to utilize the existing pipe method mentioned in 2.2.1 for use with tensile test coupons. Figure 9 is designed to have fibers wrapped around each armature and span across the length of the spool between the top and bottom armatures. This would mean the span length would be half the gauge length for aging as the fibers would be wound back to the top in a U shape. The fibers would then each be tied to one end of the span's armature. This completed fiber aging fixture would then be placed inside the pipe aging cell and could also be stacked.

The main advantage of this design is that it utilizes our industry partner's existing pipe setup and keeps the fibers from being tangled with each other during aging. Each individual spool could also be removed independently from the pipe for testing. As the whole fixture is placed inside a pipe spool for aging; the main disadvantage would be the ends of the fibers are aged with the gauge length and extra handling would be required to remove the aged fibers for tensile testing.

For detailed drawings please refer to Appendix A – Concept Drawings for Fiber Fixtures.

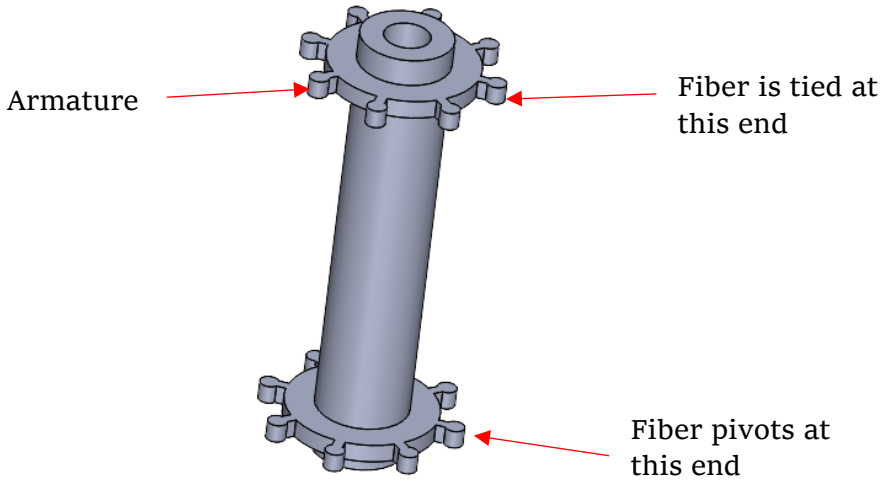

Figure 9: Design A concept of a fiber aging fixture

3.2.2 Design B

The next fiber aging fixture is based on a simple pipe spool where the fibers are wrapped around the flanges as shown in Figure 10. The aging fluid would then be circulated through the pipe spool with the nozzles on the ends. This would mean the ends of the fibers would not be aged as they are located outside of the pipe. However, the ends of the fibers could potentially be wicking fluid out if the seating stress of the gasket was not sufficient to stop capillary action. There would also be a risk of introducing another damage mechanism on the ends of the fibers if the wicking fluid carried salts that would be further concentrated via evaporation. The gasket on the ends would also need to sandwich the fibers to provide an adequate seal without a leak path, which means using two soft seating gaskets per flange instead of the norm of one gasket per flange. The cost of manufacturing this design would be low as it is made from simple piping components. Another advantage would be that the fibers would not risk entanglement with one another as they would be pinned in place by the flanges on the end, however, extra handling would still be needed for tensile testing the fibers.

For detailed drawings please refer to Appendix A – Concept Drawings for Fiber Fixtures.

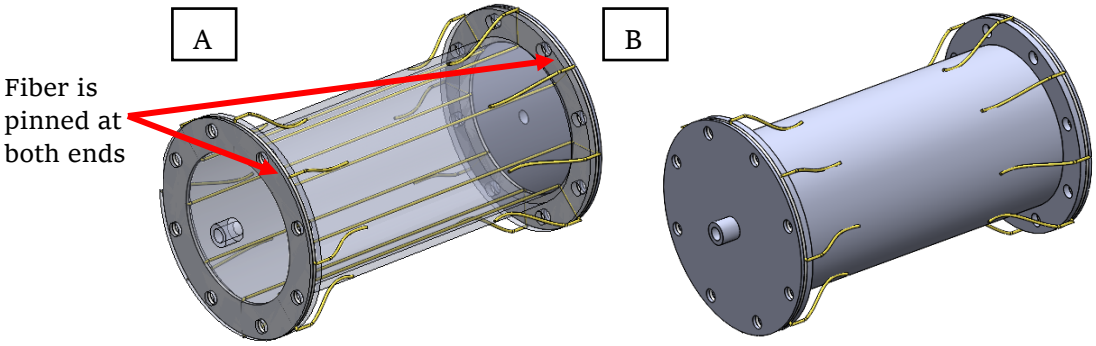

Figure 10: Design B concept of a fiber aging fixture: (A) transparent pipe spool to show fibers, (B) opaque pipe spool

3.2.3 Design C

Design C is an iteration of design B where the fibers are only placed on one end of the pipe spool as shown in Figure 11. The process fluid is similarly circulated through the pipe spool utilizing the nozzles on the flanges. This design would offer the main advantage of easier sample preparation compared with design B as only one flange would need to be removed to place the samples in place. The same aspect would then become a major disadvantage as the fibers would risk entanglement with the fluid flow unless a very low velocity was maintained. The main reason for this design was the cost of manufacturing and potential leak points could be minimized with the removal of one of the flanges from the design.

For detailed drawings please refer to Appendix A – Concept Drawings for Fiber Fixtures.

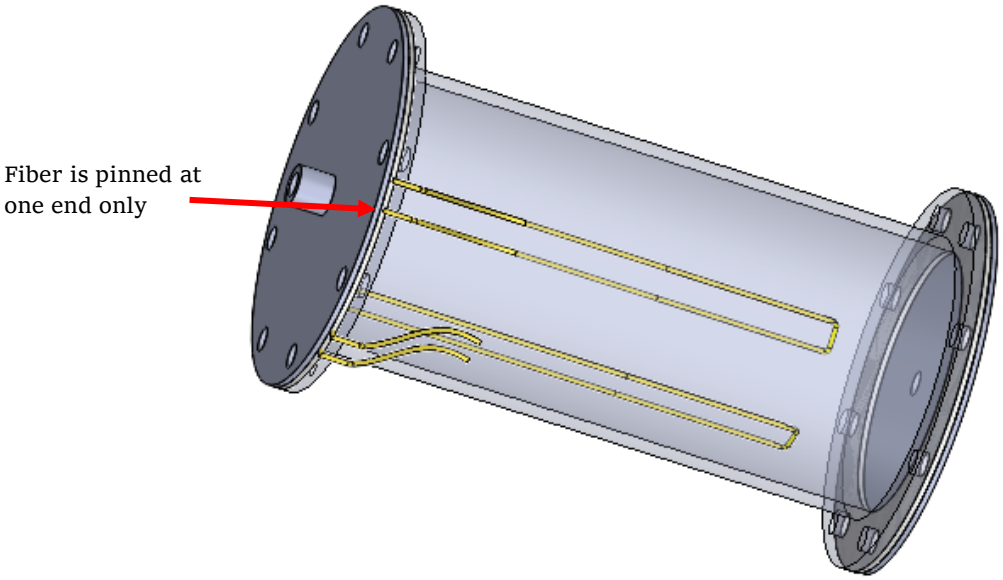

Figure 11: Design C concept of a fiber aging fixture

3.2.4 Design D

With a request for a modular design that could have a set of samples removed from the aging vessel with minimal impact on other aging samples, the Figure 12 below shows this concept. The idea is to have pegs placed into a board that can hold the fibers. Each fiber would be wound around the top two pegs and down towards the bottom peg forming a U shape. That way the length down to the bottom peg is less than half the gauge length. The locations of the pegs and their sizes can be adjusted to increase the bend radius and angles as needed to minimize stress on the fibers. This design can be scaled up as needed to accommodate other container sizes, in particular, our industry partner was interested in using a plastic tote like those described in 2.5.2 for aging using the frame design. Another advantage is the ends of the fibers can also be placed above the liquid level to minimize aging there. The design can also accommodate tensioning the fibers during aging by the addition of a threaded design to one peg where it can be turned to apply tension to the fiber.

For detailed drawings please refer to Appendix A – Concept Drawings for Fiber Fixtures.

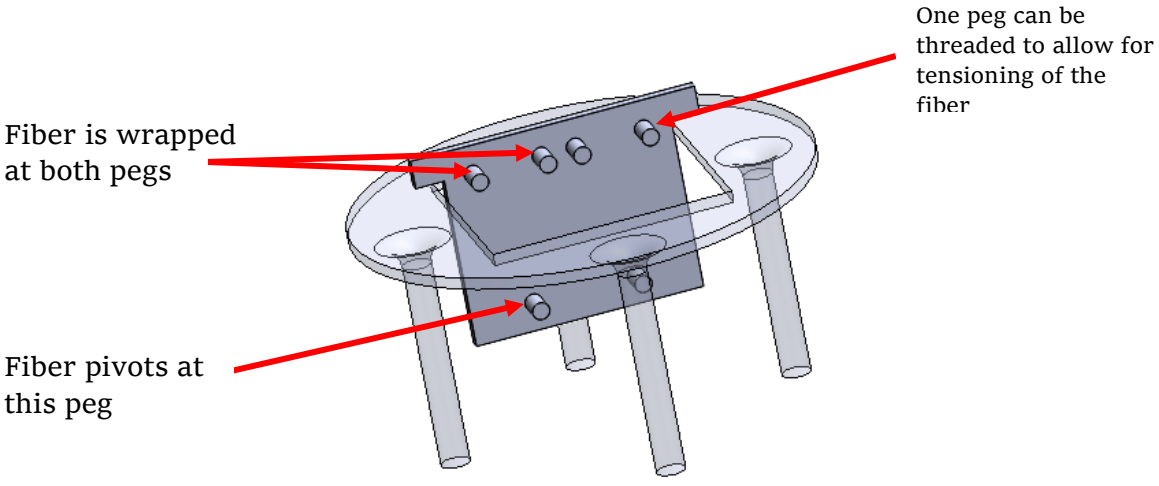

Figure 12: Design D concept of a fiber aging fixture with stand

3.2.5 Design E

Design E is based on the frame design described in 2.2 for fiber aging. The main modification is to have a simpler design without the need for welding and to accommodate double the number of samples. Figure 13 shows the frame design made from a singular piece of sheet metal that has been laser or waterjet cut to shape. The length of the inner square would be approximately the gauge length and the fibers would be secured on the opposite ends via bolting with a rubber washer. In the same manner described in 2.2, the fibers can be tensioned during assembly. The frames would be aged in plastic totes similar to what our industry partner currently uses. The concept below can also accommodate up to double the samples without having the fibers contact each other when compared with the original design by having fibers placed vertically on the front face of the plate and horizontally on the back face of the plate.

For detailed drawings please refer to Appendix A – Concept Drawings for Fiber Fixtures.

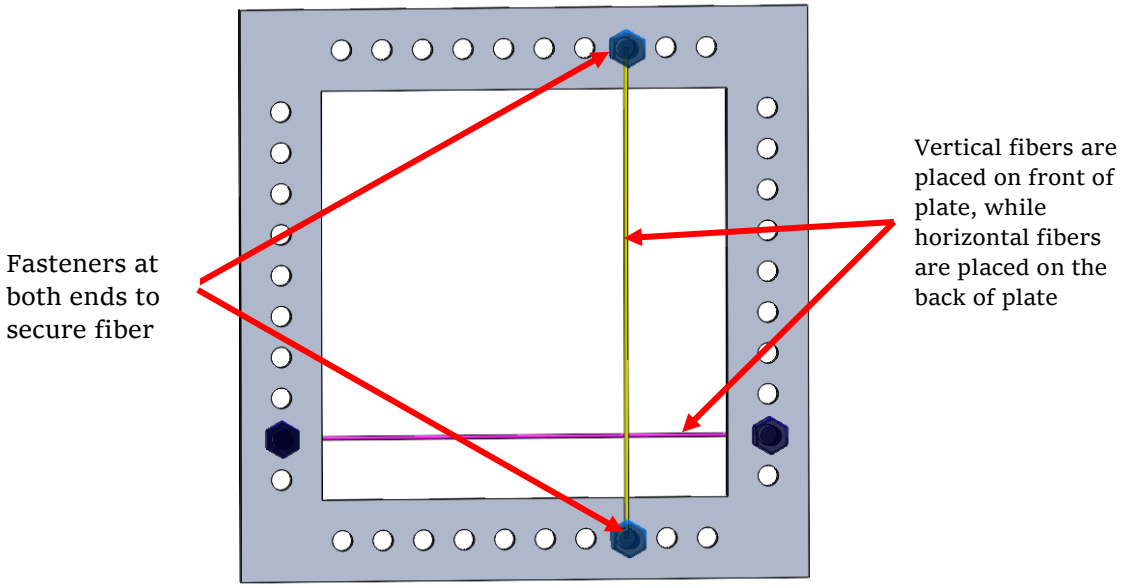

Figure 13: Design E concept of a fiber aging fixture

3.2.6 Design F

The inspiration for design F is from a combination of a clothesline and cantilevered storage racking. The concept is to create this storage rack design which would be anchored within a container. Each fiber would then be wound and glued to a piece of a steel bar as shown in Figure 14, which can subsequently be attached to another fixture for tensile testing of the fiber to minimize handling of the aged fibers. A major drawback would be accessing the lower racks to gather samples as it would be cumbersome to weave the fiber around without snagging on surfaces.

For detailed drawings please refer to Appendix A – Concept Drawings for Fiber Fixtures.

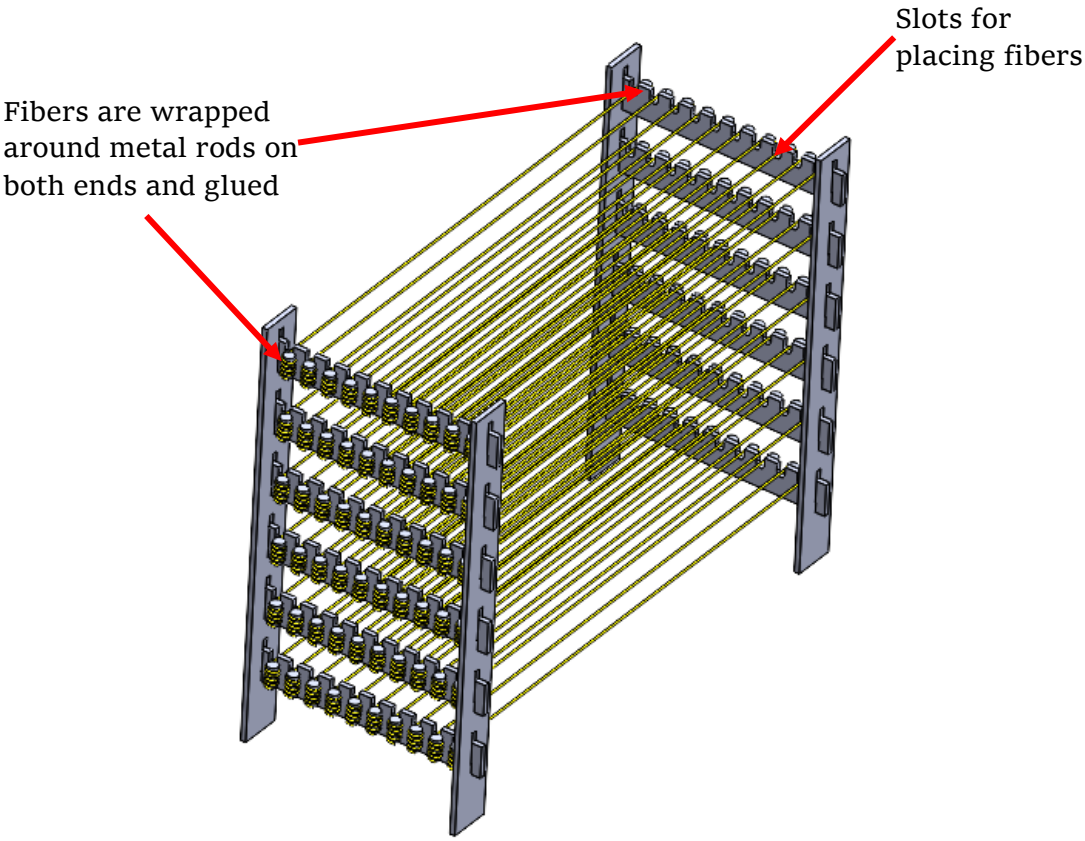

Figure 14: Design F concept of a fiber aging fixture

3.2.7 Design G

Design G gathered inspiration from the previous singular fiber testing fixture mentioned in section 2.2, but with modifications to enable cost-effective production and decreased the real estate taken up by the previous bulky design. The main body of the design would be waterjet or laser cut from sheet metal and the threaded holes tapped as shown in Figure 15. The stepped mid-section would enable it to locate the upper and lower tabs in position with just a single fastener. The fibers would be wound around each bolt and could be tensioned by tightening the bolts after assembly. The bolts are offset from the centerline of the fixture to place the fiber in the center of the tangent of the bolt shank.

The fixture is intended to be placed vertically in an aging tank such as a tote or inside of the tensile testing aging cell mentioned below in 3.3. The top hole in the upper plate is used to secure the fixture during aging and allow for ease of removal. After aging the whole fixture is secured to a tensile testing machine before the mid-section is removed; this would ensure minimal handling with the aged fibers and allow the fibers to be tested in the same fixture as it was aged.

For detailed drawings please refer to Appendix A – Concept Drawings for Fiber Fixtures.

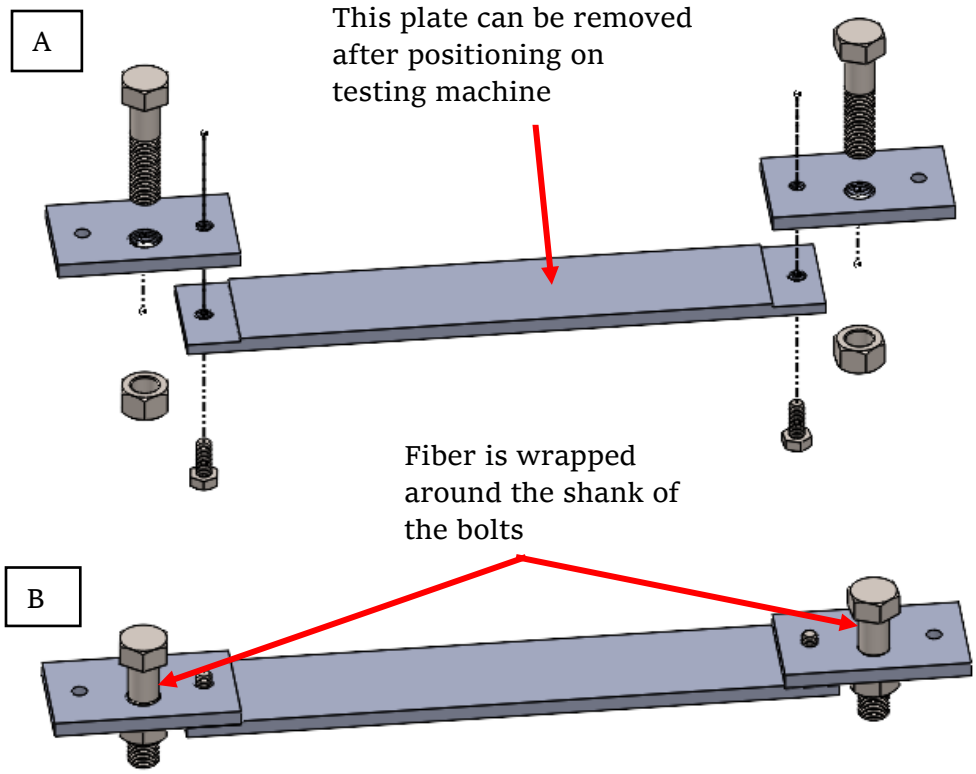

Figure 15: Design G concept of a fiber aging fixture: (A) exploded view, (B) assembled view

3.2.8 Design H

This design is another iteration of design D but with a more modular design that can be placed in the same vessel as the tensile testing aging cell in 3.3. The fibers are glued to two metal blocks that can also be mounted into the tensile testing machine to minimize the handling of the fibers as shown in Figure 16A. The metal blocks are then placed on a table located above the liquid level within the vessel; this is to prevent the aging of the fiber outside of the gauge length. The fibers can independently be removed from the aging vessel for testing. A disadvantage of this design would be that the exposed fibers could be prone to entanglement, especially with the implementation of any stirring within the vessel. This could be solved by placing mesh or perforated dividers between each of the sets of gauge blocks as shown in Figure 16B.

For detailed drawings please refer to Appendix A – Concept Drawings for Fiber Fixtures.

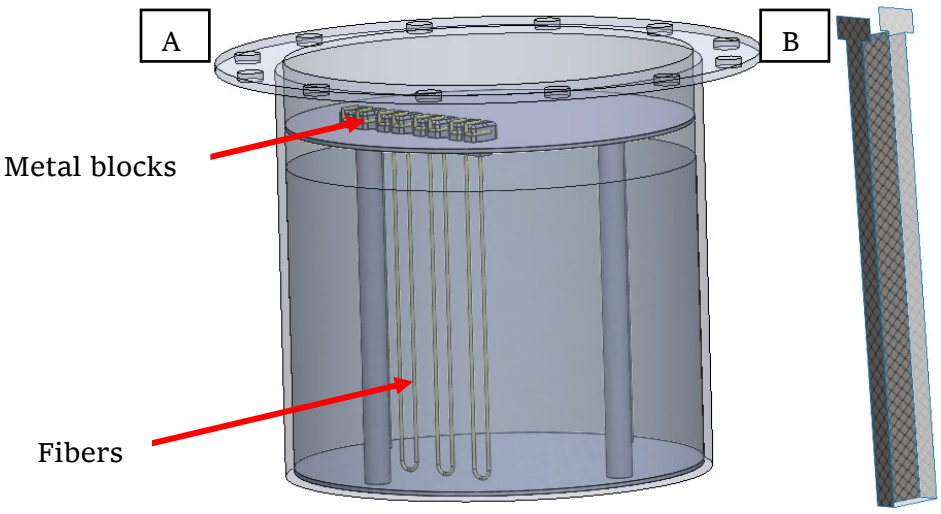

Figure 16: (A) Design H concept of a fiber aging fixture inside of aging cell, (B) mesh divider concept

3.2.9 Design I

Design I was inspired by a pineapple. Figure 17A resembles a slice of a pineapple while Figure 17B resembles a whole pineapple. The fiber aging fixture is created using 2D manufacturing techniques to minimize the cost of fabrication. Each fiber would be wound around the fixture and each fixture can be removed from the aging cell without impacting the other fixtures. This design would keep the fibers from being tangled with one another. Each fixture can then be placed into the tensile test aging cell and offset with the next to provide a more efficient stacking pattern. A disadvantage of this design would be that the whole fiber is aged and must incur some handling from aging to testing.

For detailed drawings please refer to Appendix A – Concept Drawings for Fiber Fixtures.

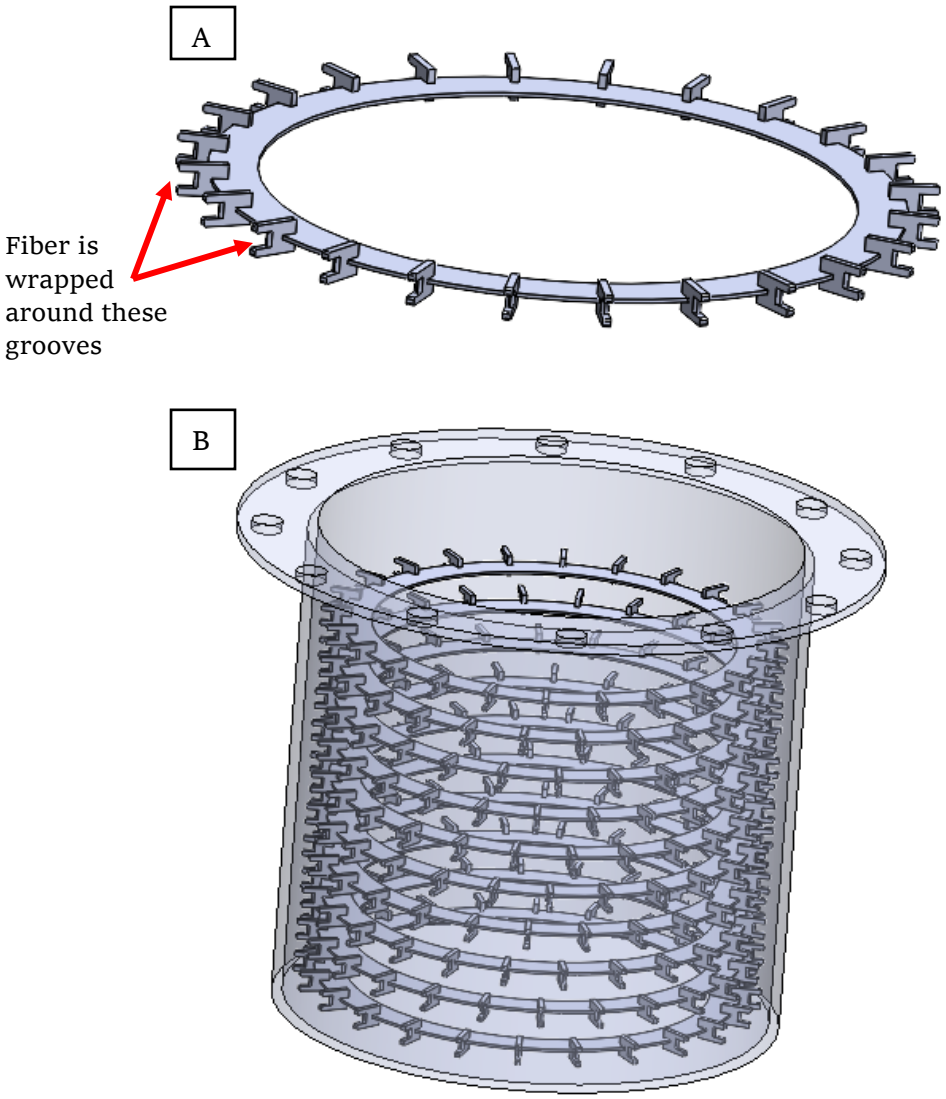

Figure 17: (A) Design I concept of a fiber aging fixture, (B) Design I fiber aging fixtures stacked inside of aging cell

3.2.10 Design J

Design J was intended to be a highly efficient and modular way to hold fibers for aging. Figure 18B shows the modular fiber aging fixture with the two support bars to be made from either a large-diameter threaded rod or machined grooves in a round bar. The original thought behind utilizing threaded rods was for their low cost relative to a custom machined part. However, the threaded rod may generate some stress concentrations on the fibers which could be undesirable. Fibers are then wound around one of the grooves and tied off on the opposing groove; in this way, many samples can be aged at once with each modular fixture. Then each fixture is placed into a carousel as shown in Figure 18A which can then be placed into the tensile testing aging cell in 3.3. Utilizing the same aging cell is ultimately the biggest advantage of this design.

For detailed drawings please refer to Appendix A – Concept Drawings for Fiber Fixtures.

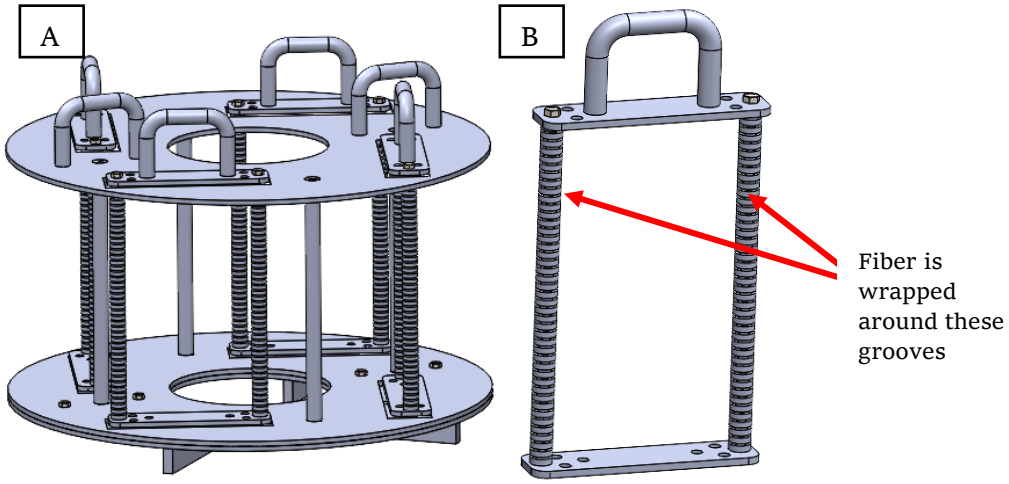

Figure 18: Design J concept of a fiber aging fixture and carousel: (A) aging fixtures inside of carousel, (B) aging fixture

3.2.11 Design K

Design K was based on design J but with a non-modular approach to reduce the stress concentrations and cost of manufacturing. To reduce the cost of manufacturing the previous design was updated to incorporate only 2D manufacturing; the vertical slats can have tabs added for attachment to the top and bottom plates, while the handles can be flatted into a shape that can be manufactured easier. This design retains the ability to be used in the same aging cell as design J. The bending radius for wrapping the fibers around for aging has been greatly increased to reduce the stress concentrations. Each fiber is wound around the entire circumference of the setup in Figure 19 and secured via tying, gluing, or taping. The disadvantage of this design is that the entire carousel would need to be removed from the aging cell to extract samples for testing. However, another design was explored that combined the 2D manufacturing concepts to Figure 18B's aging fixture to get the best of both designs. That different design has not been included in this paper as it was not pursued past the chalkboard sketches.

For detailed drawings please refer to Appendix A – Concept Drawings for Fiber Fixtures.

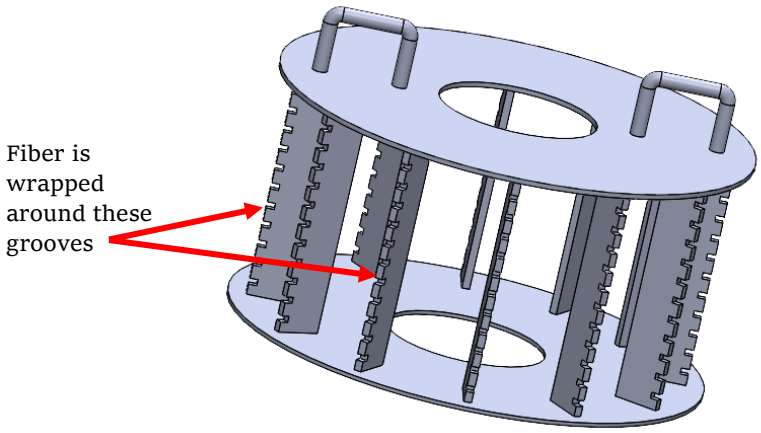

Figure 19: Design K concept of a fiber aging fixture

3.2.12 Design Selection Discussion

The aforementioned designs A through K were extensively considered for use in fiber aging experiments. These considerations will be summarized below in Table 2 with a ranking matrix to provide a relative comparative score.

Fabrication cost was ranked from 1 to 10, with 10 being the least expensive to fabricate. It is a relative cost estimate based on the complexity of the fabrication steps required, such as machining, welding and rolling.

Ease of use was ranked from 1 to 10, with 10 being the easiest to use. Operational and setup steps and complexity were both considered. For example design B (Figure 10) requires the tightening of bolts on two flanges to assemble the test setup; while design C (Figure 11) requires only tightening bolts on one flange after initial assembly as the fibers are only secured from one side as opposed to two sides in design B. This means the steps required to remove any aged fibers is halved using design C compared with design B, hence design C is ranked higher than design B.

Use of existing aging tank was ranked from 0 to 2. A rank of 2 means it can utilize the existing aging tanks; either the pipe design and/or plastic tote our industry partner currently utilizes. A rank of 1 means it can only use the newly fabricated aging cell for the carousel design. Note design I (Figure 17) can utilize both the newly fabricated aging cell and existing plastic tote, so a rank of 2 was given. A rank of 0 means it requires the fabrication of a new setup.

Fibers being able to be tensioned was ranked from 0 to 1. A rank of 1 means the fibers can be tensioned in the setup. A rank of 0 means it cannot be tensioned. Similarly the other ranks of fibers prevented from entanglement, aging of fiber ends, and handling of fibers are ranked in the same fashion with a rank of 1 being compliant and rank of 0 being noncompliant. The handling of fibers is with respect to the extra handling needed during the aging process where less handling is the higher ranking.

Fiber stress concentration was ranked from 0 to 2. With a rank of 2 providing no significant stress concentration due to securing of the fibers during the aging process. A rank of 1 means there is some stress concentration while a rank of 0 means there would be a large stress concentration. Whether the setup would be tensioned was also taken into consideration for this ranking; which means if the setup can be tensioned it was assumed to be operated with tension for the ranking process.

Modular design was ranked from 0 to 2. With a ranking of 2 providing separate modules for removal as shown in design J (Figure 18) with the four aging fixtures that can be independently removed from the carousel. A ranking of 1 means some part of the design has some modular ability but with limitations such as design H (Figure 16) or design I (Figure 17) where individual test specimens can be removed but not as a single module that holds enough test samples for one test; meaning more effort is needed to remove multiple small modules to allow for enough test samples to be collected. A ranking of 0 means the design is not modular and the entire experiment would be interrupted to extract the samples.

Lastly, the ranking for whether removal of fibers disrupts the experiments was ranked from 0 to 2. With a rank of 2 being no impact to the experiment for the removal of samples; a rank of 1 having minor impact, and a rank of 0 having major impact. For example, design J (Figure 18) was ranked 2 because the modules could be removed without impacting the other modules in the aging vessel. While design K (Figure 19) would require the whole carousel be removed each time any number of samples are needed, so hence it was ranked 0 due to the disruptive nature of the sample collection.

Design G was ranked highest then followed by design E. Our industry partner's primary criteria of cost-effectiveness and ease of use were the main deciding factors between the various designs. With designs G and E being fabricated primarily by 2D manufacturing methods and their minimal use of

machining customized parts; these two designs are by far the most cost-effective of the ones being considered. Another noteworthy point is that both designs G and E are based on the existing test fixtures our industry partner is familiar with; this sense of familiarity also adds extra points which are not considered in the above table but were noted as a possible category for consideration.

Design G provided the main advantage of being more modular and minimized the handling of fibers when compared with design E. Whereas with design E the fibers would need to be individually removed and placed into fixtures for tensile testing; design G would have the aging fixture placed directly into the tensile testing machine without future handling of the fibers. Design G also provided the flexibility to utilize either the aging cell in 3.3, the water bath, or the previous aging containers; with design E being more suitable for use in all but containers from 3.3.

In contrast, design E would be more cost-effective when comparing the cost per number of samples aged as multiple fibers can be aged per fixture. Design E would also be faster to scale up for either more or fewer fibers or to accommodate different aging vessel sizes. Whereas design G would be less flexible in its ability to adapt to changes. Design E could also be fabricated in the same manner as the original design where it consists of welded flat bar to facilitate more efficient use of materials. However, due to our research groups' ease of accessibility to both a waterjet and laser cutter, fabrication from a plate would be the preferred option.

Table 2: Fiber aging fixture design ranking matrix

Design Criteria	Weight	Design A		Design B		Design C		Design D		Design E		Design F		Design G		Design H		Design I		Design J		Design K	
		Rating	Weighted Score	Rating	Weighted Score	Rating	Weighted Score	Rating	Weighted Score	Rating	Weighted Score	Rating	Weighted Score	Rating	Weighted Score	Rating	Weighted Score	Rating	Weighted Score	Rating	Weighted Score	Rating	Weighted Score
Fabrication cost	10	3	30	7	70	8	80	4	40	10	100	5	50	9	90	5	50	8	80	2	20	5	50
Ease of use	10	2	20	6	60	7	70	2	20	8	80	4	40	10	100	3	30	7	70	4	40	5	50
Use of existing aging tank	2	2	4	0	0	0	0	1	2	2	4	0	0	2	4	1	2	2	4	1	2	1	2
Fibers can be tensioned	5	0	0	1	5	0	0	1	5	1	5	0	0	1	5	0	0	0	0	0	0	0	0
Fibers prevented from entanglement	10	1	10	1	10	0	0	1	10	1	10	1	10	1	10	0	0	1	10	1	10	1	10
Aging of fiber ends	5	0	0	1	5	1	5	1	5	0	0	0	0	0	0	1	5	0	0	0	0	0	0
Handling of fibers	10	0	0	0	0	0	0	0	0	0	0	0	0	1	10	1	10	0	0	0	0	0	0
Fiber stress concentration	2	0	0	1	2	0	0	0	0	2	4	1	2	1	2	1	2	2	4	0	0	2	4
Modular design	2	1	2	1	2	1	2	1	2	1	2	1	2	1	2	1	2	1	2	2	4	0	0
Removal of fibers without disrupting experiment	5	0	0	0	0	0	0	1	5	0	0	0	0	2	10	2	10	1	5	2	10	0	0
Total Weighted Score			66		154		157		89		205		104		233		111		175		86		116

3.3 Design Discussion – Tensile Test Coupon Aging Cell

This section covers the process from the initial design concept to the final design of the tensile test coupon aging cell. Including initial testing results, which triggered an additional change to the aging carousel to help mitigate the issue of coupons warping.

3.3.1 Initial Design

The proposed design of Figure 20 took inspiration from the previous design mentioned in 2.2.1. Improvements were made based on the industry partner's past learnings and operational issues the previous designs had. The scope of the improvements includes: an increased number of tensile test coupons one fixture can accommodate; a reduction in thermal and chemical gradients via mechanical means; material change to stainless steel for chemical compatibility as one of the process fluids (hot brine) is considered corrosive to aluminum; added handles for ease of carousel removal from the tank; addition of legs on bottom of carousel to allow debris from aging to settle below the carousel; angled test coupons to promote better mixing with the flow; changed design to be made from 2D manufacturing techniques to improve ease of fabrication; added vent and valve for sample collection with minimal impact to the aging experiments; adapted design to fit multiple sizes of test samples as needed; and increased the volume of liquid to increase thermal mass for thermal stability and reduction in the frequency of water additions due to evaporative losses.

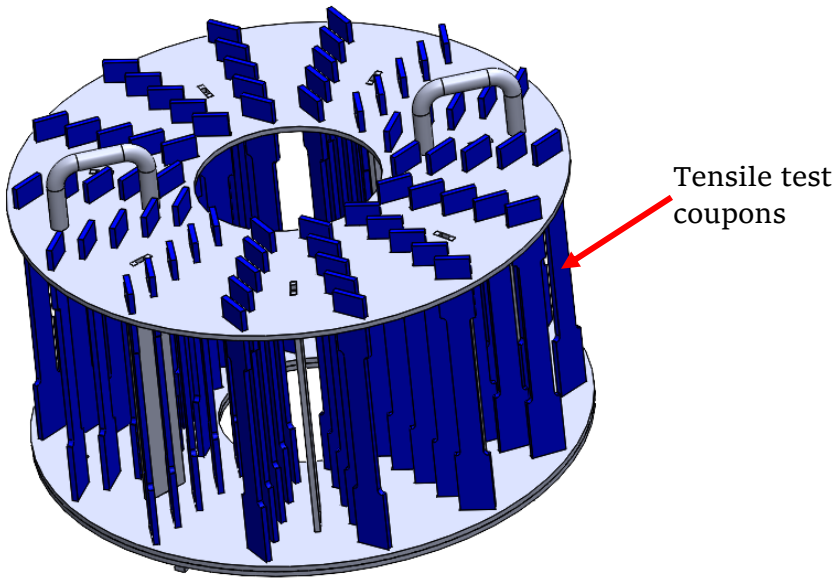

Figure 20: Carousel with tensile test coupons

Comparing the two design setups of Figure 3 and Figure 21, it is clear that the new design has increased the complexity of the setup with its additions, and therefore the cost is greater as well. However, the design was approved by the industry partner due to the clear advantages with mechanical mixing and ease of use over the previous version. The increased carousel size could accommodate 70 tensile test coupons whereas the previous design can only accommodate 50 coupons; our industry partner requires a minimum of 50 coupons for testing but requested an increase as a safety factor in case of unforeseen issues. The test coupons are also easily accessible for removal throughout the aging duration just like the earlier design. The original intent for the central hole of the carousel was to provide access for circulation from the vortex formed by the magnetic stirrer; while the tensile test coupons are angled to cause turbulence yielding better mixing and helping to eliminate dead spots from forming in the flow regime. The carousel was also raised off the tank bottom to allow the accumulation of any particles shed due to the aging process of the tensile test coupons; this was another issue noted by the

industry partner for some of their past test setups as certain coupons will foul the aging fluid with debris. The addition of a reservoir tank with circulation helps to increase the thermal mass and mixing of the system thus supplying a buffer to thermal and chemical gradients. This also puts the heating away from the aging cell as the heat tracing is then installed on the reservoir tank thereby also reducing thermal gradients. Liquid sampling can be done in the reservoir tank without disturbing the experiment. Evaporative losses can also be easily checked and topped up as needed utilizing the open vent; the frequency of fluid replenishment is also greatly extended compared with the earlier design.

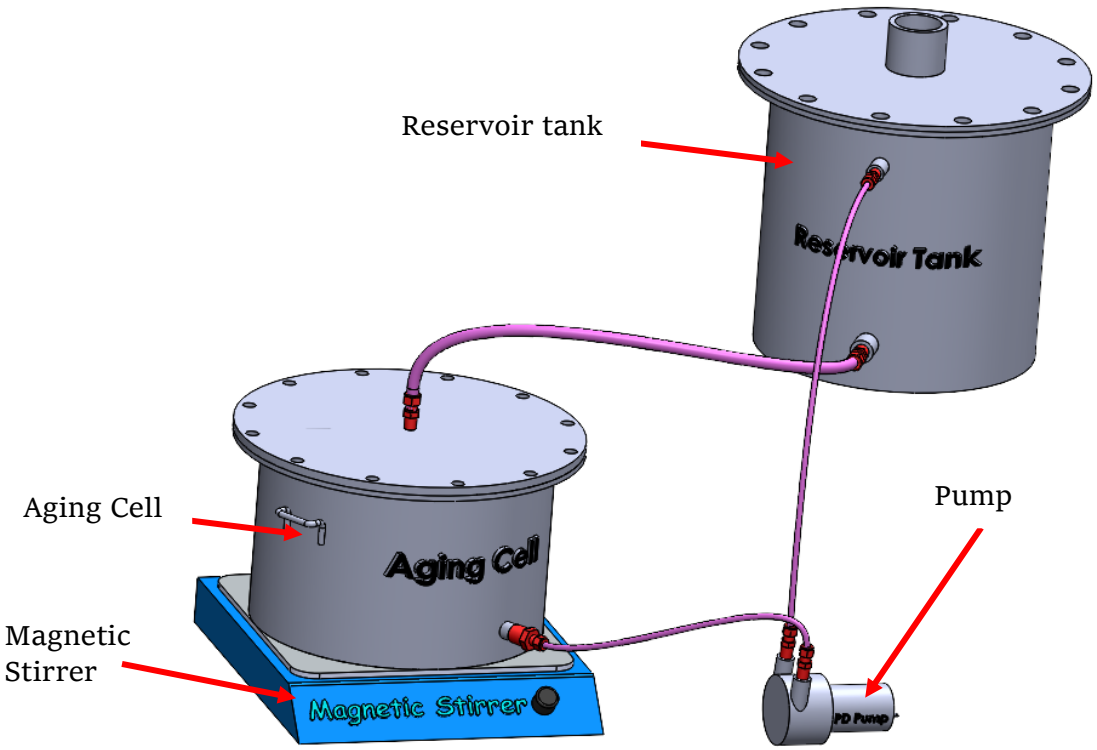

Figure 21: Initial aging design setup

The carousel from Figure 20 is placed inside of the aging cell as shown below in Figure 22. The magnetic stir bar is situated at the bottom center of the carousel with the intention to provide extra mixing to help eliminate any stagnant regions from forming. The outlet of the aging cell is positioned just above the bottom plate of the carousel as shown in Figure 22. The inlet is positioned directly above the magnetic stir bar in the hole at the top of the carousel in Figure 22. The magnetic stirrer can also double up as a secondary heat source to help mitigate issues with failures causing interruption of the primary heat source from the reservoir tank.

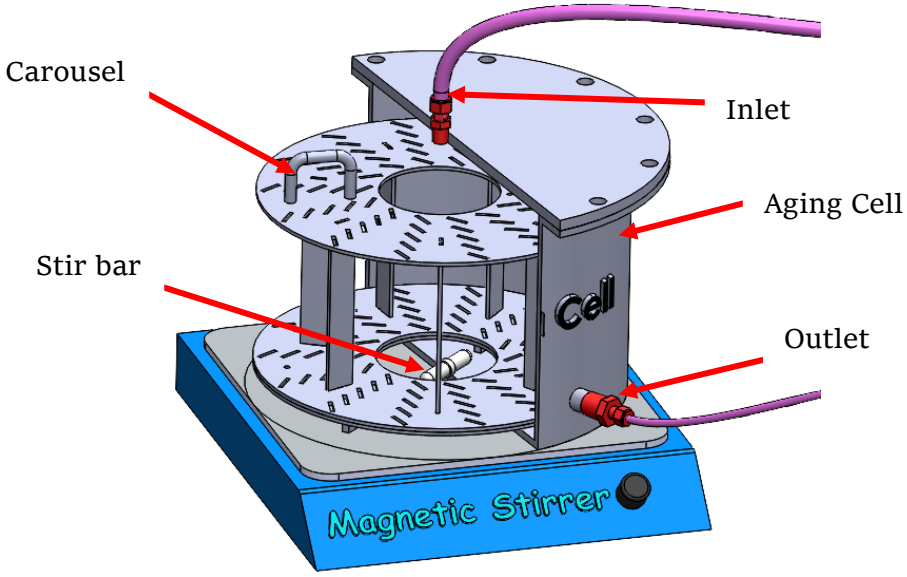

Figure 22: Close up view of aging cell showing carousel

The reservoir tank is designed with a large open vent situated at the top center of the vessel as shown in Figure 23. This serves to meet exemption for adequately vented pressure vessels under section 5.4 in AB-516 due to the reservoir tank being heated to >65°C and requiring a PSV if no adequately sized vent is present [56]. The inlet of the reservoir tank is situated near the top to be above the expected water level of the reservoir tank. The tank itself would be situated above the aging cell to provide a positive pressure head and ensure the aging cell is always water full as shown in Figure 21. The outlet of the reservoir tank is located slightly above the bottom of the tank to allow for any debris to be accumulated within the tank instead of flowing into the aging cell.

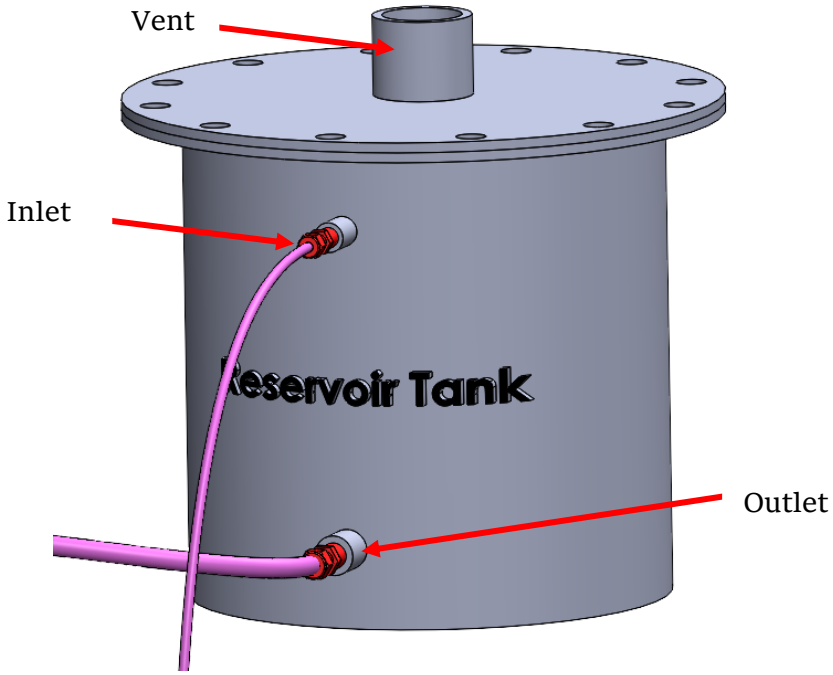

Figure 23: Close up view of reservoir tank

When compared with the industry partners' existing pipe setup for the aging of tensile test coupons, similar advantages can also be seen such as better management of thermal gradients and spacing to ensure even aging of coupons; the ability to extract fluid and tensile test coupons without disturbing the experiment; circulation of fluid compared with previous stagnant conditions; and accommodation of all test coupons within one aging cell. With the earlier pipe design, the industry partner had a limited diameter and length of pipe that could be accommodated which then limited the number of coupons. They would need multiple pipe spools to accommodate all 50 test coupons, and this was also noted as another source of potential error as there may be small differences with each setup. The overall safety of the design was also increased as the pipe spool setup had no overpressure protection in the event of overheating or localized boiling, whereas the proposed design has an open-air vent preventing any accumulation of pressure or vapors.

3.3.2 Design Changes

After much discussion with our industry partner, it was decided that both an acrylic and stainless steel setup would be fabricated. The main reason to go with acrylic was due to the cost and optical clarity it provided allowing for visual dye testing to be done to confirm flow paths and see underlying issues with any low flow regions. The stainless steel setup was needed because the industry partner's design specification requires testing with more severe conditions (such as utilizing hydrocarbon solvents) and the acrylic materials would not withstand the attack from the process conditions. The cost difference between the setups would be almost an order of magnitude owing to the cost of materials and labor differences; the acrylic can be fabricated in-house without the need for skilled tradesmen, unlike the welding and rolling of stainless steel. The lead time was also greatly shortened as the materials are all readily available locally, while the stainless steel materials would need to be ordered and fabrication labor to be contracted out.

Below in Figure 24 is the fabricated acrylic carousel with a few tensile test coupons. There were a few design changes made for ease of fabrication, for example, the handles were originally designed to be fabricated from a piece of round bar and this revised design had the handles flatted so they could be fabricated with a laser cutter. There were also holes added on the middle supports that hold the top and bottom slotted disks, these holes are there to provide support for a pin to securely position the disks. Without this pin the disks would be free to float if air bubbles were trapped below them; this occurred once before during initial testing and has led to all the tensile test coupons falling into the center of the aging cell when the tank was being filled. This stresses the importance of trialing and testing the setups before actual experiments are performed or mass manufacturing.

For general arrangement drawings of the acrylic setup please see Appendix B – Acrylic Aging Vessel and Appendix C – Acrylic Carousel.

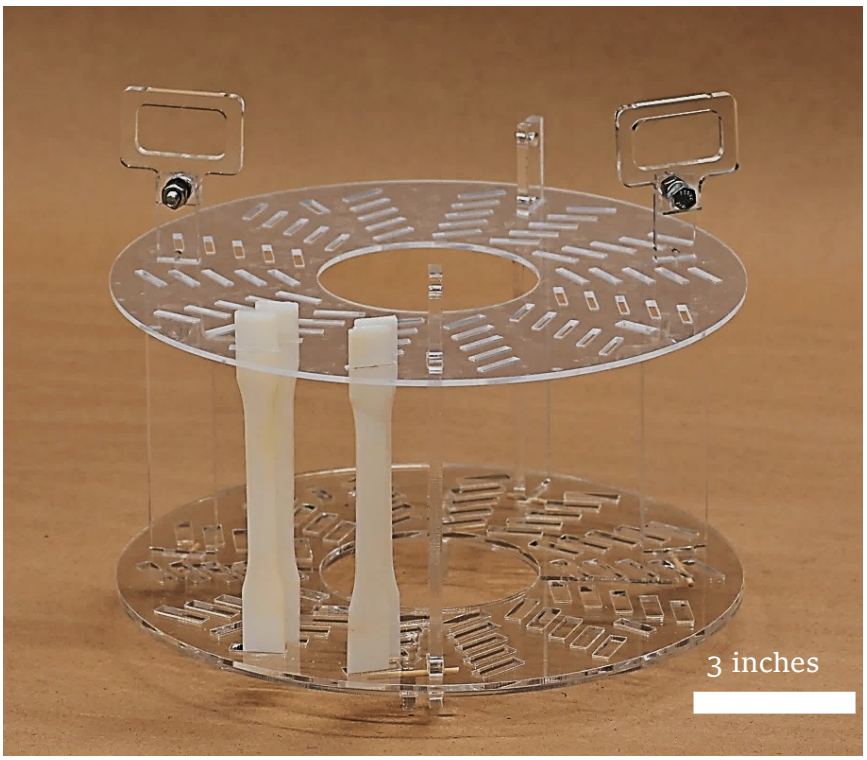

Figure 24: Acrylic carousel

Insulation was also added to the aging cell to help minimize gradients as shown in Figure 25. Half-inch polystyrene insulation was cut into rectangular slats and taped together similar in fashion to how wooden barrels are constructed. The lids' half-inch polystyrene insulation would be added in the future. This method of securing the insulation would have the added benefit of being easily removable to view the aging process during the duration of the experiments. If the heat losses were found to be very high to the point that the setup has trouble minimizing gradients, then additional insulation would be added. The acrylic pieces were attached using solvent welding with DCM.

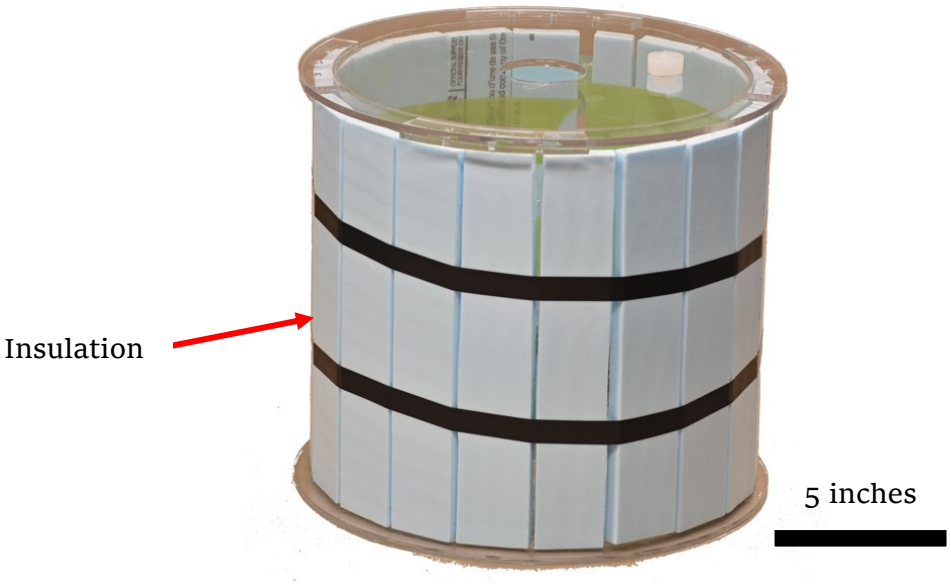

Figure 25: Acrylic aging cell with insulation

The design was then further simplified with the removal of the reservoir tank and pump. An immersion-style sous vide heater (immersion heater, Inkbird, Shenzhen, China) used in the food industry was instead placed into the aging cell in place of heat tracing as shown in Figure 26 without insulation. The open vent on the reservoir tank was then replaced by a makeshift pressure relief valve (PSV) which was created by plugging a hole in the lid with a silicone plug that has a slight interference fit. This has the added benefit of minimizing evaporative losses and offering overpressure protection while still being low-cost to manufacture. The silicone plug was custom-made by 3D printing a mold and utilizing household silicone caulking. The PSV was not necessary for the acrylic lid as it doesn't have a tight sealing flanged connection like the stainless steel version. However, the hole in the lid was still useful for accessing the tank without removing the lid.

Figure 26: Acrylic aging cell and carousel with sous vide heater

The sous vide heater shown in Figure 27 was utilized in both the acrylic and stainless steel aging cells. It has the benefit of being more cost-effective than heat tracing with a controller. The sous vide heater has built-in safety systems that standard consumer-grade electrical devices would require such as protection from running dry; where if the water level falls below the minimum level shown at the bottom of Figure 27 then the power will automatically be cut off preventing the heating element from overheating or boiling dry. The metal casing around the heating element is grounded; this would help to prevent electrocution in the event of a short in the electrical system by causing a trip in the breaker. There is also a resistance temperature detector (RTD) within the metal shroud, shown in Figure 28, which is used to control the fluid temperature to hit the control set point. Most of the wetted parts in the sous vide heater are made from 304 stainless steel which, as shown in section 3.1.4, is acceptable for our range of process conditions. It is noted that brine may cause an issue with prolonged exposure, however with the low cost of the unit, this was noted as an acceptable risk. In the event of sous vide heater failure the device would be replaced during the next working day with a spare sous vide heater; the as found temperature and time of interruption would be noted for data collection purposes. An open impeller centripetal pump is also included with the sous vide heater to provide mixing. The impeller is shown on the right of Figure 28 and the pump casing is shown in Figure 29. The casing has two openings for the outlet spaced approximately 120^{o} apart; this is an unusual design as most centripetal pump designs have casings with only one outlet opening. Hydrocarbon solvents are also not suitable for this device as the included motor for mixing has exposed contacts and would possibly provide a source of ignition for flammable vapors.

Figure 27: Sous vide heater with ruler for scale

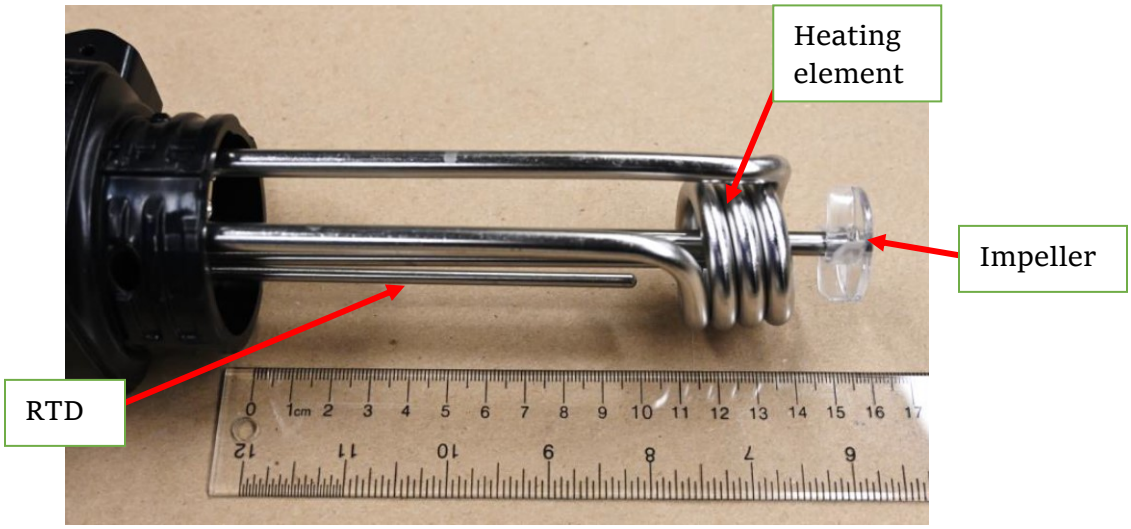

Figure 28: Inside of sous vide heater showing the RTD, heating element and open style impeller

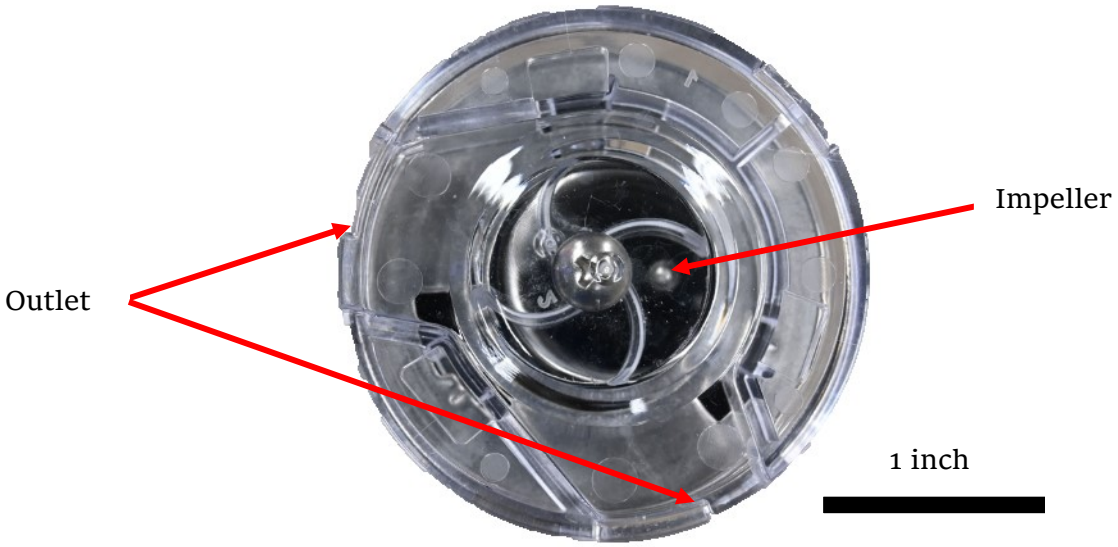

Figure 29: Bottom of sous vide heater showing the plastic centripetal pump casing with two outlets

The centripetal pump design in the sous vide heater functions by drawing liquids in through the 5 rounded rectangular slits cut into the metal shroud shown in Figure 27 and past the heating elements before being expelled through one of the two outlets. A visual representation can be seen below in Figure 30, where a green dye was added around one of the rounded inlet slits and visually shows the plume of dye being expelled out of the outlet. The need for mechanical means of flow in the design is due to the sous vide heaters' element being placed near the top of the container of liquid. Normally the immersion heating elements are located near the bottom of the vessel to allow for natural convection currents to circulate the fluid flow due to the hot water being slightly less dense than the surrounding cold water. However, in this case, the heating element is intended to be placed near the top of the vessel and thus would need the added centripetal pump to help provide adequate flow and mixing. Otherwise, there may be a large thermal gradient formed in the vessel due to inadequate mixing.

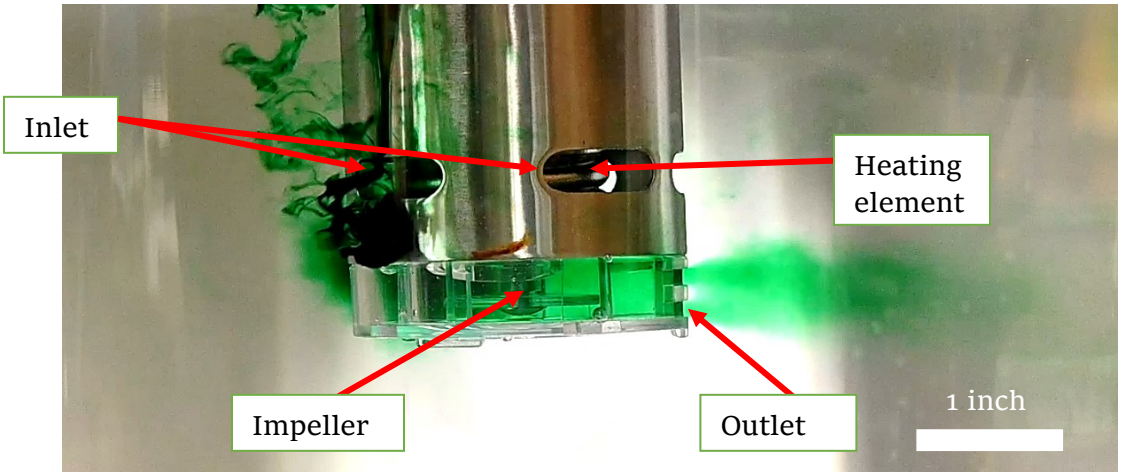

Figure 30: Sous vide heater with dye showing the flow path

The sous vide heater used has an effective heating power rating of 1000W, so it would be expected that the actual power consumption would be marginally greater than this owing to the extra power consumed by the controller. A power meter built into an uninterruptible power supply (uninterruptible power supply battery backup, APC, Manila, Philippines) was used to measure the power consumption to determine the following information: standby power 1W; Stirring power consumption 12-13W; peak heating power 890W. The manufacturer of the power meter used in this measurement does not publish the accuracy or error of the device. This power measurement data shows the devices' actual heating power was lower than the manufacturers' claim of 1000W of heating power. This is important to note as the advertised rating was 1000W of heating and the experiment may have needed the full rating to ensure adequate heating is available.

The sous vide heater power consumption during a heating cycle was metered and it provided insight into the control logic of the device. Figure 31 shows the metered power consumption over time when the aging vessel experiences a temperature change. The temperature drop was created artificially by the addition of cold water into the vessel to promote an exaggerated response from the heater. Initially, it was hypothesized that the sous vide heater would have a thermal switch due to it being a lower-cost alternative to a feedback control system. However, Figure 31 shows the response is not that of a simple thermal switch but instead a thermal gradient-based power consumption response; also known as a proportional integral derivative controller. The steady-state power consumption was also metered and supports the same observation due to the random frequency and power levels to maintain a steady state. The power levels and heating frequency appear to increase with increased heat loss of the setup. This control logic helps to provide better thermal control when compared with just a heating element with a thermal switch similar to what an electrical kettle would have. For an electrical kettle, once the thermal set point is reached and the thermal switch activates; there

is excessive boiling afterward. If it wasn't for the set point being at the boiling point of water, this setup would overshoot the target temperature set point after the thermal switch activated due to residual heat from the heating element. For the sous vide heater, since it has a throttled power response depending on the thermal gradients; it would reduce the excess thermal gradient between the heating element and vessel as the temperature nears the set point. Thus reducing the amount it would overshoot the set point by. In the same manner, maintaining the steady state temperature using a lower heating power would help to minimize the same overshooting effect.

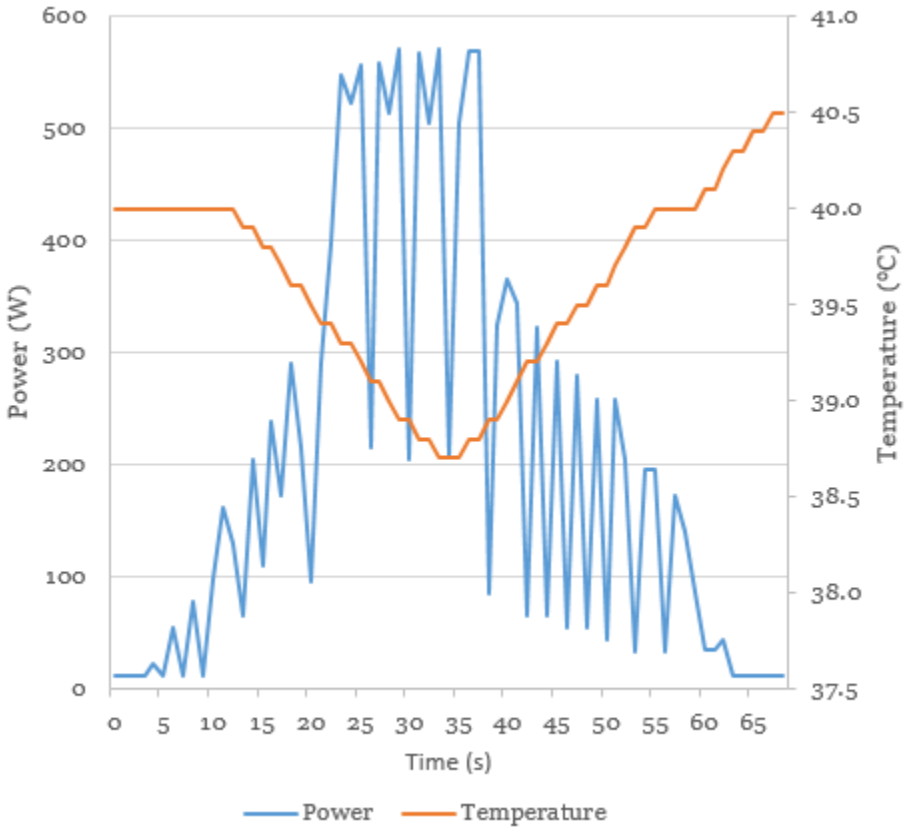

Figure 31: Sous vide heater power consumption to counteract a temperature change

Figure 32 shows the stainless steel carousel with a few tensile test coupons. This version of the carousel has a few distinct design differences compared with the acrylic version in Figure 24. The handles are located away from the support columns in the stainless steel version, whereas the acrylic version has them located on the supports due to the better load-bearing location. The acrylic top plates are greatly weakened with all the slits and resultant stress concentrations, whereas the stainless material has much higher stiffness and strength. The supports themselves have also been redesigned to allow for height adjustments on the stainless steel carousel. The slits on the carousels' top and bottom plates were also widened. This is to accommodate various sizes of tensile test coupons per the industry partner's request, as they intend to adapt this setup for other tensile test coupons.

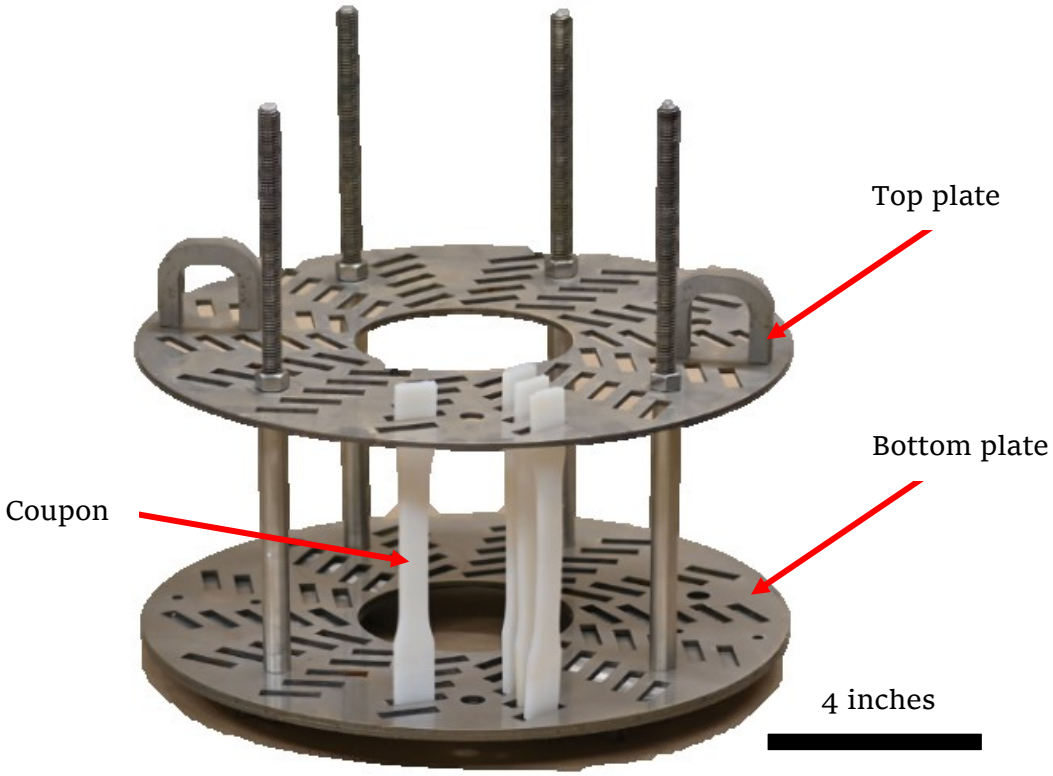

Figure 32: Stainless steel carousel

The stainless steel aging cell height was also raised to accommodate the taller threaded rods of the carousel. This led to the lid being redesigned to place the sous vide heater at the same level as the acrylic setup to get the same flow and mixing characteristics. The redesigned stainless steel lid has a box to situate the sous vide lower as shown in Figure 33. It was noted that the new design height requirement does not mean the liquid level can be increased accordingly due to the maximum water level limitations on the existing sous vide heater as it is not a waterproof unit. However, this limitation can be overcome by selecting a different sous vide heater in the future. The tank insulation was done in the same manner as the acrylic setup shown in Figure 26, Figure 34 shows insulation on the stainless steel tank.

For general arrangement drawings of the stainless steel setup please see Appendix D – Metal Aging Vessel and Appendix E – Metal Carousel.

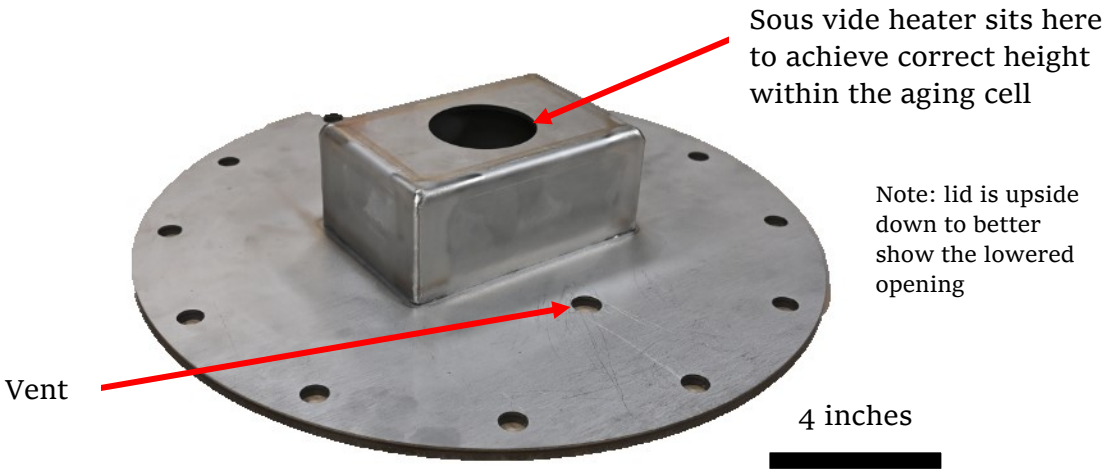

Figure 33: Stainless steel aging cell lid

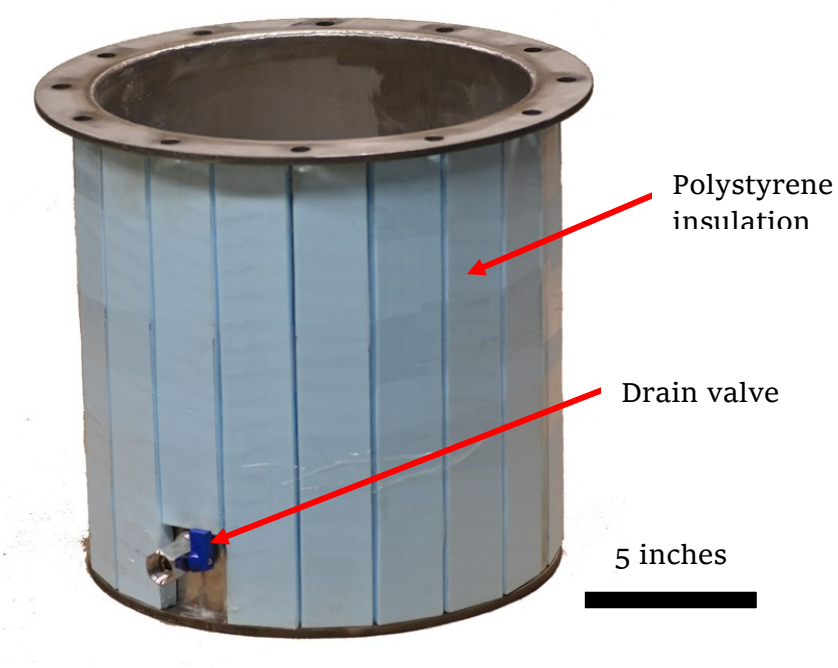

Figure 34: Stainless steel aging cell with insulation

3.3.3 Further Design Changes after Initial Testing

The initial trial testing was done using polymer coupons (exact material composition is proprietary to the industry partner) to see their interaction with water and gauge how well the test setup performs. The exact composition and test results of the tensile test coupons will not be investigated in this paper per the industry partner's wishes; as such this thesis will focus on generic observations which lead to the next design change. The first test was done at 80°C for 2 weeks utilizing the stainless steel aging cell setup. The polymer tensile test coupons were initially transparent and clear when placed into the aging carousel. After two weeks of aging at 80°C, these coupons became white and opaque with various degrees of deformation as shown in Figure 35 and Figure 36.

For example if the polymer was nylon based then the following could be a mechanism to explain the degradation. Nylon is well known for being hydrolyzed by water as the reaction to create nylon 6.6 ejects water at the amine bond between the hexanediamine and adipic acid building blocks [15]. The reverse reaction is also possible through the introduction of water to break the amine bond and thereby breaking the nylon polymer chains.

Large deformations in the coupons in Figure 36 were not expected as the aging temperature was set below the glass transition temperature. The degree of the deformation also varies from coupon to coupon within the carousel. This is hypothesized to be caused by the creep or annealing of the coupons. Whether this is creep can be validated by looking at the literature for this type of polymer and confirming if the temperature exceeded the threshold for creep, however, as the composition is proprietary to the industry partner this is not explored. The differences in the deformation make these coupons not suitable for tensile testing due to the various preloads required to straighten the coupons for fitting into the testing

machine. There was no further testing done on these coupons aside from the initial visual examination.

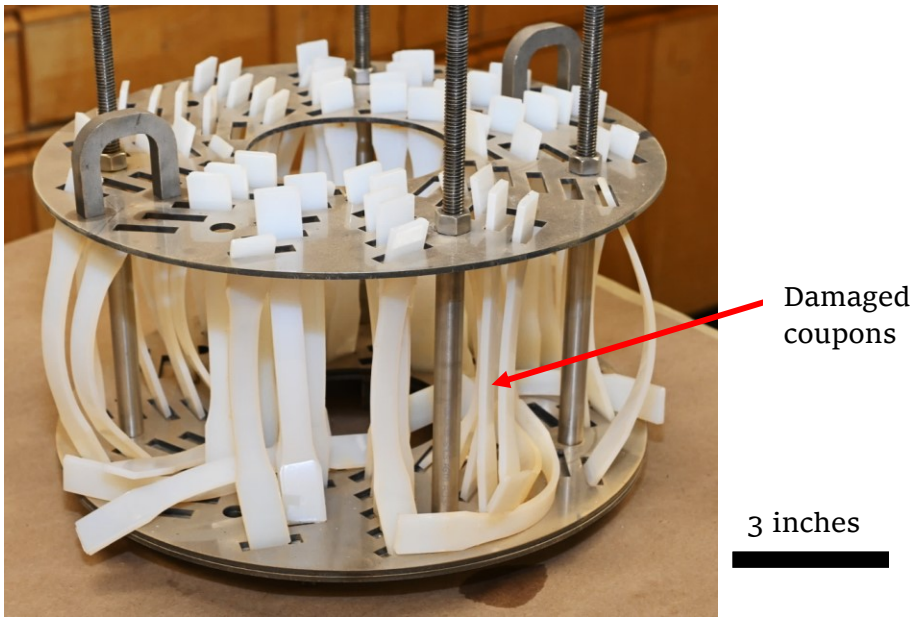

Figure 35: Carousel of damaged tensile test coupons

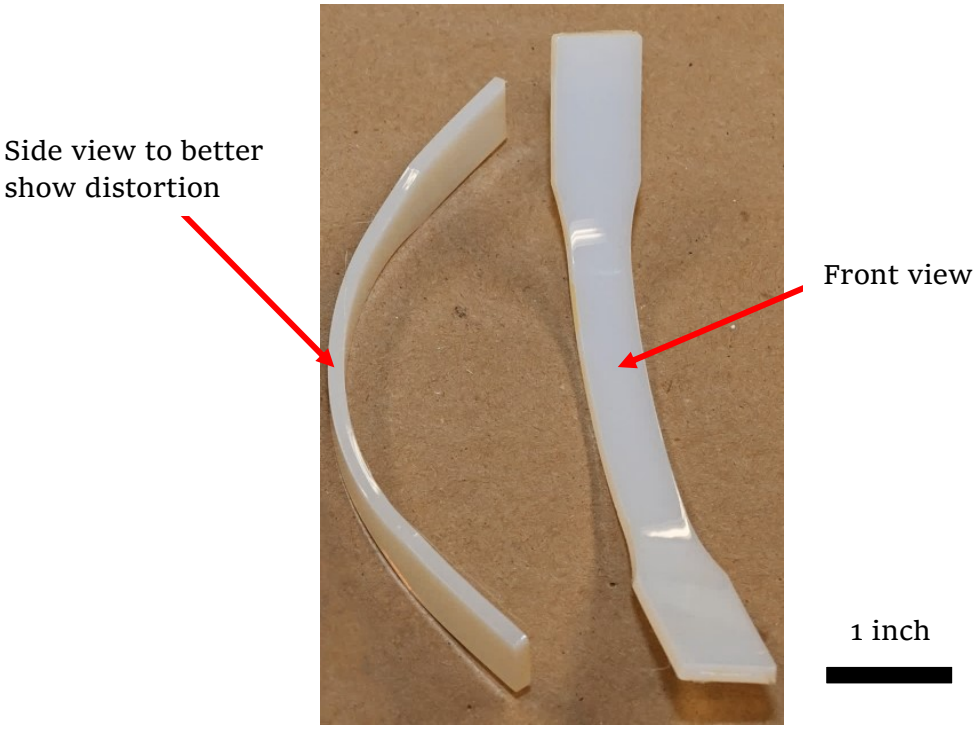

Figure 36: Close up view of damaged tensile test coupons showing the deformation

Further testing was then done using 60.0°C and 82.0°C and the visual results of these coupons are shown in Figure 37. The 60.0°C aged coupons do not appear to have visually degraded compared with the unaged coupons, while the 82°C coupons are an intermediate degradation between the previous 80.0°C and current 60.0°C coupons. The 82.0°C aged coupons showed some translucence and the deformation spread between coupons is much smaller than 80.0°C. However, the deformation is varied between coupons within each group, which is most likely explained by annealing of the coupons instead of creep. This is due to creep being impacted by same self-weight across coupons while annealing can impact them differently as it depends on the coupons' residual stresses. It is noted that it could be a combined effect of creep and annealing that is causing this deformation.

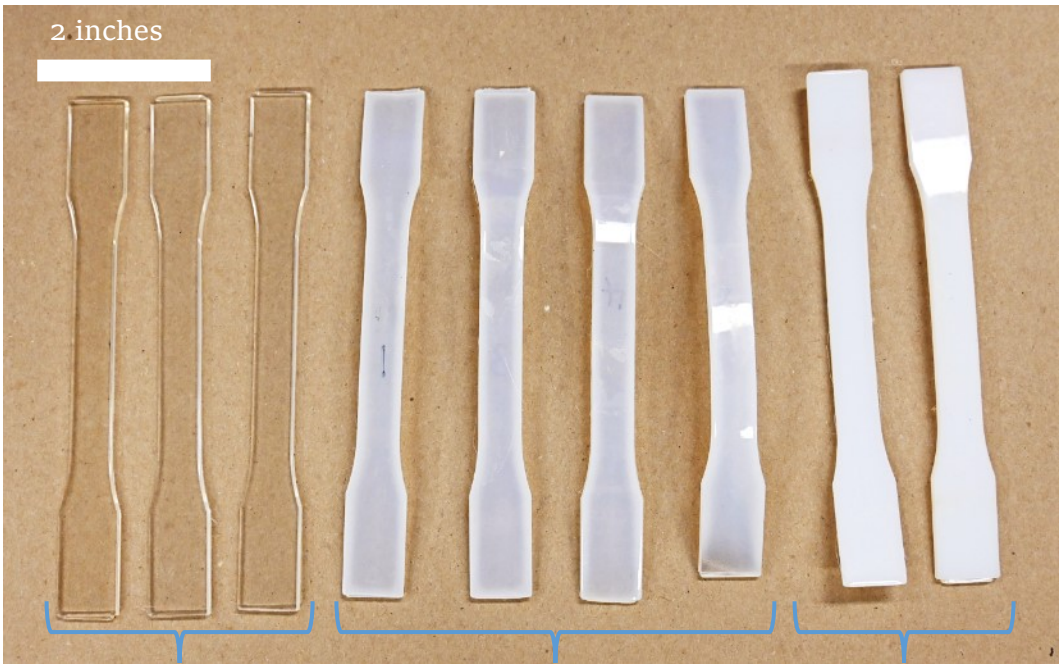

Figure 37: Polymer tensile test coupons aged at various temperatures and durations

Due to the deformation witnessed in the polymer tensile test coupons, our industry partner has requested a design change to include a middle support plate fitted halfway between the top and bottom plates of the carousel tensile test holder shown in Figure 38. The idea is the middle plate would limit the deformation of the tensile test coupons and thus allow for more accurate tensile test results of the deformed coupons.

As the Arrhenius equation is used for accelerated aging to determine the temperature dependence of the degradation; the introduction of new variables into the aging experiments would greatly complicate the analysis when a comparison is needed between unannealed coupons versus annealed coupons. The same issue would be present if other damage mechanisms occur that were not present in the other different temperature coupons.

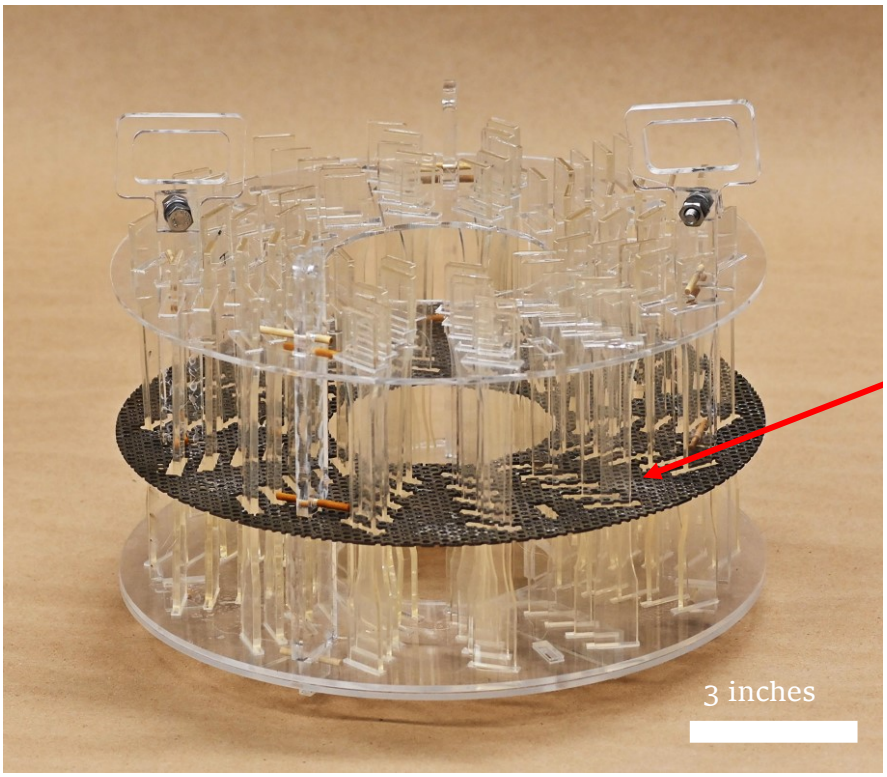

Figure 38: Acrylic carousel fitting with a stainless steel middle plate

Three different middle plate designs were fabricated as shown below in Figure 39. All three of these designs were tested with dyes to show the flow characteristics to validate the below predictions. These dye tests with the various plates will be discussed in detail in section 4.2.

The topmost plate design is a copy of the existing carousel top/bottom plates. This design was predicted to have the most detrimental effect on the existing design as it would separate the two domains within the carousel and cause two separate regions of the flow. The upper region would have a similar flow as before, with the lower region being isolated and having a much lower flow relative to the top region.

The leftmost plate in Figure 39 is an alteration of the topmost plate where skeletonized to provide areas where the flow can mix between the top and bottom regions. The term skeletonized comes from watchmaking of skeleton dial watches [57, 58]; where a standard watch is skeletonized to make all the moving parts visible by cutting as much of the watch face as possible. In this case, the middle plate is cut as much as possible to allow flow to penetrate between the upper and lower regions. This was predicted to have the best flow characteristics of the three designs. The structural integrity of this plate was noted as being sufficient but greatly weakened due to the nature of this design. Care was taken to ensure all the cut edges were rounded to minimize stress concentrations; however, the plate still physically felt very fragile during handling with a far lower stiffness compared with the topmost design.

For design drawings of the three different middle plate designs please see Appendix G – Middle Plate Designs.

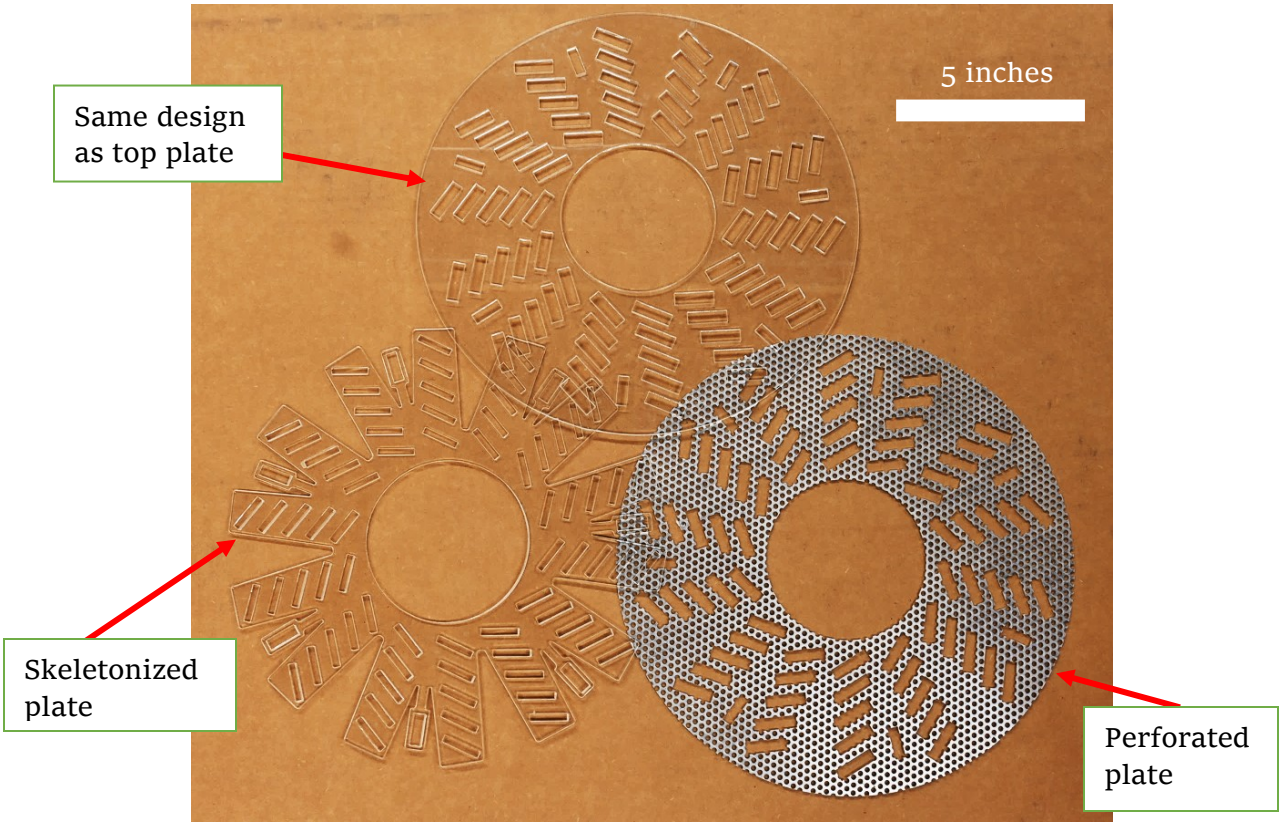

Figure 39: Various middle plate designs for the carousel

The rightmost plate in Figure 39 is an alteration of the topmost plate where perforations are added and the material has been changed to stainless steel. The material change was due to the ease of fabrication from a perforated plate and then waterjet cutting the design; where if acrylic was used then each perforation would need to be individually cut out. The perforations are predicted to allow the flow to penetrate between the two regions similar to the leftmost skeletonized design. However, a distinct difference is the skeletonized design has larger openings towards the outer diameter and gradually shrinks to no openings towards the inner diameter. This is predicted to influence the flow paths of the design compared to the carousel design without the middle plate. The perforated plate is predicted to yield the most similar flow path to the carousel design without the middle plate when compared with the other middle plate designs. The perforated plate also has more structural stiffness compared with the skeletonized plate owing to both

the design and change in materials. However, a possible issue with the perforated design is the random sharp edges that occur as a result of cutting the slits through the perforations. This can cause potential damage to the tensile test coupons in the form of scratches that can cause unwanted stress concentrations along the gauge length. Scratches can likely occur from either handling or the turbulence of the flow due to the sous vide heater and the enlarged slits. Several different ideas were contemplated regarding how to eliminate this risk from the sharp edges, such as: manually filing down the sharp edges; taping the sharp edges, and coating the sharp edges with rubberized paint.

3.3.4 Discussion of the Jar Design Change

A question was posed by the industry partner over the use of 2L glass mason jars instead of the carousel design for aging. The use of mason jars would adjust the main test parameter to become hydrostatic aging due to the lack of mechanical flow within the jars when compared with the carousel design. However, it will not be zero flow within the jars as there will be natural convection from the small temperature differences around the jar. As a result of this change the aging would then become stagnant.

With the new proposed jar method, multiple aging scenarios can be performed simultaneously within the same aging vessel while the carousel design cannot accommodate this. A different aging fluid can be utilized within each jar, thereby allowing the same material to be aged in different fluids within the same vessel all at the same time. Also different coupon types can be aged simultaneously when placed in different jars; as aging them together within one carousel poses the risk of cross contamination from their leached chemicals. As the mason jars would be in the same vessel, the aging temperature would need to be the same between the jars within the same vessel. However, the aging vessel fluid can be replaced with another fluid such as tap water when aging with other fluids such as hydrocarbon solvents.

This would reduce the cost and improve the safety as the amount of volatile solvents and their potential fumes around the surrounding environment would be decreased. It should also be noted that the current setup with the carousel design cannot accommodate flammable solvents as the setup electronics are rated only for general area classification and not the required flammable area classification. This would be another advantage with the jar method as it would be a cheap modification to allow aging with hydrocarbon solvents.

The mason jar themselves would also be a potential source of safety or contamination issues. For safety, the mason jars would need added handling when compared with the carousel. As sample removal would require the removal of the jar first, whereas the carousel allowed direct removal of the coupons from the aging vessel and the vent holes allowed for a fluid sample to be taken directly. The jars would also be hot and the extra handling (from removal of the jars to opening/closing the lids) could pose safety hazards from thermal burns due to either contacting the hot glass or accidental fluid spillage. The glass jars could also be subjected to thermal stress during handling outside of the aging vessel and pose a risk of shattering. The time of the jar spent outside the aging vessel would also allow the fluid to slowly cool down, as such it should be minimized; however, rushing to obtain the coupon/fluid samples could pose to be dangerous as the risk for accidents would increase with rushing. Proper personal protective equipment and operating procedures would also need to be utilized to minimize the potential safety hazard created from added handling of the jars.

The jars' lids have a rubber gasket seal which may not be rated for handling hydrocarbon solvents, so further investigation should be done to determine whether the lids would be compatible with the various solvents. As the jars are intended for storage of food, the manufacturer has no information regarding the compatibility with different hydrocarbon solvents.

For contamination issues, the jar themselves would leach some ions into the aging solution. Glass leaches ions such as sodium and silicon into deionized water [59]. If the coupons or fibers aged leaches the same ions or are impacted by them, then the aging inside of the glass containers are not ideal. The issue with them leaching the same ions is that fluid samples are taken for analysis to determine the number of leached chemicals/ions to determine the amount of leachate from the degradation; so, when they leach the same ions/chemicals then the amount leached from the test samples would not be able to be differentiated. For example, when glass fibers are aged in glass jars; the leached chemicals/ions would be very similar and cloud that part of the analysis. Another issue is the lid of the jars, as they are made from coated carbon steel. This can rust easily and provide another source of contamination by either leakage or contaminating the aging solution with corrosion products. For contamination of the aging fluid, that can occur when the lids rust sufficiently to become compromised and leak. That would mean the aging fluid within the jar is exposed to the fluid within the aging vessel, which could be a different fluid (like water compared with hydrocarbon solvent within the jar). This can also have an impact on the experiments and is not desired.

Below in Figure 40, it is shown how the lids of the jars rust when being exposed to hot water for two weeks in the aging vessel and contaminate the aging fluid and samples with corrosion products. The corrosion products visually discolored the test coupons slightly. Overall, rust contamination of the aging fluid is not desirable as it is another variable that may impact the test results.

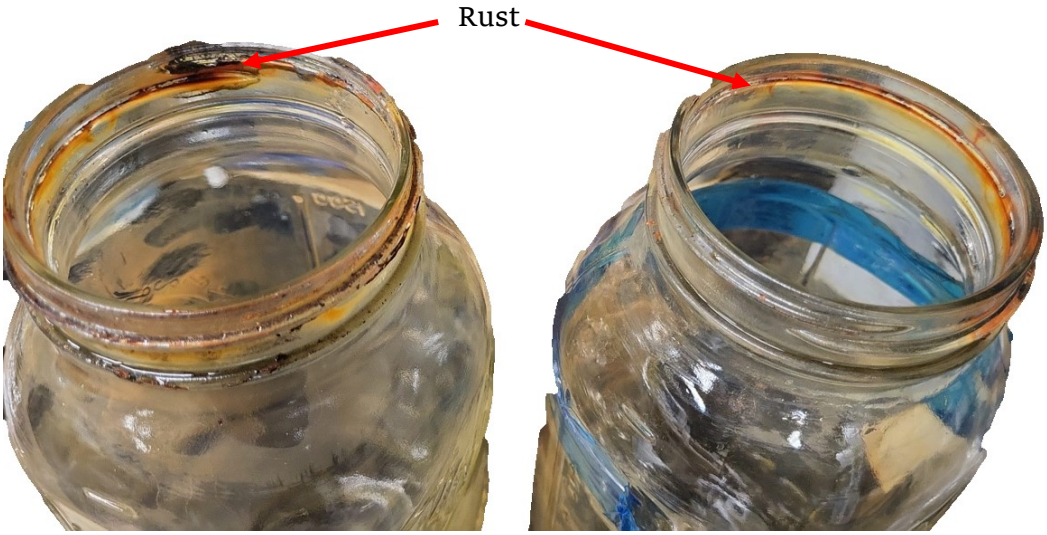

Figure 40: Rust on mason jars after 2 weeks of aging

To mitigate these impacts of rusting and possible leakage from the jars; a few changes to the aging setup would need to be introduced. The lid material for the jars should be changed, if possible, to a material that is inert relative to the aging environment, such as stainless steel. If not, then a buffer should be added to prevent the corrosion products or fluid leakage from entering the jar during aging, such as placing a sheet of plastic between the lid and the glass jar to act as a barrier. The current employed method to mitigate this contamination risk is the frequent changing (every week) of the aging fluid along with the jar. This method has its own issues, primarily that there is an increase in handing of the jars and the aging fluid is refreshed each time. The increased handling to change the jars and fluid poses an increased safety risk as there is more exposure potential to our staff. The weekly fluid change doesn't eliminate the corrosion products but rather prevents them from accumulating. It also subjects the coupons to some cooling while it is being swapped; however, this is minor as the timeframe is short relative to the aging time. The fluid change also changes the concentration of the other leached ions/chemicals by being refreshed; this allows the fluid to once again leach out more of the ions/chemicals and could impact the overall aging study

when compared with other closed loop systems where the fluid can reach saturation and cannot leach out more ions/chemicals.

For RTP, the process conditions seen in the three layers are different. The innermost layer of the RTP would see flow conditions most similar to the ones in the aging carousel with the flow from the sous vide heater; as that layer is exposed to the process conditions of fluid flow. The middle layer would see nearly stagnant conditions most similar to the jar method as the fluid would be trapped in the thin layer without much movement. The outermost layer would see natural conditions in the surrounding ground where the pipe is buried. Therefore, testing with both the jar method and the carousel design would provide insight between the stagnant and flow conditions for aging.

The main advantage of pursuing this change with mason jars instead of the carousel design was due to the cost and time constraints. There are a large number of scenarios that needed to be tested with the existing design and limited fixtures; this would mean either fabrication of more aging fixtures/vessels to run all the experiments in parallel and/or having to run the experiments back-to-back, increasing the time needed. Both of these options were less desirable outcomes when compared with swapping the carousel to jars. Changing to the jar method was seen as an easy win by the industry partner due to the above limitations.

As the proposed design change does not have a mechanism to space out the coupons; the bundle of tensile test coupons would be contacting one another. This impacts the amount of the coupons' surface area exposed to the fluid within the jar and could have an impact on the uniformity of coupon aging. The addition of any spacers to help evenly distribute the tensile test coupons within the jars was strongly opposed by the industry partner as the space was limited with the current setup utilizing jars and the addition of spacers would further limit the maximum number of tensile test coupons one setup can accommodate. The extra handling of the hot jars to remove coupons and test

or change the jars' fluids was also noted as an increased safety risk when compared with the carousel setup.

Another advantage of the jar method is that the jars are in their own domain, which means the fluid flow is not transferred between these domains. Our industry partner's main concern with the carousel or other aging methods was that the CFD results revealed how there were velocity gradients around the aging cell and perceived this variable as a potential risk in the homogeneity of the aging results. Utilizing the jar method eliminates this velocity gradient and uses the aging cell's fluid as a buffer to temperature gradients. By minimizing the temperature gradients within the jar, any natural convection-based velocity gradients would also be minimized.

3.4 Design Discussion – Fiber Aging Fixture

This section will cover the initial testing done with the selected fiber aging fixture and the future works of this design path. The future work done on the fiber aging fixture will be published by another researcher so will not be discussed in depth here.

3.4.1 Initial Tests

The fabricated prototypes of design G were initially tested without aging to determine if the tensile testing of the fibers would provide repeatable results. If they provided repeatable results then aging before testing would proceed next. However, initial results showed that the breakage occurs sometimes near the bolts shown in Figure 41 and other times in the gauge length providing a repeatable but significantly lower breaking strength compared with reference methods.

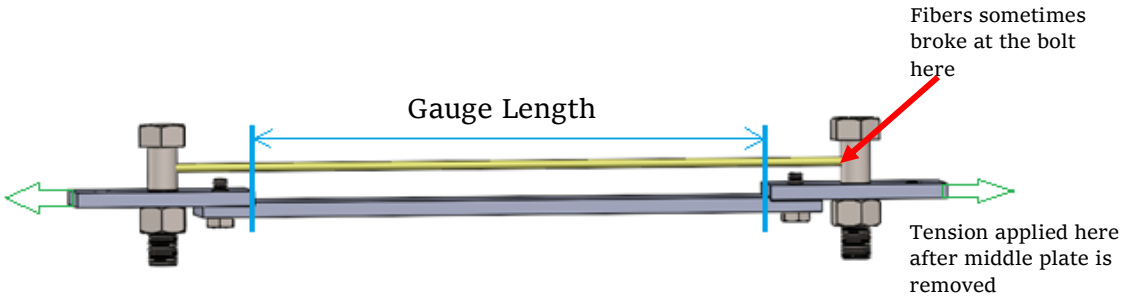

Figure 41: Design G fiber aging fixture location of breakage during initial testing

Due to this discovery, there were several iterations of changes attempting to remedy both issues. Changes to the wrapping method were explored such as: adding glues to the fibers around the shank on the bolt; changing the bolts from fully threaded as shown in the top design of Figure 42 to the shoulder bolt design in the bottom of the same figure; adding a washer to sandwich the fiber to reduce stress concentrations; drilling a hole in the shank to secure the fibers in position as shown in the bottom design in Figure 42B; increasing

the diameter of the bolt shank; and applying a preload to the fibers before testing to eliminate any stress concentrations caused by the zipper effect.

After performing the above iterations, the fibers were still failing at significantly lower breaking strengths compared with the reference methods. The results were repeatable and the possibility of a bad batch of fibers was ruled out due to the breaking strength corresponding with the reference values when tested with another method. The true cause of the lower breaking strength was not investigated further as efforts were focused on the second highest-ranked design E instead.

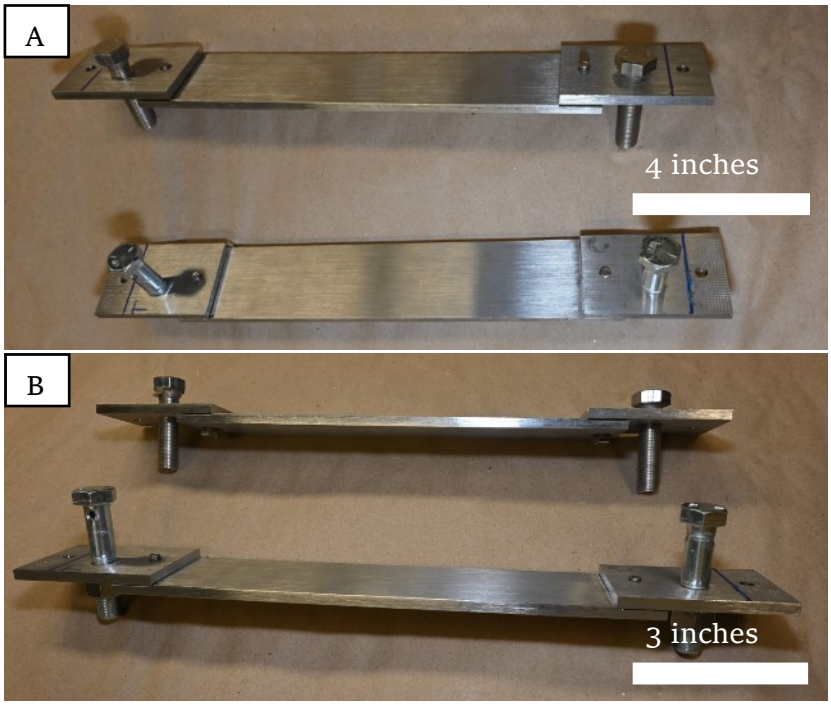

Figure 42: Design G fiber aging fixtures: (A) top view of fixtures, (B) side view of fixtures

3.4.2 Updated Design

After switching to design E instead of further developing design G, a single modification was made to have fibers in a single direction instead of in both the horizontal and vertical directions. As such the number of holes cut into the frame was also decreased by half. This was essentially the same as the industry partner's existing testing method aside from the welded nature of their frame. See below in Figure 43 for the difference between the original and modified design. Further discussion and testing of design E will not be explored in this paper since another researcher will be performing those tests and publishing those results.

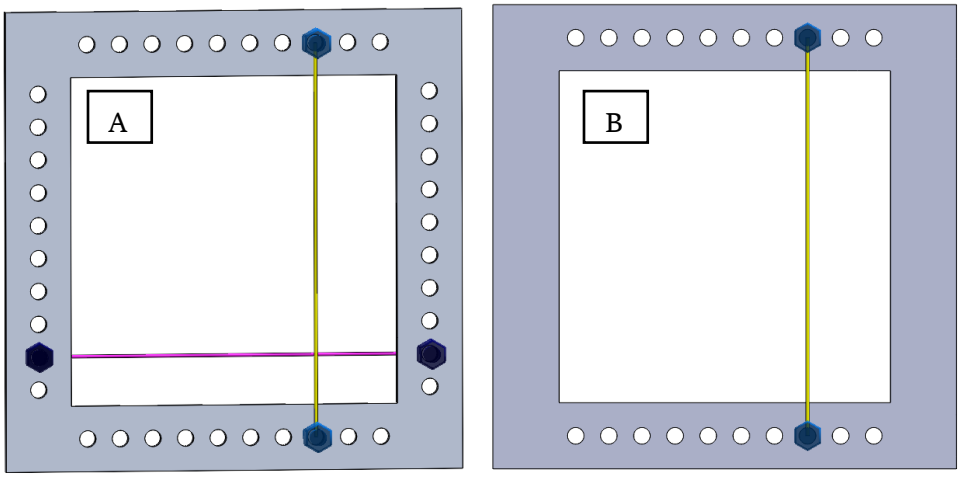

Figure 43: Design E concept of a fiber aging fixture: (A) original concept, (B) updated concept

4 Design Validation and Discussion – Tensile Test Coupon Aging Cell

This section encompasses all the design validation done on the tensile test coupon aging cell prior to the setup being deemed ready for starting the aging trials. Validation performed includes heat loss to verify the sous vide heater sizing; dye mixing and CFD analysis to minimize the number of low flow or stagnant areas; and steady-state temperature measurements to measure the gradients around the aging carousel.

4.1 Heat Loss

The heat loss of the aging cell setup was calculated by first principles and then validated using temperature measurements by allowing the setup to cool down over a period of time. The heat loss validation with temperature measurements was done at three different temperatures as the convection coefficient varies with temperature.

4.1.1 Heat Loss Calculation

One of the main objectives for thermal aging studies was determining how to maintain the correct temperature and in doing so we must first determine the heat loss of the setup.

The following assumptions were made to calculate the heat loss of the acrylic aging cell:

- Heat transfer was assumed to be uniform in each of the two unique singular directions (vertical and radial) and at steady-state conditions.
- No localized thermal gradient effects were considered.
- Losses related to the top and bottom flanges of the aging cell were assumed to be negligible.
- Materials were assumed to have homogenous properties.
- Radiation losses were assumed to be negligible.

The three-dimensional heat loss problem was simplified into three separate one-dimensional heat flux calculations to approximate the overall heat loss of the setup. Figure 44 shows the 3D model of the idealized acrylic aging cell for this heat loss calculation. The section view reference in Figure 44 is shown in Figure 45. In both figures the different materials are color coded as follows:

- Cyan is the acrylic
    - Thermal conductivity k = 0.19 W/m·°C [60]
- Light green is the polystyrene insulation
    - Thermal conductivity k = 0.014 W/m·°C [61]
- Light brown with a grain texture is the plywood of the table
    - Thermal conductivity k = 0.83 W/m·°C [62]

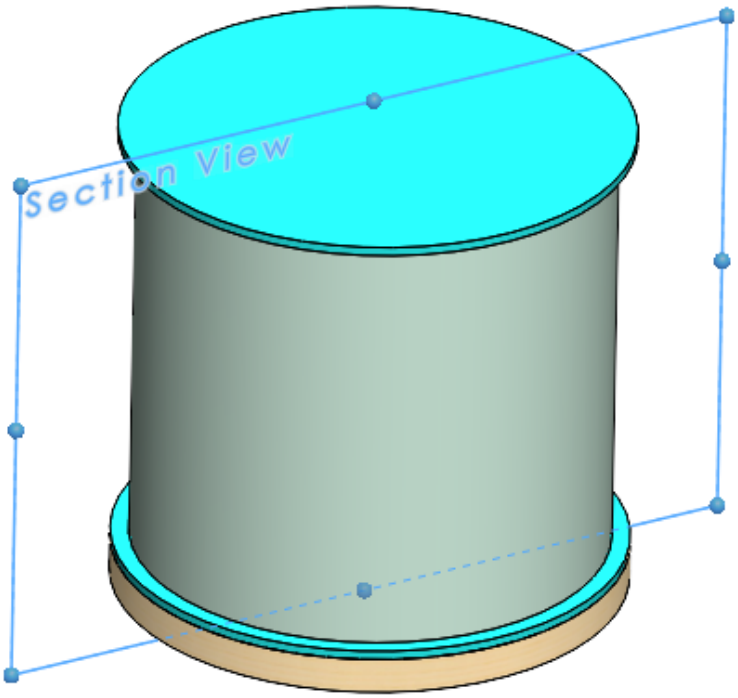

Figure 44: 3D view of aging cell for heat loss calculation

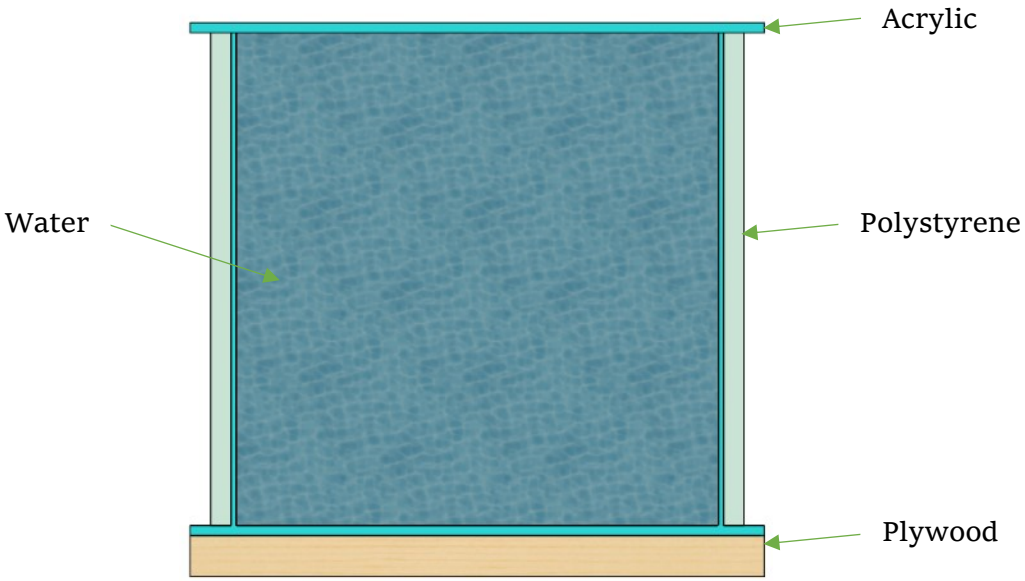

Figure 45: Cross section of aging cell for heat loss calculation

The below heat flux equations are taken from Cengel [63]. Each direction of the total heat flux in the aging cell can be calculated by a simple summation of the individual components of heat flux below (1).

$$Q_{\text{Loss}} = Q_{\text{cond}} + Q_{\text{conv}} + Q_{\text{rad}} \quad (1)$$

Where Q_{Loss} is the total heat flux and the other components are conduction Q_{cond}, convection Q_{conv}, and radiation Q_{rad}.

$$Q_{\text{cond}} = kA_s \frac{T_1 - T_2}{L} \quad (2)$$

Conduction (2) is dependent on the material thermal conductivity k through the thickness of the plane L and across the surface A_s. It is also linearly dependent on the temperature difference presented as T_1-T_2 in (2). This equation is derived from Fourier's Law of Heat Conduction. The separate values of k used for the calculation are shown previously with the materials.

$$Q_{\text{conv}} = hA_s(T_{\text{surface}} - T_\infty) \quad (3)$$

Convection (3) takes on a very similar form to (2) for conduction but without being dependent upon the thickness as it is a boundary effect of the heat transfer between a solid and fluid interface. Therefore, the variable h in (3) represents the convection heat transfer coefficient between these two mediums. Equation (3) is sometimes referred to as Newton's Law of Cooling. It should be noted that for this heat loss calculation, the convection on both the inner and outer surfaces is considered to be free convection. While in operation the inner surface is forced convection due to the immersion heater's built-in pump circulating the fluid. The reason for assuming free convection on the inner surface is due to the comparison later with validating the heat loss of the aging cell where the heater is unplugged thus causing the forced circulation to be stopped. The values of h chosen were from Cengel's book with h_{air} having a range of 2 to 25 W/(m^2·^{o}C) and a value of 5 W/(m^2·^{o}C) was chosen; h_{water} having a range of 10 to 1000 W/(m^2·^{o}C) and a value of 50 W/(m^2·^{o}C) was chosen [63]. These chosen values for the heat transfer coefficient were estimated to compute the total heat flux and in the next section will be compared with the measured total heat loss. The important thing to note here is the range of possible heat flux values that can be obtained with the varying heat transfer coefficients.

$$Q_{rad}=\varepsilon\sigma A_s(T_{surface}{}^4-T_\infty{}^4) \tag{4}$$

Thermal radiation (4) losses occur as photons are given off from the surface into the surrounding space. This is due to the radiation emitted from the temperature of the body itself. The surface and how closely it resembles a blackbody is denoted by the variable Ɛ for emissivity. With the variable σ presenting the Stefan-Boltzmann constant. However, for our case, we will be assuming the radiation losses to be insignificant compared with the conduction and convection due to how radiation is dependent on the fourth power of temperature and with our temperatures being fairly low.

$$R_{Loss} = R_{cond} + R_{conv} + R_{rad} \tag{5}$$

$$R_{\text{cond}} = \frac{L}{kA_s} \tag{6}$$

$$R_{\text{conv}} = \frac{1}{hA_s} \tag{7}$$

$$R_{\text{rad}} = \frac{1}{h_{\text{rad}}A_s} \tag{8}$$

$$h_{\text{rad}} = \frac{Q_{\text{rad}}}{A_s(T_{\text{surface}} - T_\infty)} \tag{9}$$

$$Q_{\text{Loss}} = \frac{T_1 - T_2}{R_{\text{Loss}}} \tag{10}$$

The thermal resistance concept (5) allows the summation of the various conduction and convection components of heat transfer and more easily calculates the overall heat flux Q_{Loss} (10); this is similar to electric circuits and how resistances can be added up. This method does not need the surface temperatures between components but only the fluid temperatures on the outside of both surfaces. As mentioned previously, the R_{rad} is assumed to be negligible for this setup and thus ignored in the next steps.

The topmost surface heat flux comprises two convection steps and one conduction through the acrylic top; combining (6) and (7) with (10) to calculate the heat flux.

Similarly, the bottom surface heat flux is done in the same manner except since the aging cell sits on top of a piece of plywood that is also taken into consideration.

$$R_{\text{cond\_radial}} = \frac{\ln(r_{\text{outer}}/r_{\text{inner}})}{2\pi L_{\text{height}}k} \tag{11}$$

$$R_{\text{conv\_radial}} = \frac{1}{2\pi r L_{\text{height}}h} \tag{12}$$

Resistance equations for the cylindrical section of the aging cell need to be adjusted from the previous steps due to the radial nature of the geometry. The adjusted equations are shown in (11) and (12). For the aging cell, it's a summation of the radial resistances then equation (10) is utilized to calculate the radial heat flux.

A summary of the calculated data is shown in Table 3 below for the ambient room temperature of 20.0°C.

Table 3: Calculated resistances and heat losses

Description	Resistance [°C/W]	Heat loss at 60.0°C [W]	Heat loss at 80.0°C [W]	Heat loss at 95.0°C [W]
Top surface	3.01	13.3	19.9	24.9
Bottom surface	3.37	11.9	17.8	22.3
Radial surface	3.83	10.5	15.7	19.6
Overall	N/A	35.6	53.4	66.8

4.1.2 Heat Loss Measurements – Limitations/Positioning

K-type thermocouples (CO3-K, Omega, Quebec, Canada) utilized in the temperature measurements were factory standard and conforms to ANSI/ASTM E230 standard limits of error. The manufacturer's stated standard of error for the k-type thermocouple above 0°C is the greater of ±2.2°C or ±0.75% of the temperature measurement [64]. The calibration of the thermocouples were not confirmed prior to their usage, therefore the standard error was used.

The thermocouples could have been individually calibrated to provide an adjusted curve instead of using the default reference tables in order to give a lower error than the standard error from the manufacture. A grounding loop could have been provided to adjust for any stray electromagnetic fields impacting the measurements. For example, any nearby transformers and motors could produce an electromagnetic field that could impact the measurements of the thermocouples. With a grounding loop, the stray electromagnetic fields could be measured at the same time as the data logging and its impact deducted from the results.

The thermocouples were positioned strategically around the carousel in order to capture the gradients predicted by the CFD model. The goal was to validate the CFD model predictions with the measurements. For the initial temperature measurements in the acrylic aging cell (Figure 46) only five thermocouples were available with the data logger, so their positions were as follows:

1. Channel 3 - Positioned in the upper half of the carousel near one of the sous vide heater outlets.
2. Channel 5 - Positioned in the upper half of the carousel near the other sous vide heater outlet (note that this means the first two thermocouples are positioned near the outlets).

3. Channel 2 - Positioned in the upper half of the carousel 90° clockwise from channel 3.
4. Channel 4 – Positioned in the lower half of the carousel 45° clockwise from channel 3.
5. Channel 1 – Positioned in the lower half of the carousel 45° counterclockwise from channel 5.

The thermocouples were failing after initial setup of the experiment, so each of the trials had one thermocouple that would fail quickly after the start of the experiment and was thus removed. The failures were briefly investigated and attributed to one main mode of failure being a break in the connection; this was supported by the connection being lost if the thermocouple wires were moved slightly and could be regained after more movement. The plug connection on the data logger was also problematic as some of the connectors were slightly loose compared to others. However, repeated attempts to plug and unplug would eventually lead to a stable connection if the data logger was not disturbed afterwards. So, while the connector issue could be a contributing factor, it was believed that the wiring was the main culprit.

Due to the large standard error of the thermocouples, the small gradients within the heat loss measurements were not clearly distinguishable from the noise. A measurement was also taken during the initial warm up phase of the aging cell as the outlet temperature of the sous vide heater would clearly be warmer than the average temperature within the cold aging cell. However, this was also not fruitful due to the noise and large standard error in the measurements.

4.1.3 Heat Loss Measurements – Acrylic Aging Cell at 60°C

Measurements were taken from the acrylic aging cell to validate the previously calculated heat loss.

Figure 46 shows the thermocouples strategically positioned around the aging carousel before initiating the heat loss measurements. The aging cell was then heated up to 60.0°C and held at a steady state for some time before the power to the sous vide heater was disconnected. The room temperature was 20.2°C according to the thermostat at the time the power to the heater was disconnected. It is assumed the 20.0°C temperature set point of the room thermostat represents the average temperature of the space during this experiment.

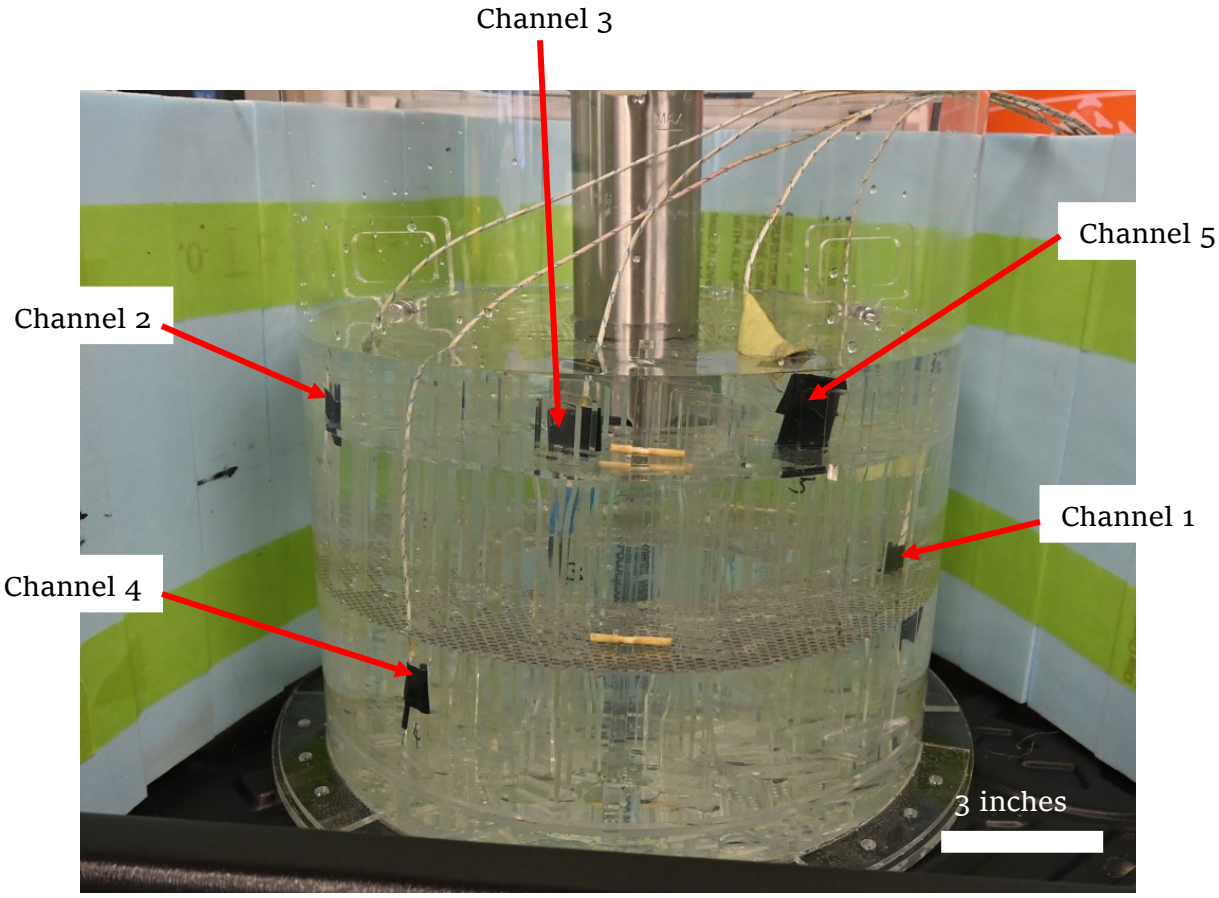

Figure 46: Acrylic aging cell with thermocouple setup

Temperature logging every 30 seconds was done for approximately 20 hours as shown in Figure 47. Channel 3 was discovered to not be in operation and thus removed from the results. The remaining four channels showed that with time there was a minor temperature gradient being developed within the aging cell. When the average temperature of the aging cell was at 59.0°C, the temperature spread in the thermocouple readings was between 58.7°C and 59.4°C. Compared to when the average temperature drops to 35.0°C with a spread of 34.5°C to 35.7°C. The gradient, therefore, increases from 0.7°C to 1.2°C across this cool-down experiment.

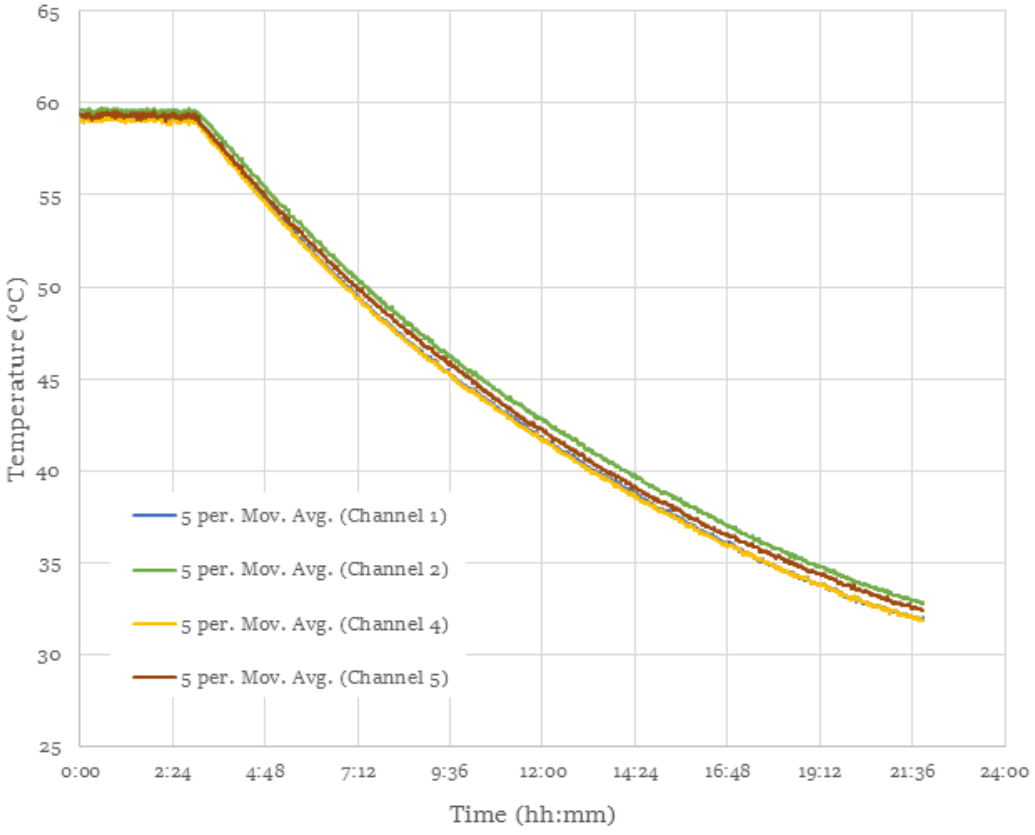

Figure 47: Acrylic aging cell cool down curve at 60°C

The heat loss of the acrylic aging cell was calculated by taking the average temperature across the four thermocouples over a period of time for a 5.0°C drop. The change in temperature of the volume of water [65] in the aging cell was then used to determine the average energy loss over the period shown in Table 4. The heat loss calculated from a smaller data set of the first 50 data points per thermocouple showed a higher value of 39.7W. This is expected as the value in Table 4 is over a larger period and the heat loss is proportional to the temperature difference.

Table 4: Measured average heat loss over time of acrylic aging cell

Temperature [°C]	Measured heat loss [W]	Calculated heat loss [W]	Time interval [s]	Cumulative time [s]
60.0 to 55.0	37.5	35.6	5,910	5,910
55.0 to 50.0	32.8	31.2	8,460	14,370
50.0 to 45.0	27.0	26.7	10,260	24,630
45.0 to 40.0	20.9	22.3	13,290	37,920
40.0 to 35.0	16.7	17.8	16,560	54,480

4.1.4 Heat Loss Measurements – Metal Aging Cell at 82°C

In the same fashion the same setup as 4.1.2, the experiment was repeated for the metal aging cell but instead from a temperature of 82.0°C. This time only four thermocouples were used as the previous test one thermocouple was not functional. However, similar to the previous test a single thermocouple was not functional and again removed from the results. Figure 48 shows the thermocouple layout inside of the metal aging cell with channels 3 and 4 positioned directed in front of the sous vide heater outlet to try and attempt to capture the temperature difference of the heated water at the outlet. All four thermocouples are of the K-type and secured to tensile test coupons positioned near the middle of the carousel.

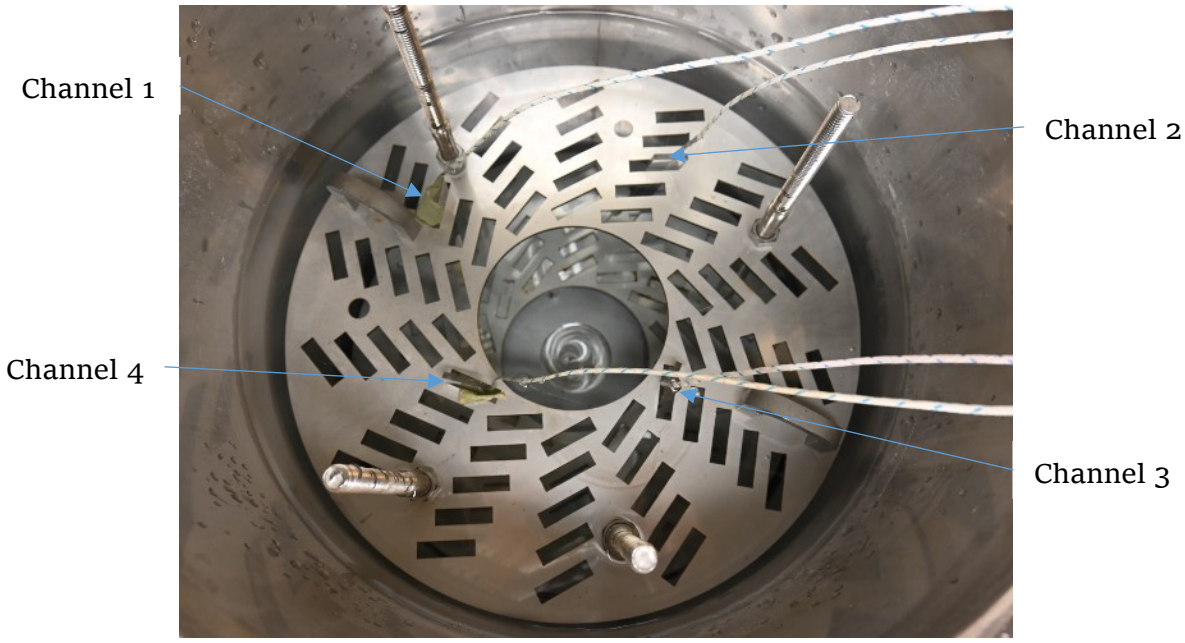

Figure 48: Thermocouple placement in the 82°C test

The cooling down experiment was run for approximately 26 hours with a portion of the data shown in Figure 49. Updating the calculation done in 4.1.1 for the 82.0°C set point and metal material yields a calculated heat loss of 53.4W compared with the calculated average heat loss of 158W over 5.0°C.

Note the steady state data collected from the thermocouples has a much larger range than the previous 60.0°C test. The variations in the temperature during steady state were within the normal error of +/- 2.2°C expected per the thermocouple type. There was also no noticeable difference in the temperature measurements of the sous vide heater outlet and positions further away. This could be explained by the thermocouples' large range of error compared with the expected temperature difference. Also, the relatively high specific heat capacity of the water contributed to dampening any noticeable gradients between the sous vide outlet and the inlet.

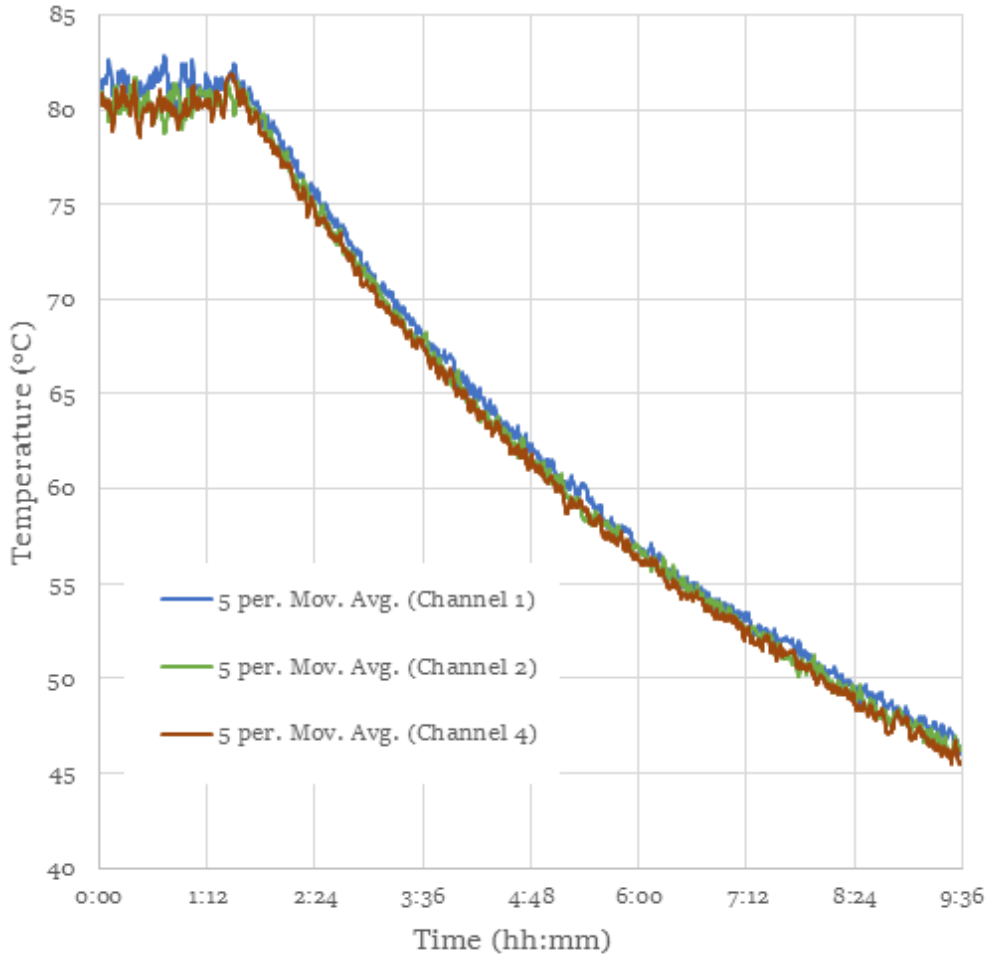

Figure 49: Stainless steel aging cell cool down curve at 82°C

4.1.5 Heat Loss Measurements – Metal Aging Cell at 95°C

In the same fashion the same setup as 4.1.2 and 4.1.3, the experiment was repeated at 95.0°C. Due to thermocouples failing, only two K-type thermocouples were used and they are positioned hanging in the middle of the carousel instead of attached to tensile test coupons. The setup was the same as 4.1.3 aside from the thermocouple differences.

The cooling down experiment was ran for a shorter time of four hours due to time constraints and the larger heat losses providing enough of a temperature change for heat loss calculations. Figure 50 shows the collected data from the cooling down experiment. Updating the calculation done in 4.1.1 for the 95.0°C set point and metal material yields a calculated heat loss of 66.8W compared with the calculated average heat loss of 209W over 5.0°C. Similar to the 82.0°C where the steady state temperature readings were less stable than 60.0°C; the 95.0°C steady state temperature readings were also less stable but within the expected +/-2.2°C variation for the thermocouple type. One observation was that the two thermocouples had a temperature difference of about 2.0°C after the cooling down experiment began. This was likely due to one of the thermocouples floating up above the top plate of the carousel as this was noticed upon removal of the lid to the aging cell. This shows there is potentially a 2.0°C temperature gradient between the centers of the aging cell plates compared with the headspace above the top plate. However, the data suggests this potential gradient is steady throughout the cooling down experiment.

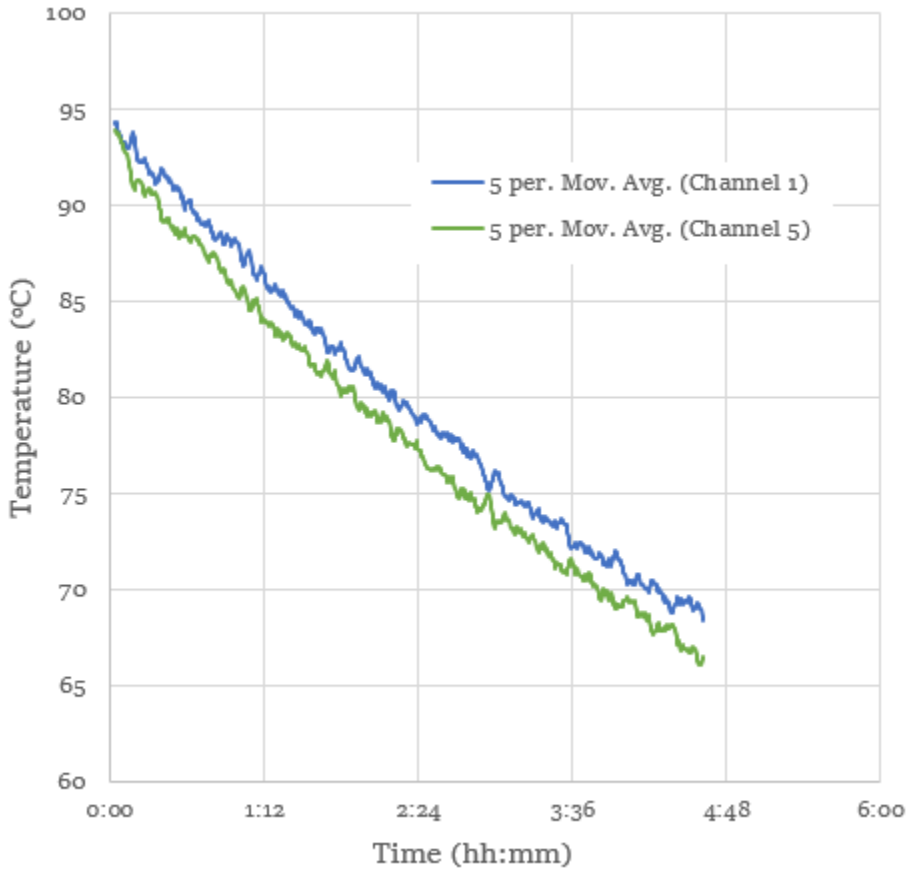

Figure 50: Stainless steel aging cell cool down curve at 95°C

4.1.6 Discussion on Heat Loss Measurements

Comparing the three different measurements of heat losses it is clear there is a large difference with the higher temperatures compared with the calculation in 4.1.1 as shown in Table 5. For the lower temperature range, a smaller convection coefficient was selected as there would be lower driving forces to generate natural convection with a smaller temperature difference. By goal seeking, the correct combination of convection current coefficients for the lower temperature case can be obtained. However, this solution is just one of many that can satisfy the total heat loss measured and be within the stated coefficient ranges per Cengel [63]. The range of possible convection current coefficients to obtain a heat loss of approximately 200W is within the range stated by Cengel [63]. Therefore the calculations provided in 4.1.1 would also be supported by the actual measured values of the heat losses in all three of the test cases, however, the heat transfer coefficients would need to be recalculated for the higher temperature cases.

Table 5: Comparison of measured to calculated heat losses

Temperature [^{o}C]	Measured heat loss* [W]	Calculated heat loss [W]
95	209	66.8
80	158	53.4
60	37.5	35.6

*measured heat losses are calculated over a 5^{o}C average

The measurements from 4.1.3 and 4.1.4 both had a limited number of tensile test coupons within the carousel compared with 4.1.2. This would be another source of error as the reduced number of tensile test coupons would provide fewer obstructions for natural convection currents to occur within the carousel. Also, the water/air volumes within the aging cell were not the same due to the slight size differences of the aging cells but their different water volumes were taken into account for the heat loss calculation.

The calculation in 4.1.1 did not account for the air space in the head of the aging cell. This would be another source of error as the air space there would provide an area for potentially more convective or evaporative losses. The specific heat capacity and conductive properties of the carousel and tensile test coupons were also not included; however, this impact is expected to be small and thus not accounted for as the main object is to qualitatively determine relative mixing homogeneity and not a quantitative one.

4.2 Mixing Homogeneity

In this section, the mixing homogeneity of the carousel setup will be discussed in detail. First beginning with the visual dye tests to qualitatively assess areas of low flow or stagnant regions. Then a simple CFD analysis was performed to help further analyze the results from the visual dye testing and other setup configurations. The goal of this analysis is to locate the regions of low flow within the design and compare with other designs over the amount of these low flow regions.

4.2.1 Dye Mixing – Sous Vide and/or Magnetic Stirrer

Utilizing the clear acrylic aging cell and carousel, a visual test was done by injection of dye into the center of the carousel to help visualize the flow paths and mixing homogeneities of the different setups. The mixing homogeneity is a function of the time for the dye to disperse and visually seeing if zones of recirculation or low flow occur. The purpose of this exercise was to empirically determine the relative flow paths and mixing homogeneity of the different combinations.

The first series of tests were done to determine how well the sous vide heater and the magnetic stirrer would perform in terms of mixing homogeneity. Figure 51 shows how quickly the dye disperses in the aging cell with both types of stirring. There did not seem to be any noticeable regions of low flow or recirculation with the highest flow being in the direct paths of the sous vide heater outlets and closest to the magnetic stirrer.

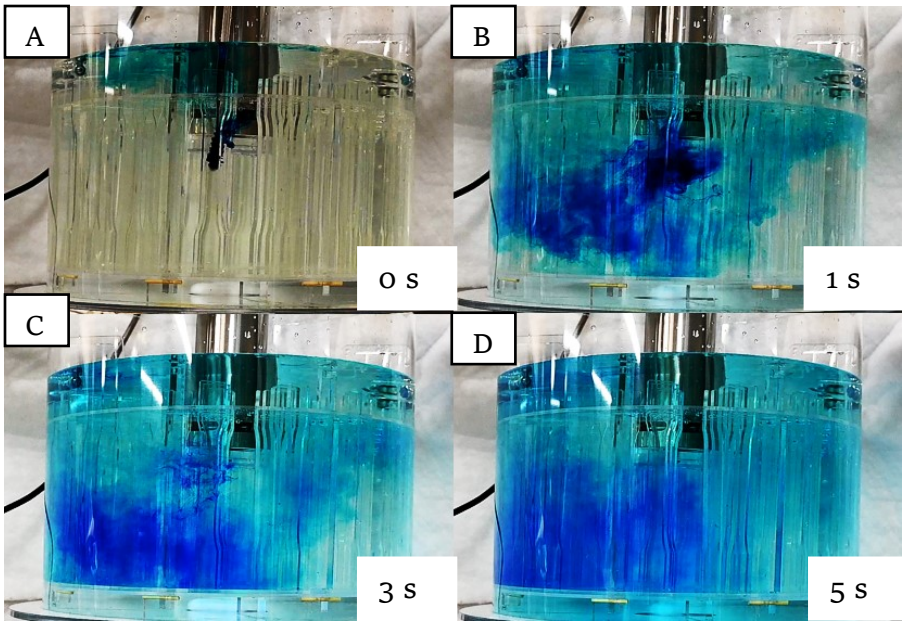

Figure 51: Dye test on initial carousel design with both magnetic stirring and sous vide heater on: (A) time at 0s, (B) time at 1s, (C) time at 3s, and (D) time at 5s

The next test is with the magnetic stirring only to gauge how well it performs as the intended use of this magnetic stirrer was for beakers and smaller containers. Figure 52 shows how slowly the dye mixes compared with the previous Figure 51. Visually there was a vortex forming in the center of the aging cell due to the stirrer as expected. However, due to the large size of the container, the velocities generated are diminished and hence the mixing homogeneity and turbulence as well. A toroid shape is generated by the mixing currents within the confines of the carousel with a region of low velocity at the center of the toroid and above the top plate of the carousel. Overall this test showed how slowly the magnetic stirrer was at mixing compared with the combination in Figure 51.

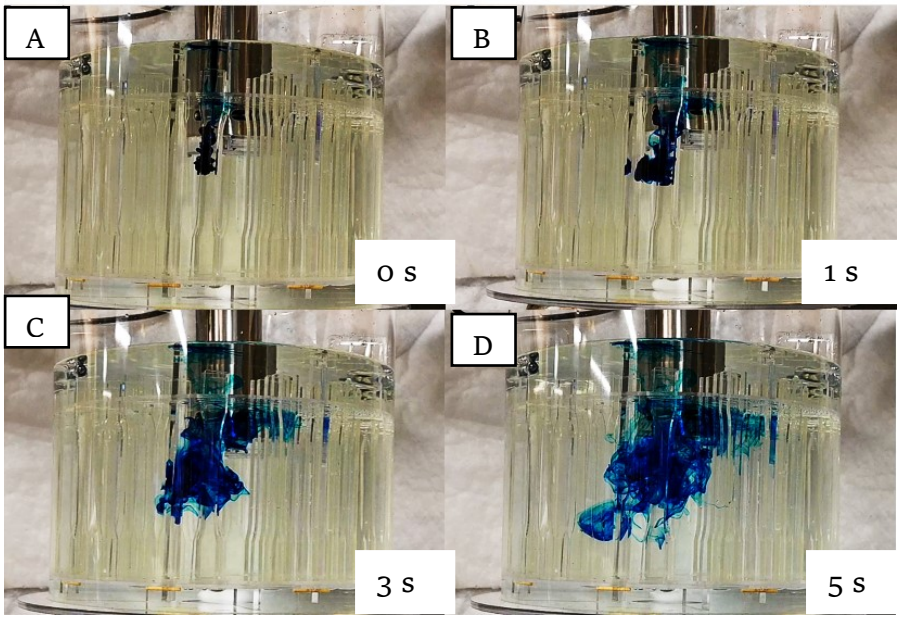

Figure 52: Dye test on initial carousel design with magnetic stirring only: (A) time at 0s, (B) time at 1s, (C) time at 3s, and (D) time at 5s

Due to the lack of performance indicated by the previous test in Figure 52, it was expected that the sous vide heater contributes the majority of the homogeneous mixing seen in Figure 51. Below Figure 53 confirmed this expectation that the sous vide heater provides the majority contribution of the pair. There was no noticeable difference between this test and the previous one with the magnetic stirrer and sous vide heater in terms of the overall time for the dye to evenly disperse. The bottom center portion of the aging cell was noticed to be slightly slower moving compared to the test with the magnetic stirrer but still moving at a significant velocity. It should also be noted there was no formation of a vortex in the bottom center of the carousel, unlike the tests with the magnetic stirrer. The area above the top plate of the carousel was the last region to have dye evenly dispersed.

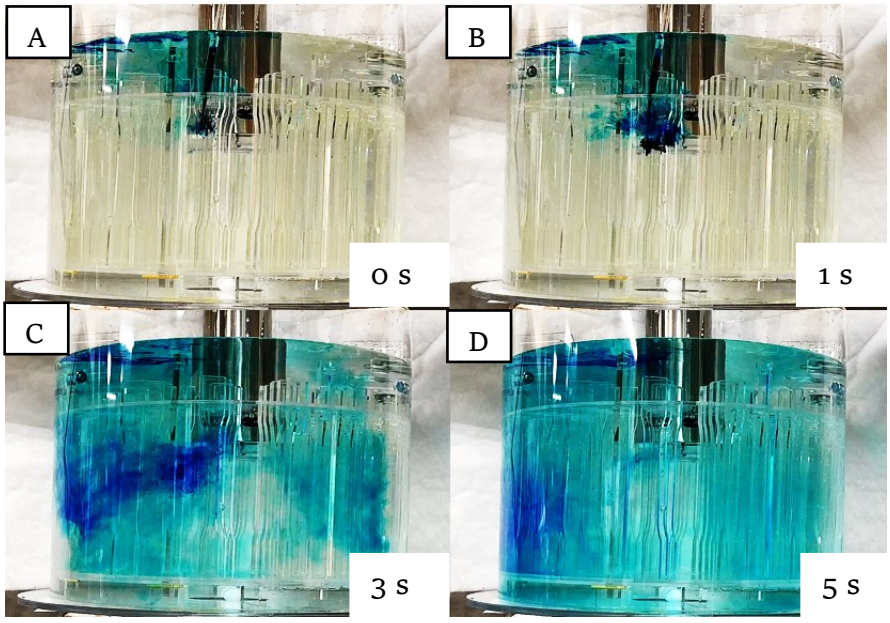

Figure 53: Dye test on initial carousel design with sous vide heater only: (A) time at 0s, (B) time at 1s, (C) time at 3s, and (D) time at 5s

4.2.2 Dye Mixing – Middle Plate

The same volley of testing was done for each of the middle plate designs of the carousel as done previously with the carousel design without the middle plates. The first middle plate design tested was a copy of the top plate as shown in Figure 39's top dead center. The intent for this series of tests was not only to gauge its mixing effectiveness but also the impact of the middle plate on the mixing performance.

The hypothesis was that the middle plate would act as a barrier to the flow and cause two segregated flow regions. This hypothesis was proven correct by Figure 54 showing the two regions. The mixing was much slower than the previous test in Figure 51 but not as slow as the test in Figure 52. Overall the test was roughly a few times slower to reach the same homogenous dye dispersion for the previous tests. The middle plate blocked the sous vide heater's powerful outlet jet from forming the large circulation zone throughout the entire carousel that so effectively mixed the previous tests.

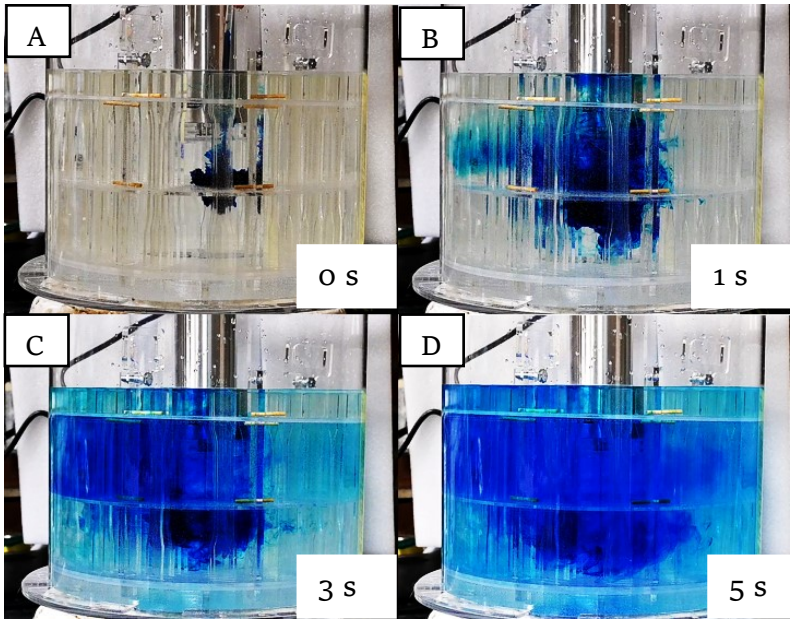

Figure 54: Dye test on modified carousel design with both magnetic stirring and sous vide heater on: (A) time at 0s, (B) time at 1s, (C) time at 3s, and (D) time at 5s

With the sous vide heater turned off the same test was repeated. Figure 55 showed how the divided flow region had a more pronounced impact on the magnetic stirrer. The upper half of the carousel was entirely a low-velocity region and the dye appears to only be mixing through diffusion aside from the very center of the carousel which still had the vortex from the stirrer. However, this vortex had a very limited impact to the point that it was barely noticeable. The lower half showed a slightly faster rate of mixing compared with the sous vide heater only in Figure 56. Overall this test showed that for the carousel with a middle plate, the magnetic stirrer's only option was by far the least desirable due to the poor mixing homogeneity.

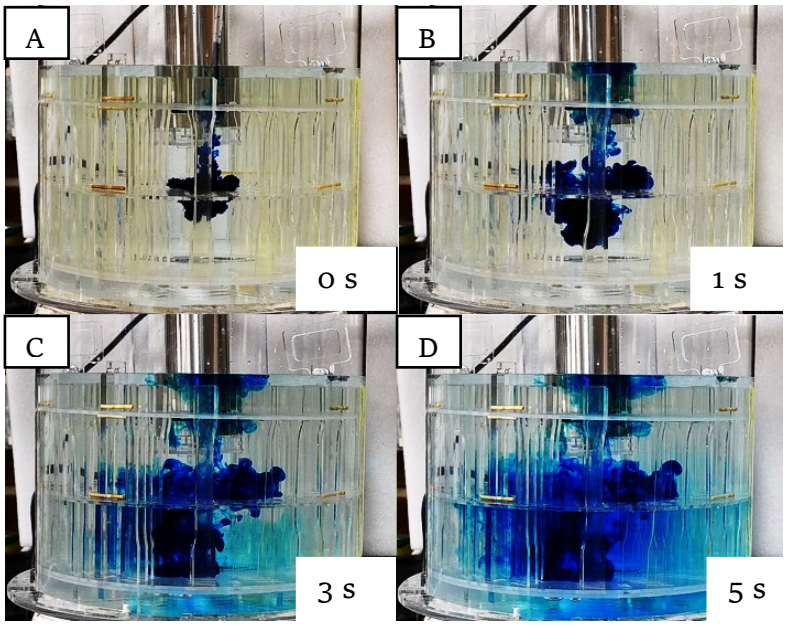

Figure 55: Dye test on modified carousel design with magnetic stirring only: (A) time at 0s, (B) time at 1s, (C) time at 3s, and (D) time at 5s

The sous vide heater-only test also showed how dividing up the regions reduced the mixing homogeneity. The lower half of the carousel was worse than the magnetic stirrer-only option as mentioned above. As the flow path out from the sous vide heater is more like a jet, adding the middle plate truncated the flow path and redirected it toward the center. Thus the bottom region has very limited flow velocities and would be mostly mixing through diffusion rather than the active flows.

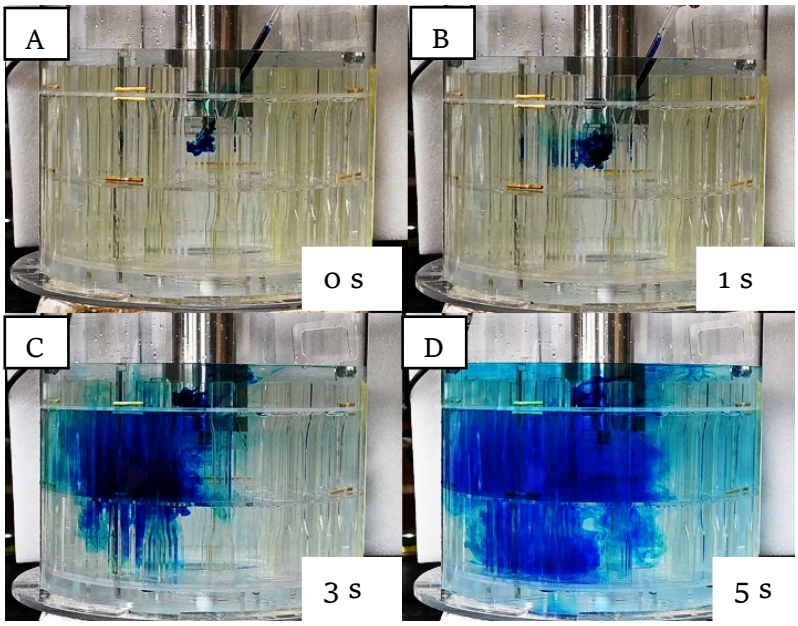

Figure 56: Dye test on modified carousel design with sous vide heater only: (A) time at 0s, (B) time at 1s, (C) time at 3s, and (D) time at 5s

4.2.3 Dye Mixing – Comparing Middle Plates

Due to the issues seen from utilizing the top plate design as the middle plate, the other two middle plate designs were created to help alleviate the mixing issue. The same series of testing was done on the remaining two middle plate designs. However, as the main interest was the impact on the sous vide heater's mixing homogeneity only those tests are shown below; the combined effects and magnetic stirrer only were not significantly different from those seen in 4.2.2.

The skeletonized middle plate showed the most promising mixing homogeneity improvement over the previous results in 4.2.2 as shown in Figure 57. The large cutouts of the skeletonized middle plate allowed for the flows from the sous vide heater to pass through to the bottom region and generate a more complex mixing path than previously without the middle plate. However, it should be noted that there is still a slight region of lower velocity as indicated by the dark spot of dye in Figure 57D.

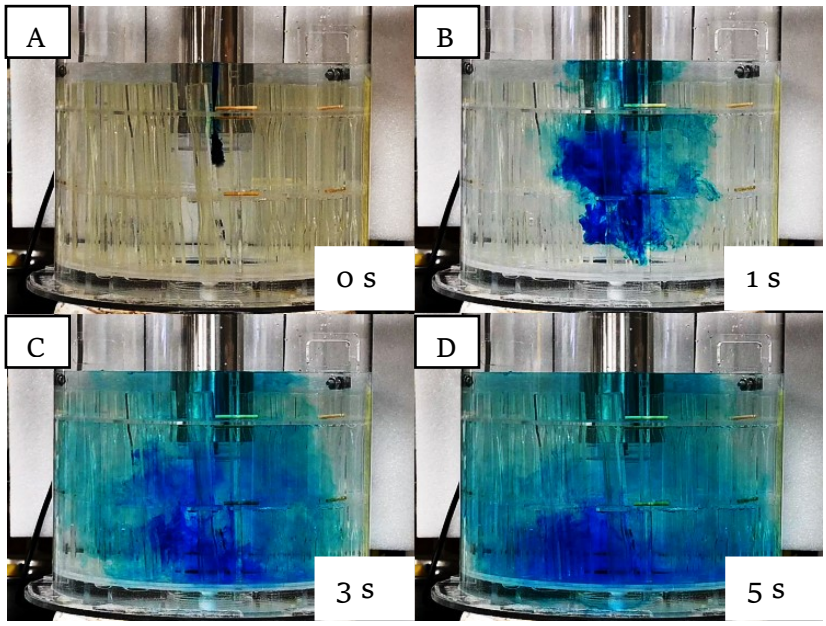

Figure 57: Dye test on skeletonized middle plate with sous vide heater only: (A) time at 0s, (B) time at 1s, (C) time at 3s, and (D) time at 5s

Lastly, the perforated middle plate design was tested in Figure 58. This design provided a similar result to the skeletonized plate in terms of the overall mixing homogeneity and time for the dye to completely disperse. The same region of lower flow exists in Figure 58D as shown in Figure 57D. However, instead of distinct flow paths between the top and bottom regions, like those in the skeletonized plate design above, the perforated plate provided numerous locations for smaller currents to carry the dye to the lower region and back. This provides a more uniform velocity overall compared with the skeletonized plate's flow paths between regions being focused in the large openings. Both designs provide very similar mixing homogeneity and times for dye dispersion. However, the perforated plate was selected as the best of the three designs due to the lower velocity gradients and increased structural stability of the middle plate. There was also an added advantage in manufacturing as the same laser cutting or water jetting file could be used as the top plates with just a change of material as opposed to a different design being created.

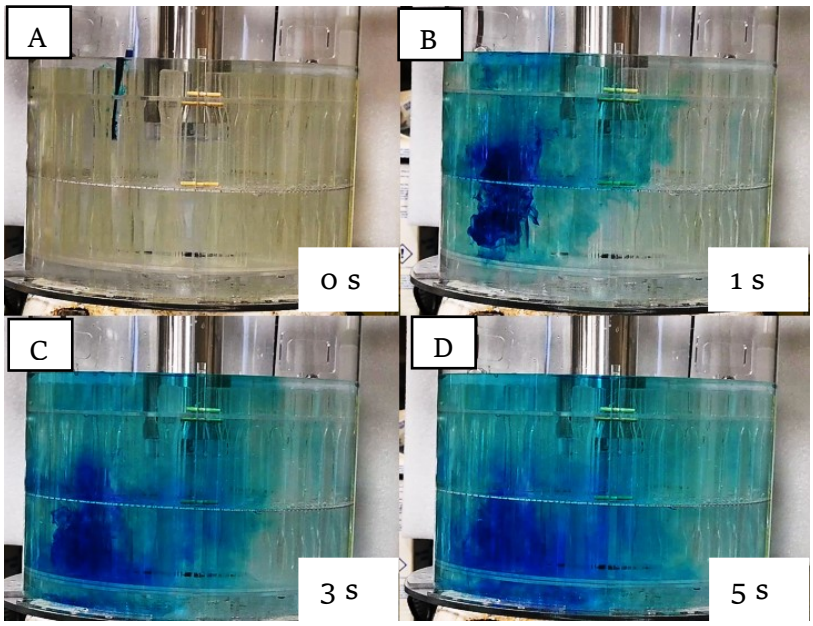

Figure 58: Dye test on perforated middle plate with sous vide heater only: (A) time at 0s, (B) time at 1s, (C) time at 3s, and (D) time at 5s

4.2.4 CFD Model Setup

SOLIDWORKS Flow Simulation was utilized to perform a simplified computational fluid dynamics (CFD) analysis of the aging cell model to help further understand the flow patterns and provide more detail than the dye tests in the previous sections. As there are many possibilities to be evaluated, computer modeling and simulations would be deemed a more efficient approach than empirical analysis. More detailed analysis may be performed in future works to refine the simulations on the final iteration of the test setup.

The model geometry was simplified from the acrylic aging cell. The sous vide heater was integrated into the lid as a tube with the inlets and outlets projected onto the tube's surface as shown in Figure 59. The CFD domain is comprised of the volume enclosed by the lid and tank. The domain air space was assumed to be fluid filled to simplify the model. The sous vide heater outlet was set at the manufacturer's rated flow rate divided evenly across the four opening slits. The sous vide heater inlet boundary condition was set as the ambient pressure to provide more flexibility in the model to adjust the flows. The process fluid was set to water at atmospheric conditions of one atmosphere pressure at a temperature of 20°C. The boundaries of the domains were set as walls with zero velocity at the surface and a defined heat loss per the heat loss ratios calculated in 4.1.1 and adjusted to match the heat losses as per the actual measurements for 95°C.

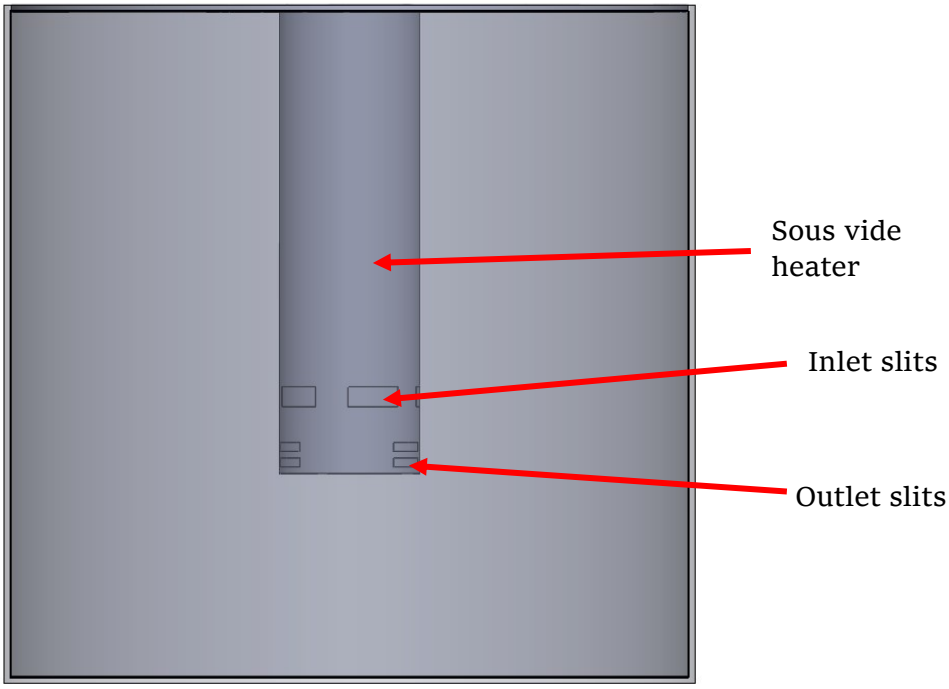

Figure 59: CFD domain with sous vide heater

The carousel was added with a full complement of tensile test coupons as shown below in Figure 60. The simulation was set to treat the entire carousel as an adiabatic entity; primarily to ignore the effects of conduction and capacitance for the simulation. The tensile test coupons were fixed into position and cannot move. The entire carousel was also fixed into a static position with the legs touching the bottom of the domain and centered on the aging tank. The effects of thermal expansion and their corresponding stresses were also assumed to be negligible and set to be ignored in the simulation.

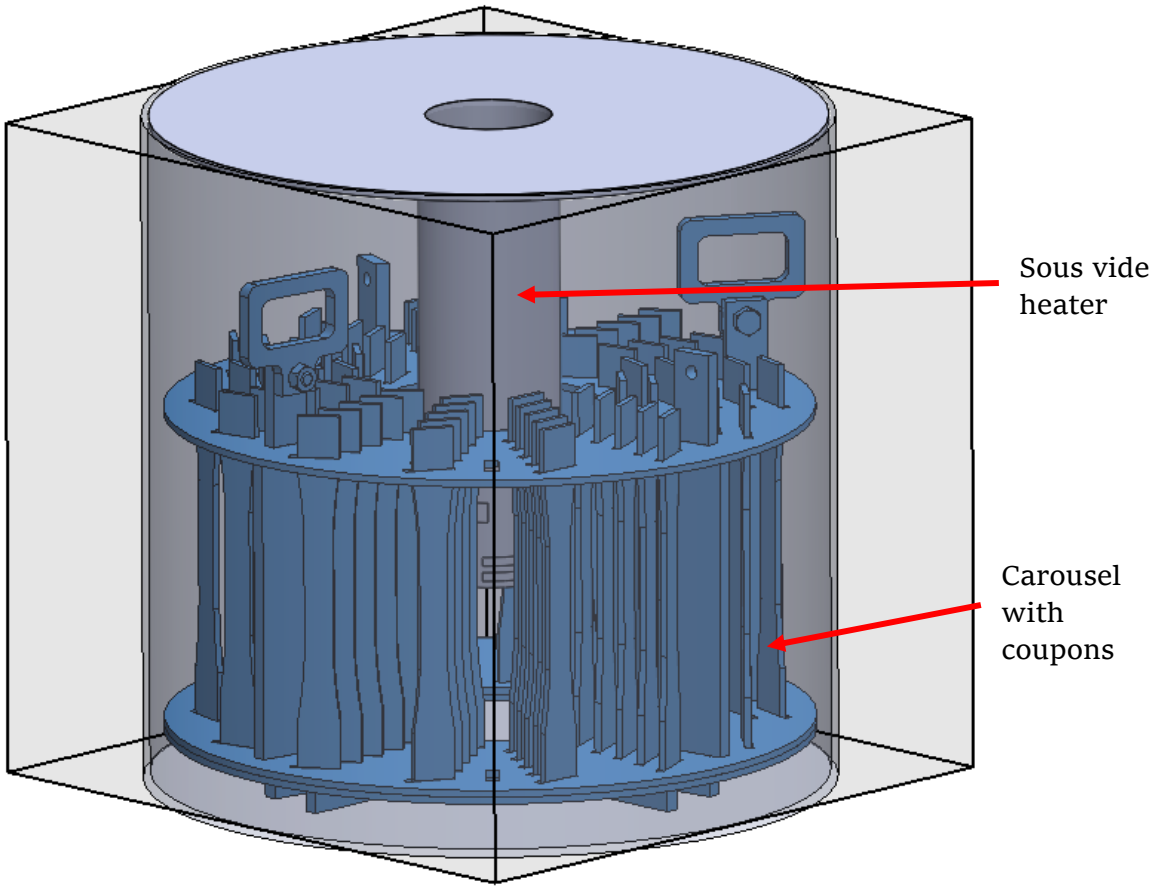

Figure 60: CFD domain with carousel

A mesh refinement of level 4 was used shown below in Figure 61 with the middle plate carousel design. Rectangular elements were utilized with a size of between 16mm to 1mm. SOLIDWORKS rectangular elements make use of their proprietary SmartCells technology where multiple control volumes are adaptively generated within one element when it is near the boundary layer in order to increase the accuracy by refinement within the localized area [66]. By utilizing the SmartCells, SOLIDWORKS can provide a much more accurate numerical solution utilizing less elements when compared to most other CFD codes [62]. A refinement of level 0 would utilize a rectangular element of 16mm; with each level of increasing refinement halving the element size down to a refinement of level 4 giving a 1mm rectangular element as shown in Figure 62. The mesh size distribution was determined by the SOLIDWORKS

optimization algorithm which aims to fit at least two elements across the width of any feature while utilizing larger elements where possible to minimize the total number of elements needed. The algorithm will also slowly transition between refinement levels, meaning it can lower or increase the refinement levels by one at a time. Figure 63 shows the detail of the level 4 refinement around the perforated plate. Utilizing traditional CFD software, this level of refinement would not sufficient to accurately simulate the boundary layers but only the bulk flow; however, with SmartCells, SOLIDWORKS can provide a more accurate solution with less elements at the boundary layers [62]. The limitations in access to computational power was also a factor in this decision as the number of simulations needed to be ran was fairly large and it was the comparative differences between simulations with respect to their qualitatively ability to eliminate stagnant regions that was important. Which can then be validated using the visual dye testing.

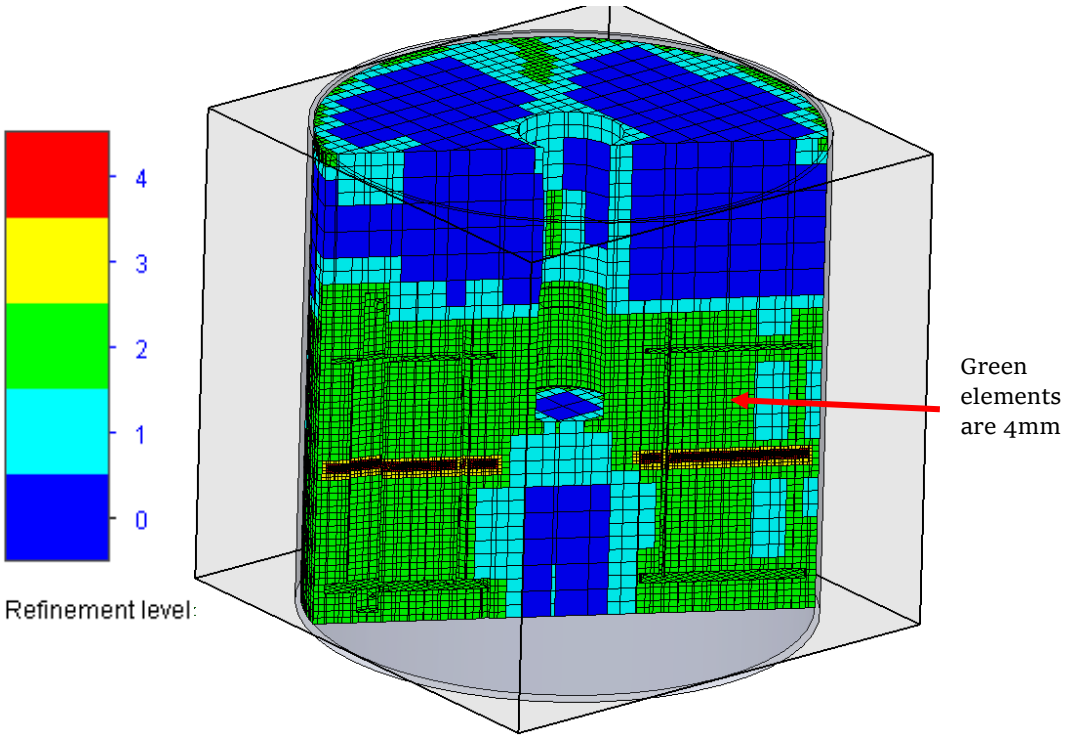

Figure 61: CFD mesh typical

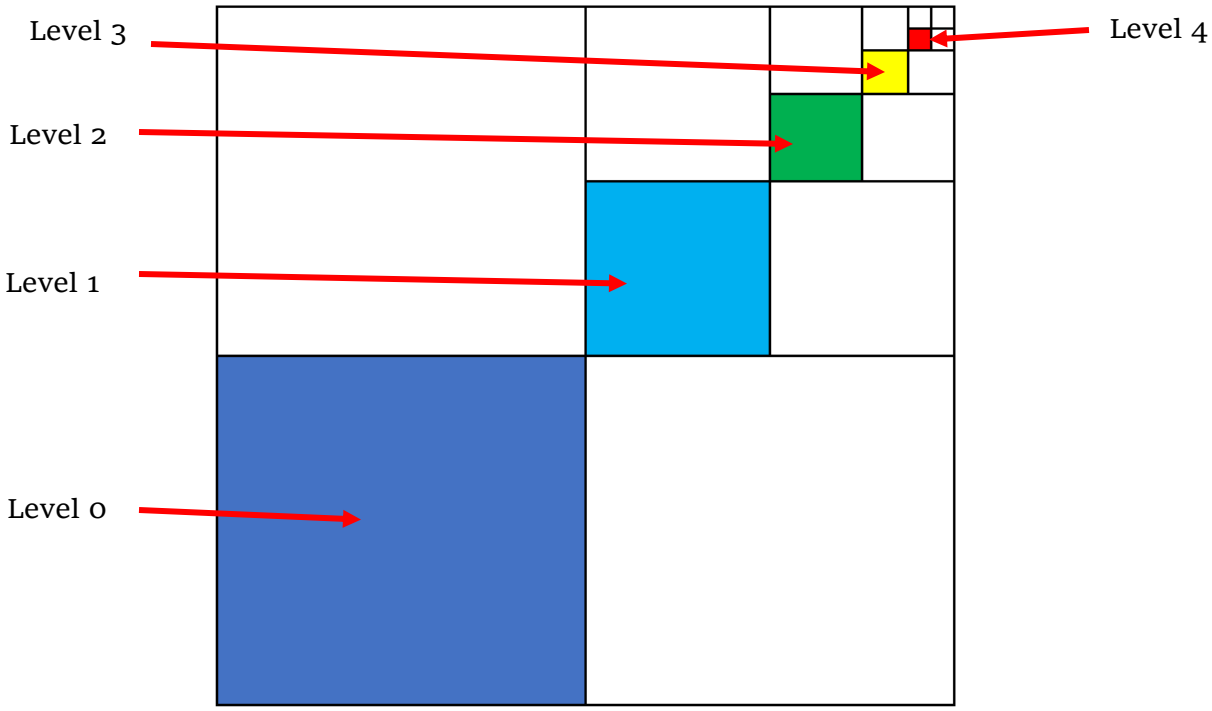

Figure 62: CFD mesh refinement size figure

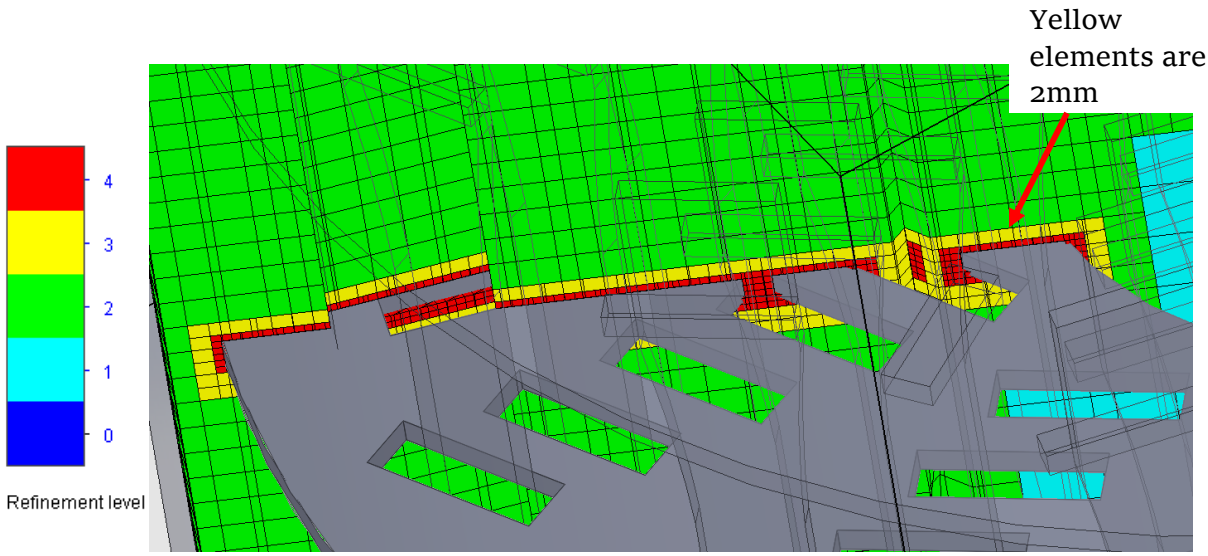

Figure 63: CFD mesh refinement detail

There are two primary checks that are needed when doing numerical analysis; one check is for the numerical solution to reach convergence and another is to validate the solution. To check for numerical convergence, the difference between the same reference point or value of each iteration in the CFD is compared to each subsequent iteration. This can be a singular average global value, such as the global velocity of the domain, or a value at a certain node. The difference between the values of each sequential iteration is called the residual or delta. The plot of the residuals should show a decreasing and converging trend. A threshold of the residual would also need to be established with the decreasing trend to provide the criteria for when a solution can be considered numerically converged.

To validate the numerical solution, a common approach is to compare different key values with experimental data or calculated values. Calculated values for comparison are done according to well-established approaches for a value within the CFD model, and then compared to calculate the variance or error between the expected (calculated) and CFD value. Another method is to compare with experimental data, for example like comparing velocity or temperature measurements at a certain point in the model with the experiment setup. To validate the CFD models a combination of visual dye testing and temperature measurements were taken. The visual dye testing agreed with the general flow paths seen in the CFD models and gave further insight of the locations of low flow regions. By using this new insight, past visual dye testing video footage was reviewed and these new low flow regions was confirmed to be in the previous video footage but was not noticed during the initial testing. Temperatures measured within the different aging cell setups were also in agreement with the CFD simulations within the error expected from the thermocouple measurements.

The CFD cases had the convergence criteria set to both the global velocity and temperature values. For the case of the lowered sous vide heater; the SOLIDWORKS algorithm set the average velocity convergence to a residual of <0.000546m/s and average temperature convergence to a residual of <1.13°C. The velocity criteria converged very early on and yielded a velocity residual of 0.0000316m/s. The temperature convergence took more iterations as the initial boundary conditions of the aging fluid was set the same as the room temperature and yielded a temperature residual of 1.12°C when convergence was achieved. The solver stops the iterations and considers the solution has converged once both residual criteria are met. See the residual plots in Figure 64 and Figure 65 for velocity and temperature respectively, the shapes of these two graphs agree with the mesh size converging to a stable solution. All other CFD cases had similar convergence criteria and residuals as the aforementioned. The larger number of iterations was driven by the temperature due to the difference between the initial starting conditions at room temperature of 20°C and the sous vide heater set point at 95°C. By utilizing the average condition as the convergence criteria, the convergence is dominated by the largest values and there is a possibility the regions of low velocity and temperature may not have reached convergence; however, as the comparisons were done based on the magnitude of the differences and considering the bulk average value differences, this was deemed to be acceptable.

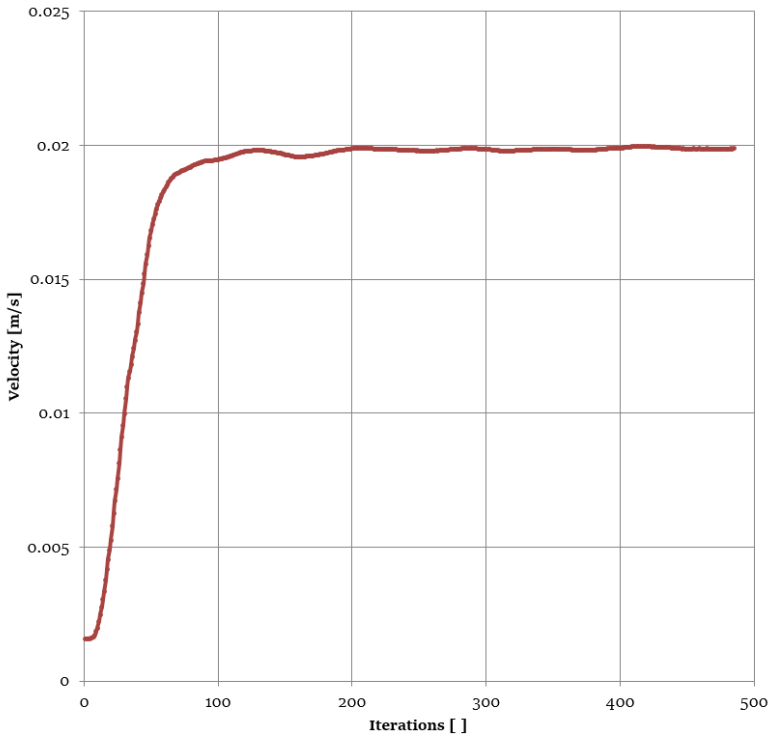

Figure 64: Velocity convergence plot for the lowered sous vide heater case

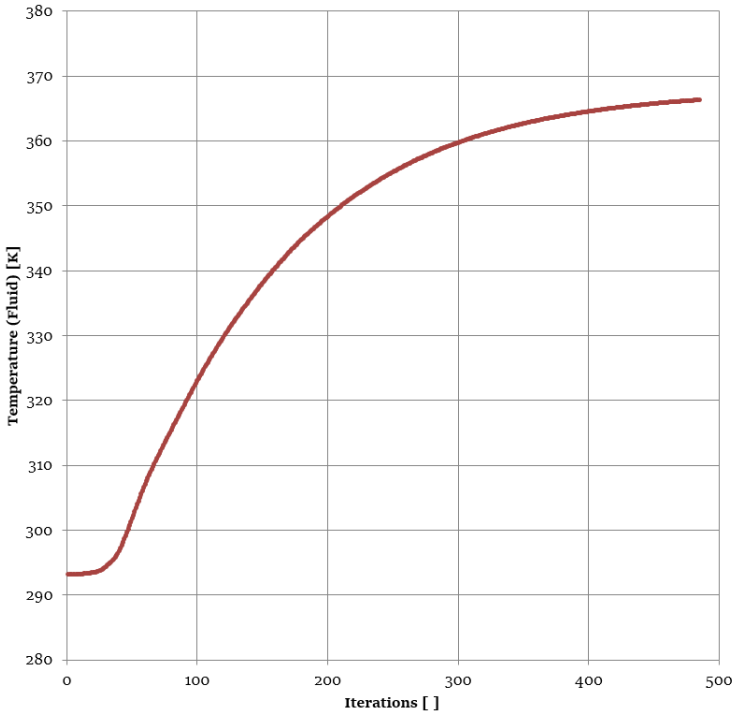

Figure 65: Temperature convergence plot for the lowered sous vide heater case

4.2.5 CFD Analysis of Magnetic Stirrer

The magnetic stirrer was ruled out initially as a poor choice for its mixing ability when compared with the sous vide heater in the case of the aging cell. However, the magnetic stirrer case for the middle plate was modeled in CFD to compare with the visual dye testing results from Figure 55. The boundary conditions were modified from the other CFD simulations. The domain boundary heat loss was set to zero and the sous vide inlet/outlet was also set to zero flow. A small circular disk region with the same angular velocity as the magnetic stirrer was added at the bottom face of the aging cell to simulate the magnetic stirrer. Convergence was based on the average velocity only as there were no temperature gradients to consider.

The result is shown in Figure 66 and resembles those seen from the visual dye testing in Figure 55. The density of the velocity vectors shown correlates to the relative velocity, hence the highest velocity region would occur at the lower half of the carousel. The overall magnitude of the velocity vectors far away from the magnetic stirrer is much smaller when compared to those in the other CFD simulations. This is also supported by the visual dye tests as the rate at which the dye mixes into a homogenous state is greatly longer compared with the sous vide heater.

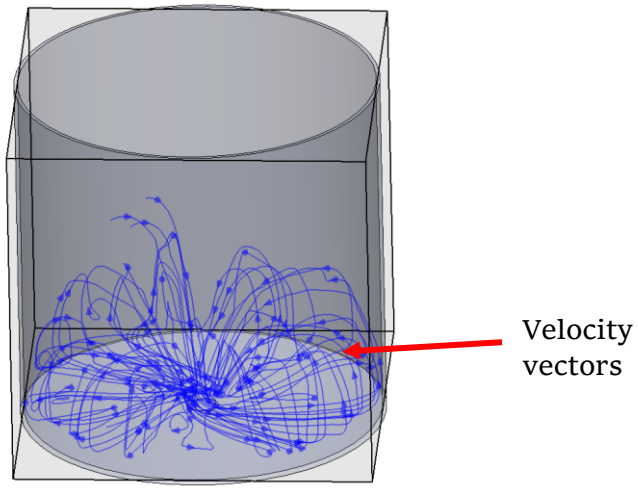

Figure 66: Velocity vectors of magnetic stirrer in aging cell

4.2.6 CFD Analysis of Carousel with Sous Vide Heater

The initial intent behind the CFD analysis of the sous vide heater setup was to provide a verification of the results seen from the dye testing in 4.2.3 and give further insight into the fluid dynamics of the different setups. However, as the scope was further refined a new objective of testing different setups came up. As CFD testing would be more efficient than building a prototype of each model.

Upon initially modeling the carousel and sous vide heater setup, it was apparent that the high position of the sous vide heater caused a region of low flow in the lower half of the carousel as seen in Figure 67A. This was not initially obvious with the dye tests, however, after this information was revealed by the CFD analysis it became very apparent when reviewing the past dye testing video footage. Initially, the height of the sous vide heater was set by the placement on top of the lid of the aging cell with no design feature added to adjust the height. To provide a more uniform flow, the sous vide heater was centered within the carousel as seen in Figure 67B. This helped to eliminate the region of low velocity seen in Figure 67A. The CFD computed average velocity was higher at 0.026m/s for the raised sous vide heater case when compared with 0.023m/s for the centered sous vide heater case. This result was caused by the new formation of a larger low-flow area above the carousel when comparing Figure 67A to Figure 67B. What is important here for the aging studies is to have uniform flow within the carousel, and thus the centered sous vide heater case would be more favorable when compared with the raised position in this regard.

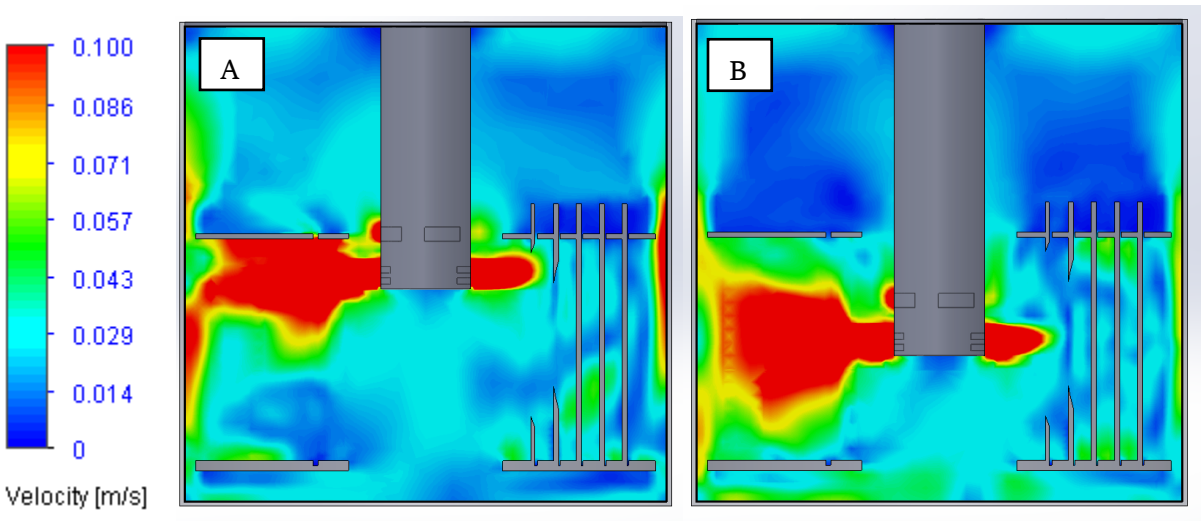

Figure 67: Vertical cross section of velocity profile with no middle plate: (A) raised case, (B) centered case

The horizontal cross-section of the velocity profiles in the bottom quarter of the carousel shown in Figure 68 shows there is still a velocity gradient between the two setups within the carousel on the left half with the tensile test coupons. This variance in gradient is due to the sous vide heater design where the flow is concentrated in two nozzles at 120° apart causing a region of lower flow within the carousel along the larger arc length between the outlets. It should be noted that the regions of low flow are by no means stagnant and just the flows are lower compared with the shorter arc length segment. This is still a large improvement compared with the original designs in 2.2.1 where no mechanically induced flow exists. In future designs, this region of low flow may be compared with design changes to help minimize the flow differences.

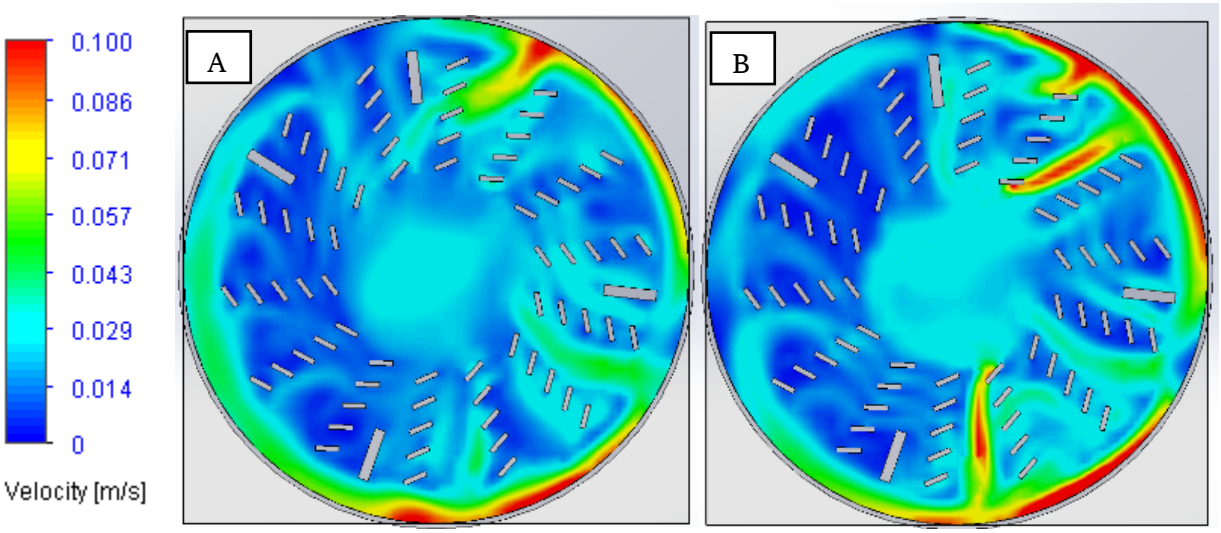

Figure 68: Horizontal cross section of velocity profile for the: (A) raised case, (B) centered case

4.2.7 CFD Analysis of Carousel with Perforated Middle Plate

The addition of the middle plate inside of the carousel causes a more distinct separation of the flow in the visual dye tests done in 4.2.3. The CFD results also align with the visual dye tests and indicate this separation. Figure 69A shows how the outlet of the sous vide heater flow is mostly localized to the upper half of the carousel and causes a region of low flow on the bottom half of the carousel. This low-flow region has a lower average velocity as indicated by the darker blue color when compared with Figure 67A. When the sous vide heater is lowered to have the outlet slits centered on the middle plate as shown in Figure 69B, the outlet flow is split into two streams with one heading into each region of the carousel. This causes a more even distribution of flow to occur within the carousel and it is a more critical detail than compared with the design with no middle plate. The other middle plate designs will be compared in the next section 4.2.8.

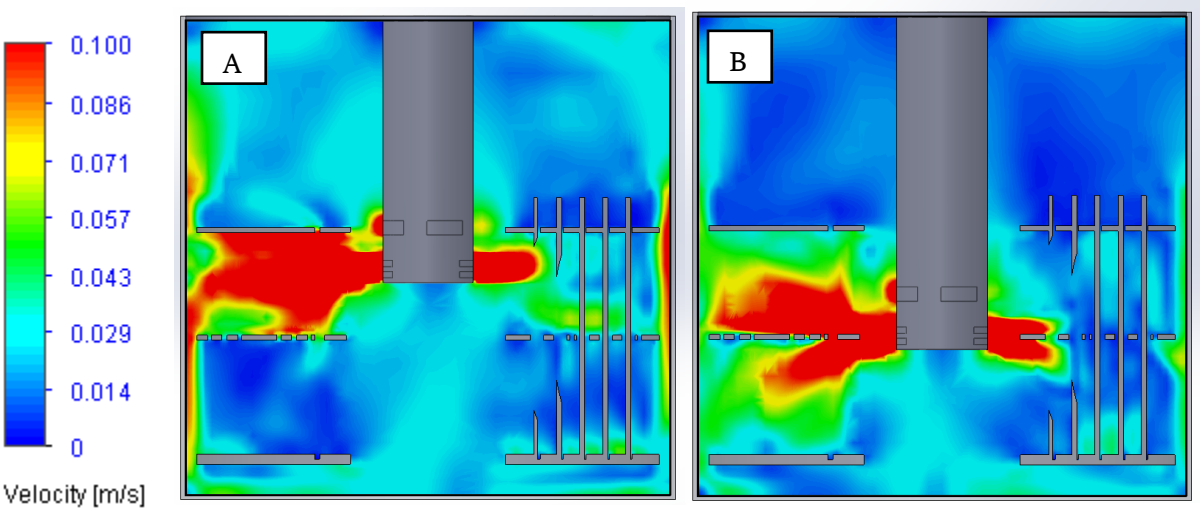

Figure 69: Vertical cross section of velocity profile with the perforated middle plate: (A) raised case, (B) centered case

The temperature gradients simulated in CFD were also compared between the two designs with the sous vide heater raised and centered. As expected with the less evenly distributed flow of the raised design, it could cause a larger temperature gradient to form in Figure 70A compared with Figure 70B. These temperature gradients are formed by the flow paths pushing the lower-temperature water from the aging cell walls back into the region of low flow. These regions would therefore form a temperature gradient compared with the regions of higher flow where proper mixing between the cooler water and heated water occurs. It should be noted that both figures show minor modeling inaccuracies due to the convergence criteria which are based on the average temperature and velocity. As the average is dominated by the highest values, the almost stagnant zones would therefore possibly not have converged yet. Separate convergence criteria with points located in these regions could be applied to rectify this issue, however, as this is deemed a first pass comparative analysis this was not done.

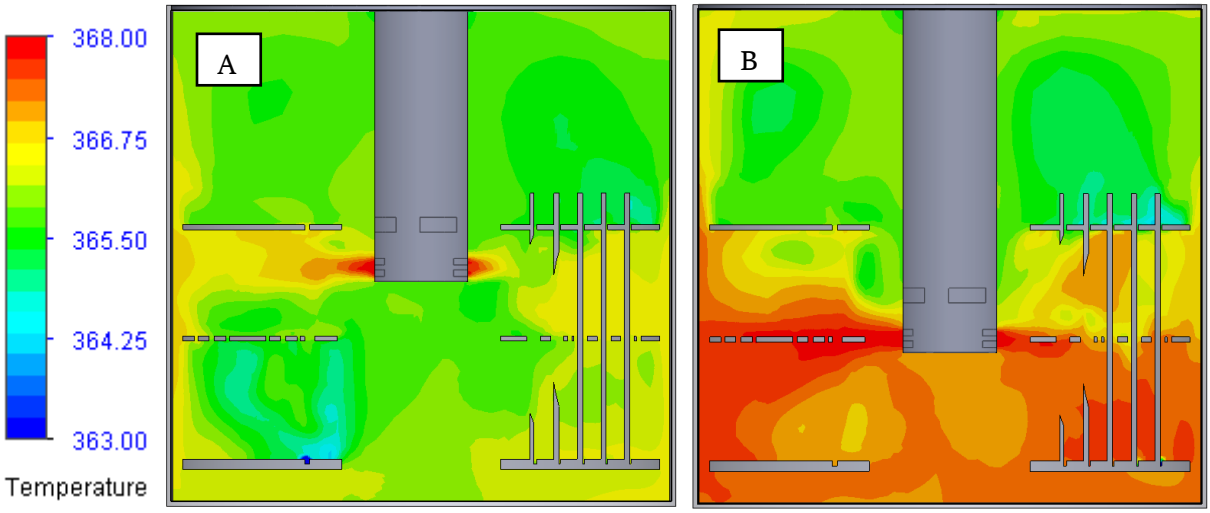

Figure 70: Vertical cross section of temperature profile with the perforated middle plate: (A) raised case, (B) centered case

4.2.8 CFD Analysis of Different Middle Plates

Previously in 4.2.3, the three different middle plate designs were compared with visual dye testing, this section will go on to compare the CFD results between the same three middle plate designs and discuss similarities and differences between these results.

Comparing the velocity profiles of the three designs in Figure 69B and Figure 71A and Figure 71B; they all look very similar with the jet from the sous vide heater outlet being almost symmetrically divided between the two regions separated by the middle plate. However, the biggest difference lies in the bottom half of the carousel for the area on the left of the three graphics. The difference is the velocity of that area increases from the full middle plate design to the skeletonized middle plate, and lastly, the highest velocity would be the perforated plate design. This increased velocity provides the high flow needed to minimize gradients seen throughout the aging cell. The lower flow region on the right side of the graphics with the tensile test coupons is very similar between the three, with nothing significant to mention.

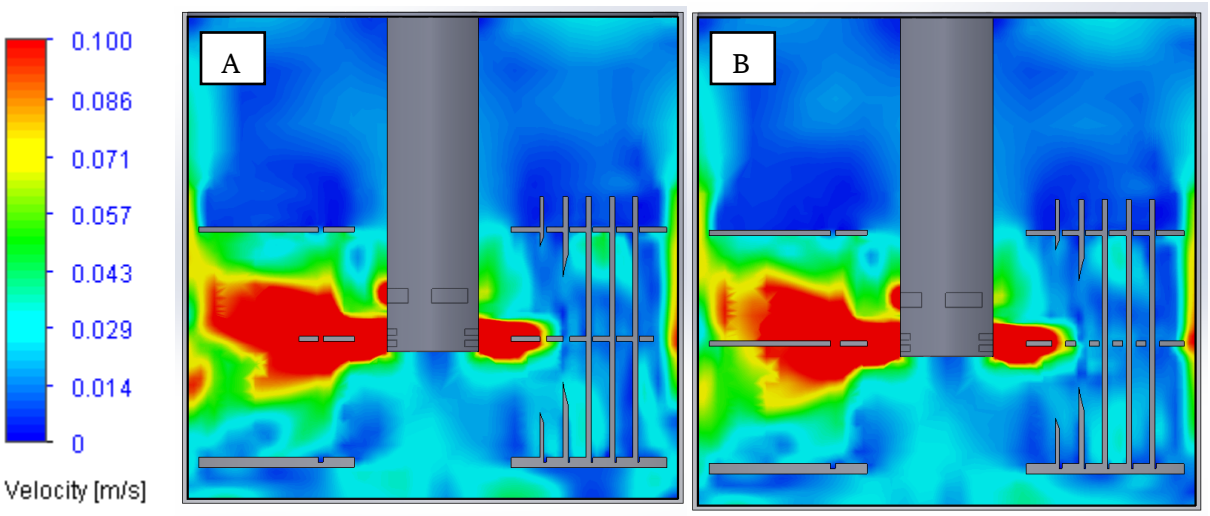

Figure 71: Vertical cross section of velocity profile with: (A) skeletonized middle plate, (B) full middle plate

Looking at the horizontal cross-sections of the velocity profile just below the sous vide heater outlet in Figure 72, it is clear they are still very similar. The full middle plate design of Figure 72C was seen as the worst performer of the three during the visual dye testing and still is in the CFD analysis so far. Figure 72B has a bit more velocity near the larger openings of the skeletonized middle plate on the outer diameter when compared with Figure 72C. Figure 72A has the greatest velocity around the outer diameter when compared with Figure 72B and Figure 72C, taking note of both the areas near the sous vide heater jet and around the 10 to 12 o'clock position.

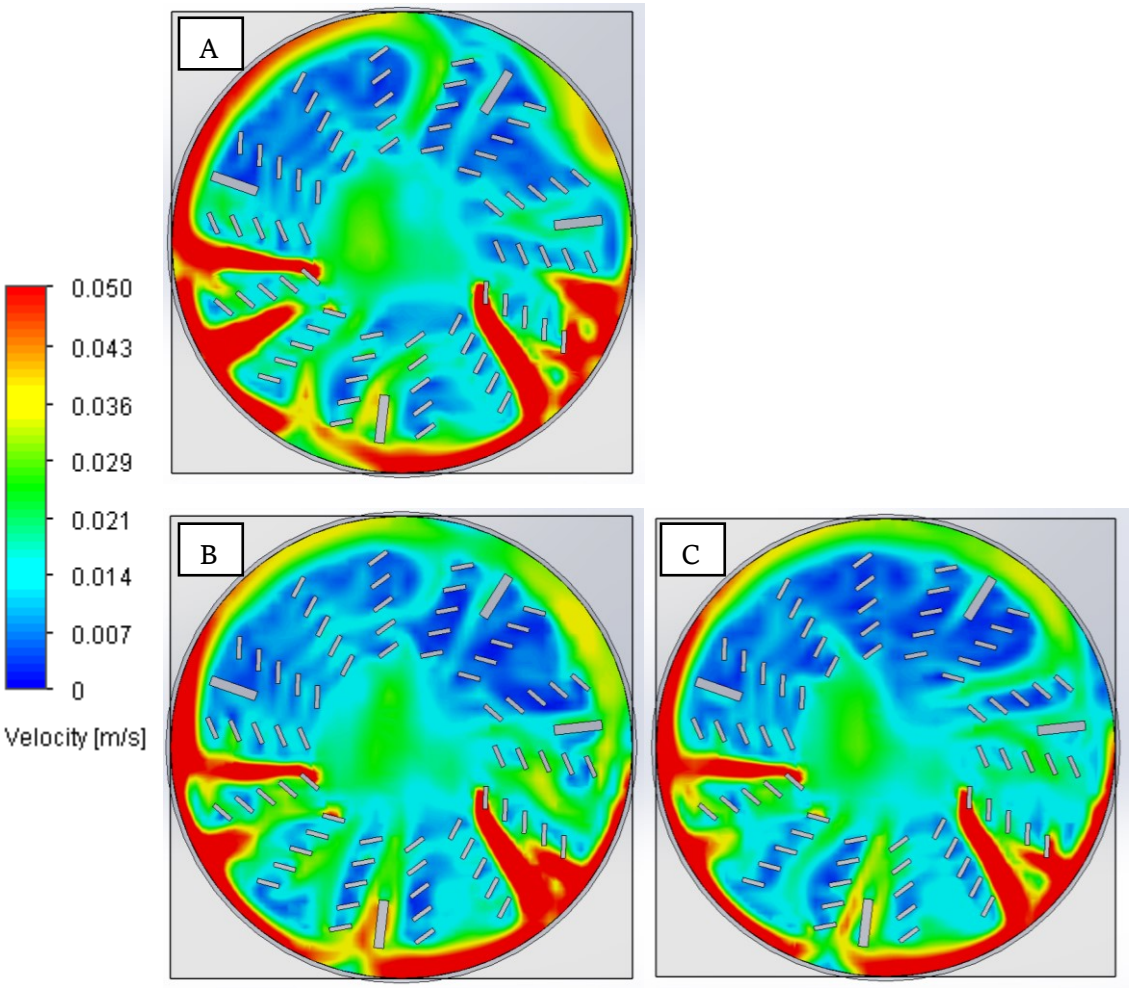

Figure 72: Horizontal cross section of velocity profile for: (A) perforated middle plate, (B) skeletonized middle plate, (C) full middle plate

The vertical cross-section of the thermal gradients paints the same picture as the velocity profile. Figure 70B shows the most uniform temperature gradients within the carousel; the perforated plate helps to allow a more uniform flow within the carousel's upper and lower regions and agrees with what was seen in the visual dye testing. Figure 73A is the next best with the skeletonized plate; it is interesting to note that the gradients above the carousel are the smallest in this design when compared with the other three. However, this is not important as the gauge length of the tensile test coupons is within the carousel boundaries with only the grip areas being exposed above, so it was not taken into consideration when deciding which design had a better thermal gradient for aging. Figure 73B was predicted and confirmed as the worst design for uniform thermal gradients of the three due to the full plate design blocking off the lower region and the visual dye testing also confirmed a region of low flow to exist below the middle plate.

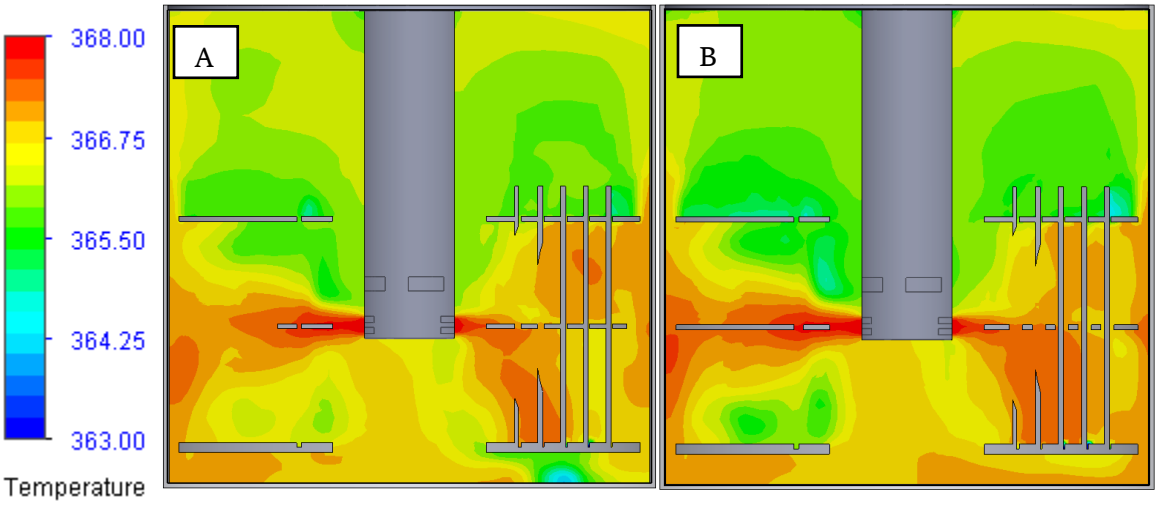

Figure 73: Vertical cross section of temperature profile with: (A) skeletonized middle plate, (B) full middle plate

4.2.9 CFD Analysis of Jar Design

The 2L jars would be the largest the current test setup could accommodate with only a few millimeters of space between the jars and the tank walls or sous vide heater. CFD modeling was done for the three and four glass jar cases. The CFD setup was modified from the previous setups with the addition of subdomains within the jars and solid elements to allow heat conduction between the inner and outer domains. For simplicity, the materials for the lids of the jars were set as glass; the jars were assumed to be floating within the domain and not contacting any surfaces; and the jars were filled to the brim with fluid without tensile test coupons.

Comparing the velocity cross sections of Figure 74 and Figure 75, it is clear that the velocities within the jars are approximately an order of magnitude difference compared with the aging cell. This was expected due to the different mechanisms that generate the flows, with the aging cell being the mechanical motion from the sous vide heater and the jars being natural convection currents that occur due to the temperature gradients. The CFD model of the jars do not have any coupons which would generate further blockage and reduce the flow within the jars. It should also be noted that the three jars are not the same for their velocity gradients due to the surrounding temperature gradients which will be discussed later in this section.

Comparing the velocity cross sections of Figure 74 to Figure 76, it is clear that at this elevation for the horizontal cross section with three jars the average velocity is higher for the fluid as there are fewer obstructions in the fluid flow from the four jars. With the three jar setup in Figure 74B, the jars are spaced perfectly apart to allow the gaps to coincide with the 120° separation between outlets of the sous vide heater and thus provide less of a flow restriction when compared with the four-jar setup's spacing of 90° in Figure 76B.

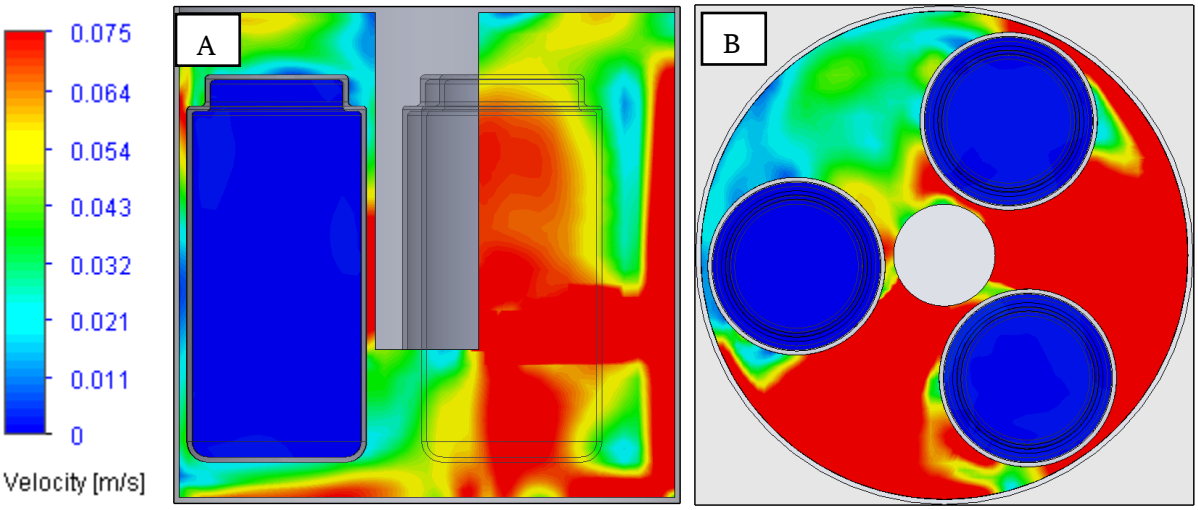

Figure 74: Cross section of velocity profile for the three jar case: (A) Front cross section, (B) horizontal cross section at the sous vide outlet

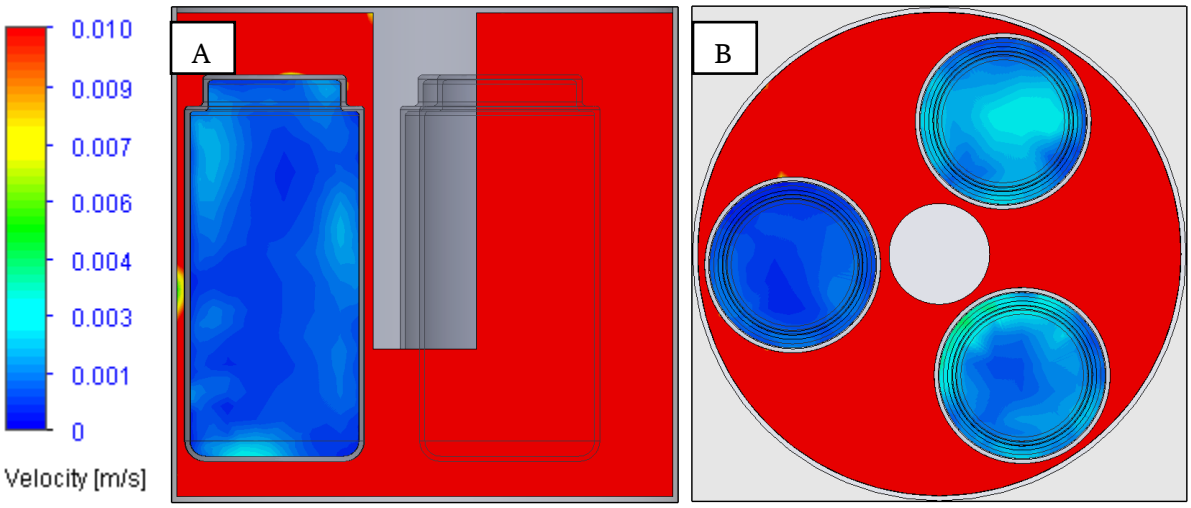

Figure 75: Cross section of velocity profile for the three jar case: (A) Front cross section, (B) horizontal cross section at the sous vide outlet

Comparing the velocity cross sections of Figure 76 and Figure 77, it is also clear that the velocities within the jars are approximately an order of magnitude different than the ones within the aging cell for the same reasons mentioned previously for the three jar scenario. The velocity within the aging cell for the four jar setup is also lower than the three jar setup due to the blockage caused by the placement of the four jars compared with the locations of the sous vide outlet shown in Figure 76B. For more clarity on the outlet placement see Figure 78B. The larger velocity gradients from this setup also causes larger temperature gradients to develop within the aging cell from the heat losses on the walls, this will be discussed further later in this section when the temperature cross sections are shown. But these temperature gradients would drive more natural currents to occur within the jars as seen in Figure 77A/B compared to those seen in Figure 75A/B.

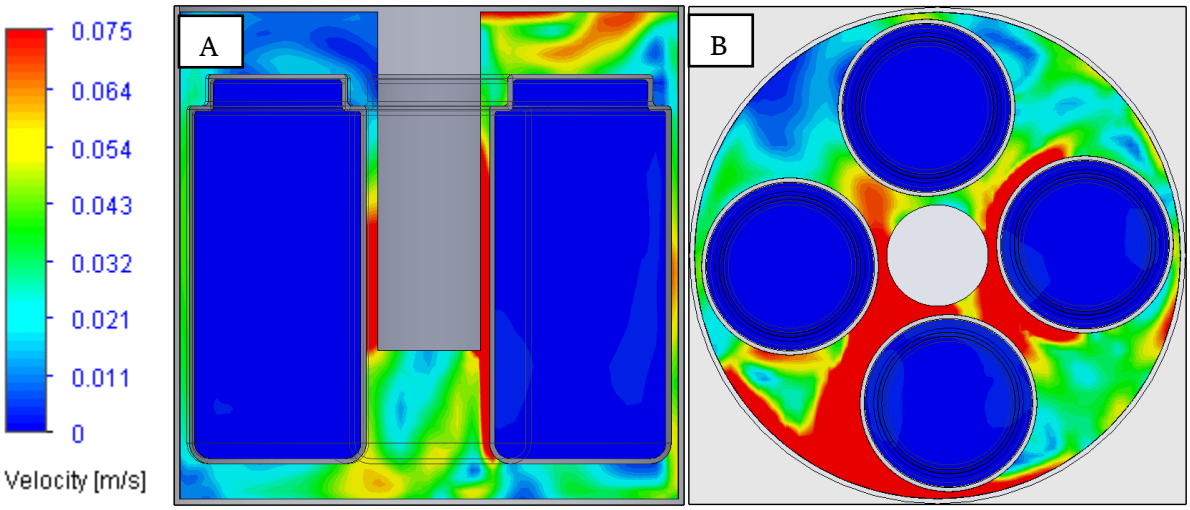

Figure 76: Cross section of velocity profile for the four jar case: (A) Front cross section, (B) horizontal cross section at the sous vide outlet

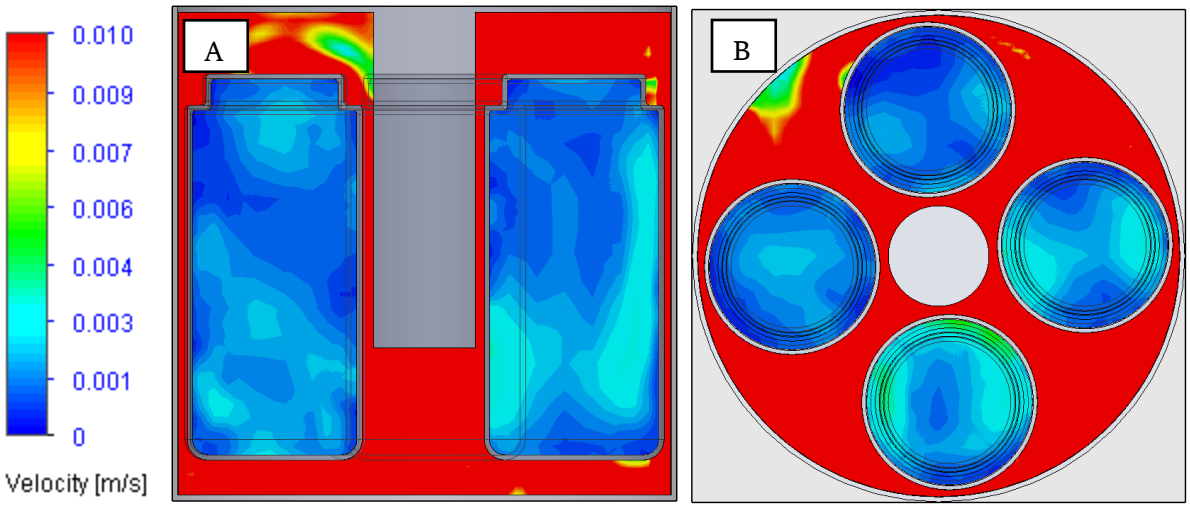

Figure 77: Cross section of velocity profile for the four jar case: (A) Front cross section, (B) horizontal cross section at the sous vide outlet

With the higher flow in the three-jar case, it is expected that there will be a lesser thermal gradient and the CFD results agree with this expectation. The comparison of the three jar to four jar thermal gradients are shown in Figure 78. Figure 78A clearly shows the sous vide heater outlet being unobstructed by the jars and how a slight gradient forms oppsite to the outlets on both sides at the 10 o'clock and 4 o'clock regions. Figure 78C shows only one jar in the cross section due to the layout of the jars, but it is clear that the gradients within the jar is very minor. Figure 78B shows the sous vide outlet being blocked by the jar at the 3 o'clock position and partially obstructed by the jars in the 9 o'clock and 6 o'clock positions. This obstruction causes the larger gradient to form between the 9 o'clock to 2 o'clock position in green shown in Figure 78B. Comparing Figure 78C with Figure 78D it is seen that the lower blockage of the 3 jar setup for this scenario yeilded a slightly higher average temperature than the more blocked 4 jar setup.

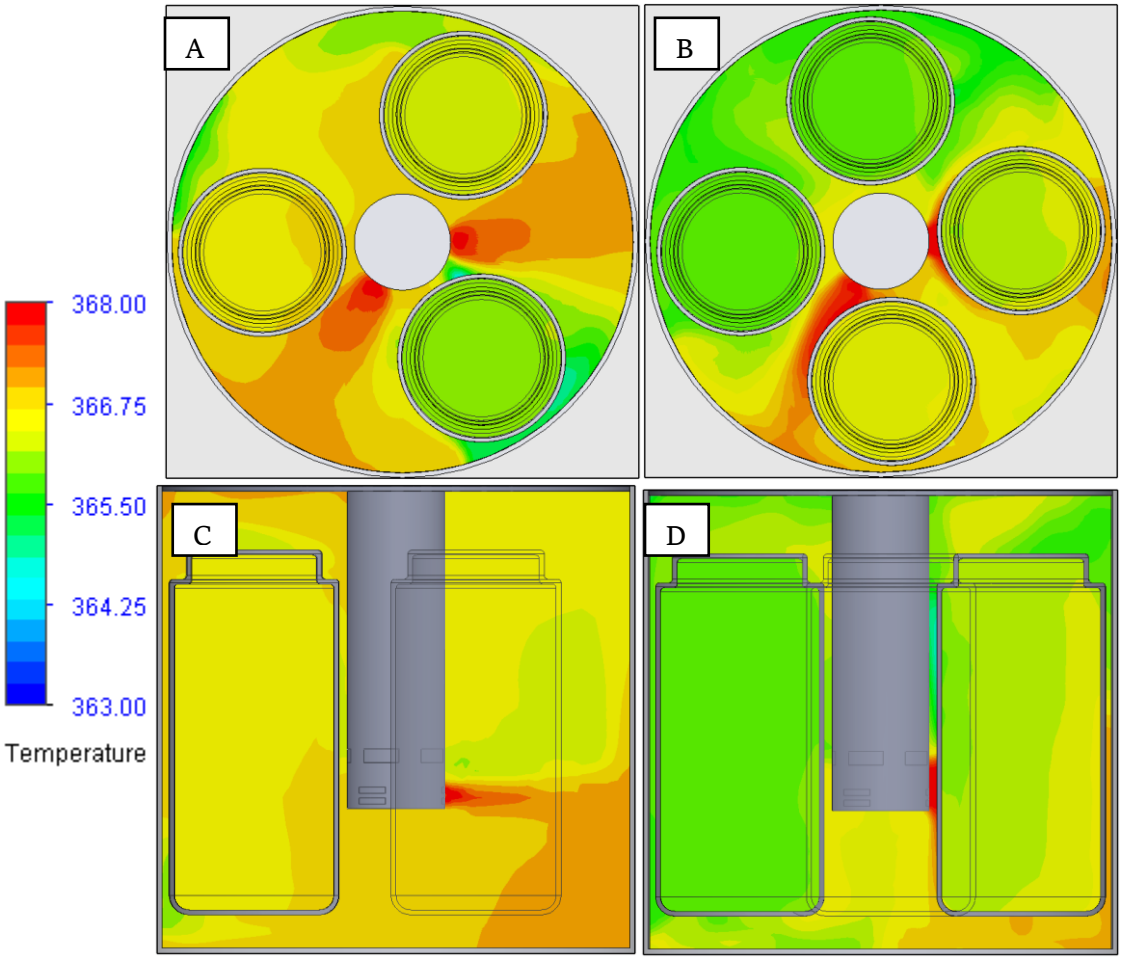

Figure 78: Cross section of temperature profile for the: (A) horizontal for the three jar case, (B) horizontal for the four jar case, (C) vertical for the three jar case, (D) vertical for the four jar case

4.3 Temperature Distribution

This section will discuss the measured thermal gradients of the aging setup utilizing the carousel at three different temperatures. The three temperatures were chosen based on the criteria set by the industry partner for the aqueous aging temperatures; this is to cover the lower, middle, and upper limits of the aqueous aging process conditions. Each test was held at a steady-state temperature for at least 24 hours. It should also be noted that the K-type thermocouples used here generated a decent amount of noise when compared to the newer T-type thermocouples used after the initial data collection. T-type thermocouple results are not shown or discussed here as another researcher performed the work and will be publishing that separately.

4.3.1 Measured Thermal Gradients at 60.0°C

With the same setup as mentioned in 4.1.3, a cumulative 24-hour steady-state temperature average was generated from the thermocouple data. The thermocouples logged data at 30-second intervals over 24 hours at various locations throughout the acrylic aging cell. The thermocouple error is +/- 2.2°C, however; it would be more useful to utilize all of the data and show the error as the standard deviation as shown in Figure 79. The error bars thus show the spread of the data across all the thermocouple measurements within one standard deviation. This shows the spread of the data is very tight when compared with the 82.0°C and 95.0°C tests. There is also not much variation or gradients within the measured sample. The data points shown are based on an hourly average of the data. Averaging the data shows a more realistic true temperature and eliminates some of the random variations due to the error in the thermocouple readings. However, this method also diminishes the effect of any minor gradients seen in the experiment.

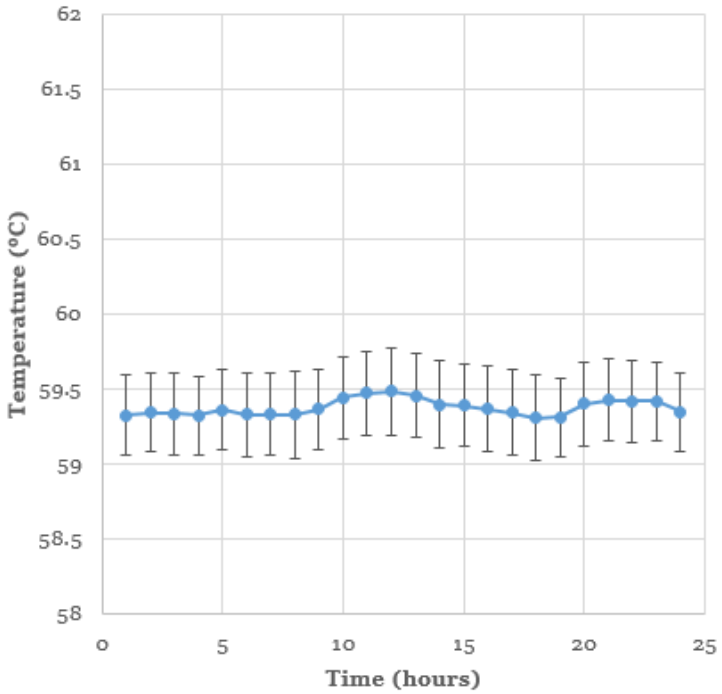

Figure 79: Acrylic aging cell measured thermal gradients over 24 hours at 60.0°C

4.3.2 Measured Thermal Gradients at 82.0°C

The same setup as 4.1.4 was used along with the same data collection frequency and graphs as 4.3.1. The average temperature of the aging cell is shown in Figure 80 and is stable like in Figure 79. The standard deviation, represented by the error bars, is much larger than those of the previous test. As the same data logging instruments were used this difference is caused by a combination of the different setups and temperature ranges. The stainless steel aging cell has a larger surface area due to the two inches taller height and is at a higher temperature; this combination of factors will greatly increase the heat losses and as shown previously.

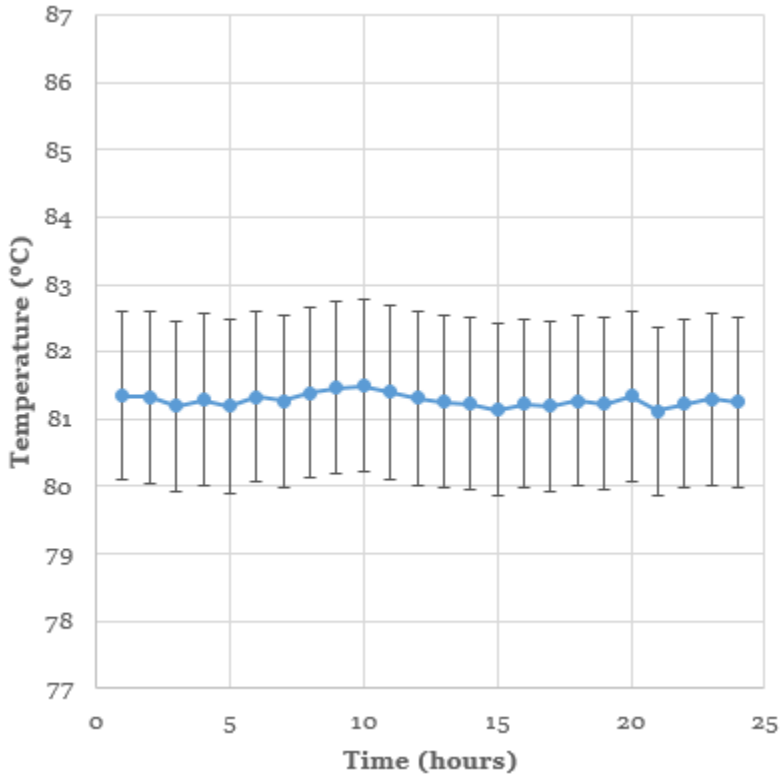

Figure 80: Stainless steel aging cell measured thermal gradients over 24 hours at 82.0°C

The idea that larger gradients are forming within the aging cell at higher heat losses is intuitive. The layer of water nearest to the walls would be cooler and generate some natural convection currents, but would still be dominated by diffusion as the temperature differences are small. As diffusion is a slow process this thus allows the gradients to form.

4.3.3 Measured Thermal Gradients at 95.0°C

The same setup as 4.1.5 was used along with the same data collection frequency and graphs as 4.3.1. The results of the 95.0°C test showed very similar results to the 82.0°C test. The average temperature in Figure 81 was steadier than in Figure 80 but more varied than in Figure 79. The standard deviation was large and in the same range as Figure 80.

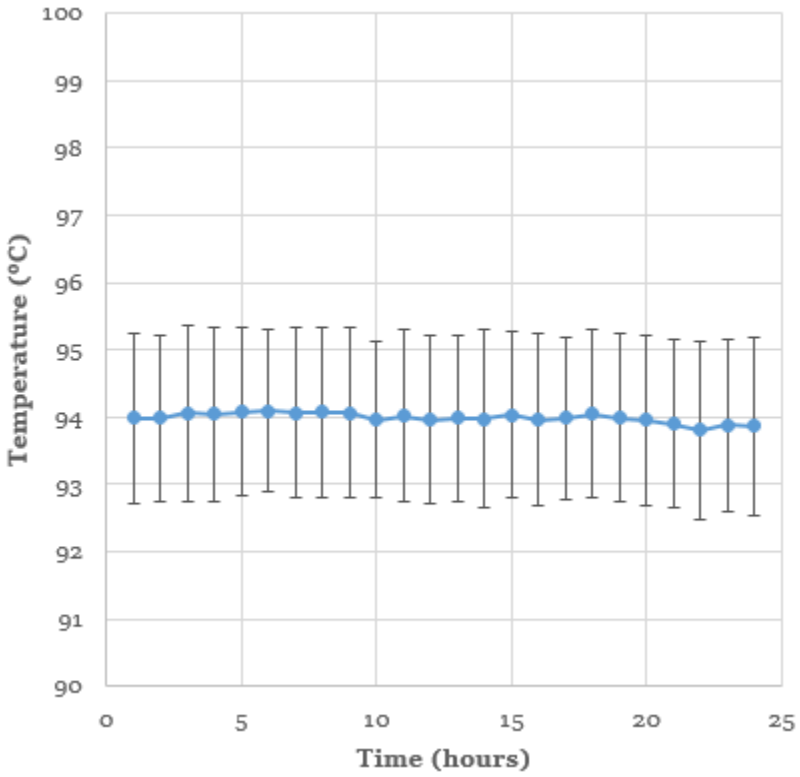

Figure 81: Stainless steel aging cell measured thermal gradients over 24 hours at 95.0°C

5 Ongoing Activities

Due to our industry partner's direction, the coupon aging activities have been delayed one year as of writing this thesis. To validate the performance of this setup, testing has begun with flexible fiber tapes; due to their buoyancy, the jar method was utilized to contain the tapes being placed in the aging tank. Two types of fiber glass tapes are being tested, each either impregnated with high density polyethylene (HDPE) or polypropylene (PP). The results of this aging study will be published by another researcher; so it will not be discussed here in depth. However, the main points regarding the utilization of the aging setup are delineated.

After running both metal and acrylic aging setups for ten continuous weeks, no major deficiencies were found and the setup performed as expected. The metal aging setup was set at 96.0°C and the acrylic aging setup at 60.5°C with weekly samples of the fiber glass tapes removed for testing. No equipment failures or abnormal temperature deviations were noticed. The only deficiency noted was the power supply in the lab; the breaker had tripped on a few occasions when other activities were being performed in the lab. This caused a temporary interruption to the power but no significant effects were noted as the power was restored within minutes each time. The 15 amp breakers in the lab were shared with other equipment and were overloaded accidentally causing the trips.

Evaporative losses for both metal and acrylic aging setups were noted as minimal; with approximately 1cm of water height loss within the aging cell per week. This amounts to approximately one liter of evaporative loss per week. About the same amount of evaporative loss was noted for these setups regardless of the temperature difference between them. This is due to the metal aging cell having a gasket seal on the lid while the acrylic aging cell does not. This balances out the expected losses due to the higher temperature

of the better sealed metal aging cell with the lower temperature of the less well sealed acrylic aging cell.

Gradient measurements at various locations in the aging cell showed a max deviation of +/-1.0°C, which is within the rated accuracy of the T-type thermocouples. It is hypothesized that the actual thermal gradients are smaller, but without a more accurate measurement instrument this cannot be confirmed at this time. Both setups utilized tap water as the buffer fluid (within the aging tank) and deionized water within the jars containing the fiber glass tapes.

Of note, the standard deviation from Figure 81's dataset for the 95.0°C test utilizing K-type thermocouples was 1.26°C while another test done at the same temperature utilizing more accurate T-type thermocouples yielded a standard deviation of only 0.177°C. The mean temperature from the 95.0°C test utilizing K-type thermocouples was 94.0°C compared with the same test utilizing T-type thermocouples mentioned above yielding a mean of 94.8°C, both of these values are within the accuracy of the thermocouples (K-type being +/-2.2°C and T-type being +/-1.0°C) from the set point of 95.0°C on the sous vide heater controller. The data taken utilizing the T-type thermocouples were therefore much less noisy when compared with the previous data taken utilizing K-type thermocouples.

Below in Figure 82 are some samples of the fiber glass tapes in their various states of testing. The HDPE fiber glass tapes began to curl at the onset of aging and was prone to catastrophically breaking during the tensile testing; so the ends of the tapes had to be reinforced prior to testing to provide repeatable results. The PP tapes remained straight after the aging process and was not prone to catastrophically breaking during the tensile testing. After two weeks of aging at 96.0°C in deionized water the PP fiber glass tapes degraded by 35% of its tensile strength and the HDPE fiber glass tapes degraded by 50% of its tensile strength. The manufacturer of these tapes did not provide

published aging degradation values for comparison. However, the successful tests over the four weeks have provided evidence that the experimental setup functions as intended. The tape samples in Figure 82 had a length of 9 inches with a gauge length of 5 inches.

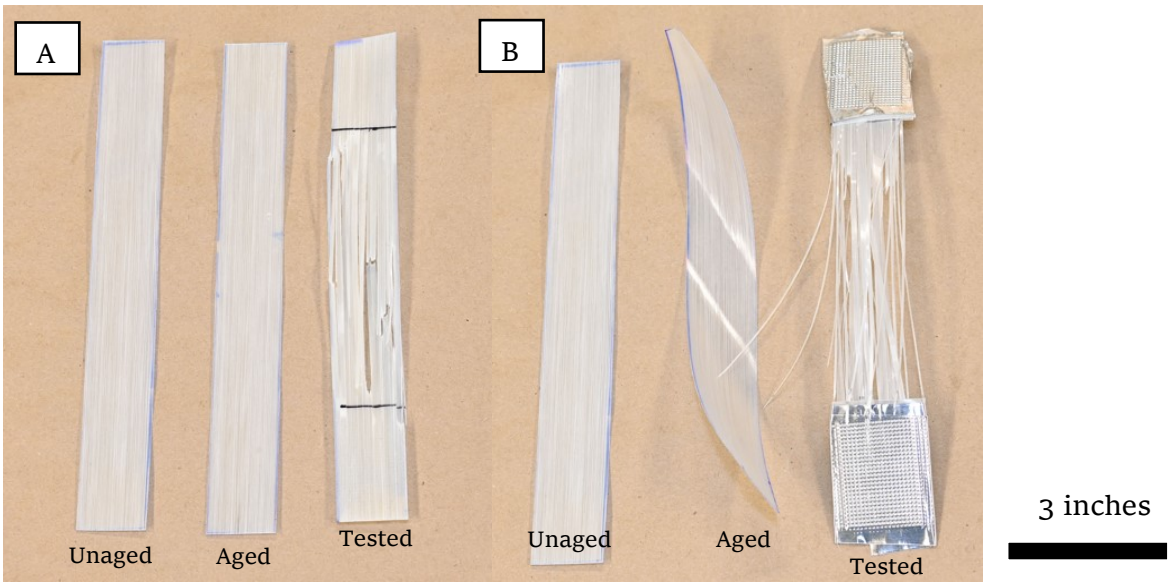

Figure 82: Fiber glass tapes: (A) PP impregnated from left to right unaged, 2 week aged, 2 week aged and tensile tested; (B) HDPE impregnated from left to right unaged, 2 week aged, 2 week aged and tensile tested

6 Conclusions

It was hypothesized that by investing time and innovation into a design, improved testing processes and thus comprehensive insights into material degradation mechanisms can be achieved. Not all of the investments yielded successful results, however, much was learned from this experience. The author hopes that this work will benefit others in their future designs and experiments. One can learn a lot from others' works and this can be a small stepping stone for someone.

6.1 Fiber Aging Fixture

The chosen fiber fixture, design G, was not successful in providing a low-cost alternative that could satisfy the industry partner's objectives. The root cause of this was not fully investigated as the industry partner directed efforts towards another concept design providing a small improvement of their existing design; to yield quicker results as their internal deadlines were fast approaching. The next chosen design E lacks one key objective, which was to minimize the handling of the aged fibers as they can be quite fragile after aging. However, design E can utilize the existing water bath setups but not the new aging cell setup.

6.2 Coupon Aging Fixture

The aging carousel met all the design objectives set forth by the industry partner. The carousel provides excellent access to the test coupons and allows for removal of them with minimal impact on the experiment; provides adequate mixing as indicated by the dye tests and CFD simulations; can accommodate the number of coupons required; can accommodate various sizes of test coupons; and ease of manufacture owing to the use of readily available parts and 2D manufacturing.

6.3 Aging Setup

The aging setup has met all the design objectives set forth by the industry partner. The setup provides a relatively large heat capacitance due to the volume of water and minimizes the impact of thermal gradients. The large volume also provides an adequate buffer for evaporative losses and allowance for the replenishment or steady exchange of test fluids with uncontaminated fresh fluids. Insulation on the tank is minimal at the moment but easily can be scaled up to reduce heat losses and improve upon the already minimal thermal gradients. Thermal gradient measurements are very promising and much lower when compared with the industry partner's previous setup. The setup can also accommodate the many different test fluids owing to the resilience of stainless steel against the harsh process conditions; some small aspects of the setup would need to be upgraded in certain applications such as with hydrocarbon solvents or higher temperatures. The aging setup is cost-effective and smaller compared with the commercially available alternative.

7 Future Work

Ongoing aging activities currently include validation testing on the design setup utilizing the jar method as mentioned in the previous section. Below are the key points for future work on the improvement of the aging setup.

7.1 Fiber Aging Fixture

Fiber fixture design G should be investigated further for the root cause of why it caused the fibers to fail prematurely compared with the other methods. Design changes and iterations can be used to help reveal the root cause of the discrepancy. For now, design E will move forward as it yields consistent results. As mentioned previously, another researcher will be continuing work on these fiber fixtures and their aging.

7.2 Coupon Aging Fixture

Aging trials should be conducted between both the final iteration of the carousel design and the jar method our industry partner proposed. The differences between the two setups can be quantified experimentally by the thermal gradient measurements and the repeatability of the tensile test data compared with published results. Further improvements can be made to the carousel to more evenly distribute the flow around the test coupons. The jar method for tensile test coupons can be investigated further as per the industry partner's direction.

7.3 Aging Setup

Utilization of the more accurate T-type thermocouples is highly recommended for all future data collection as it is shown to have much lower noise and higher accuracy when compared with the K-type thermocouples. Extra insulation should be added to the aging cell focusing on covering the uninsulated areas as they provided the highest heat losses; more insulation will help further reduce thermal gradients and reduce power consumption which will generate cost savings for the long-duration aging experiments.

Pressurization of the aging setup can be explored as the industry partner wishes to conduct experiments at higher temperatures where pressurization is required to maintain the fluids as liquids. However, specific emphasis should be placed on the safety and adherence to the pressure vessel regulations in our province as the current setup was intended for non-pressurized service.

Utilization of different aging fluids and temperatures may also require design changes to the existing aging setup. The current sous vide heater will need to be changed to maintain above 100°C with a glycol and water mixture. For utilizing hydrocarbon solvents, the electrical devices area classification along with the tank sealing methods should also be revisited as flammable hydrocarbon fumes poses a new hazard from the existing setup.

References

[1] ASTM, D638 Standard Test Method for Tensile Properties of Plastics, West Conshohocken, PA, USA: Library of Congress, 2010.

[2] ASTM, A370 Standard Test Methods and Definitions for Mechanical Testing of Steel Products, West Conshohocken, PA, USA: Library of Congress, 2016.

[3] ASTM, D3039 Standard Test Method for Tensile Properties of Polymer Matrix Composite Materials, West Conshohocken, PA, USA: Library of Congress, 2000.

[4] ASTM, E3205 Standard Test Method for Small Punch Testing of Metallic Materials, West Conshohocken, PA, USA: Library of Congress, 2020.

[5] Shawcor, "Linepipe Products," Shawcor, [Online]. Available: https://www.shawcor.com/composite-systems/composite-linepipe/linepipe-products. [Accessed 22 06 2023].

[6] SoluForce, "What is a Reinforced Thermoplastic Pipe (RTP) or Flexible Composite Pipe (FCP)?," SoluForce, [Online]. Available: https://www.soluforce.com/product-overview/what-is-an-fcp-rtp.html. [Accessed 25 06 2023].

[7] Fabco, "FRP Pressure Pipe," Fabco, [Online]. Available: https://www.fabcoplastics.com/product-detail/frp-pipe-1?cid=14. [Accessed 26 06 2023].

[8] Topolo, "RTP Pipes," Topolo, [Online]. Available: https://topolocfrt.com/reinforced-thermoplastic-pipe/. [Accessed 26 06 2023].

[9] ASTM, F1980 Standard Guide for Accelerated Aging of Sterile Medical Device Packages, New York: ASTM, 2002.

[10] ASTM, D3045 Standard Practice for Heat Aging of Plastics Without Load, New York: ASTM, 2003.

[11] ASTM, E1640 Standard Test Method for Assignment of the Glass Transition Temperature by Dynamic Mechanical Analysis, New York: ASTM, 2020.

[12] F. Micelli and A. Nanni, "Issues related to durability of FRP reinforcement for RC structures exposed to accelerated aging," in *American Society of Composites 16th Annual Conference*, Blacksburg, 2001.

[13] S. Shah, J. Daniel and D. Ludirdja, "Toughness of Glass Fiber reinforced concrete panels subjected to accelerated aging," *PCI Journal,* vol. 32, no. 5, pp. 82-99, 1987.

[14] M. A. Silva, B. Sena da Fonseca and H. Bis, "On estimates of durability of FRP based on accelerated tests," *Composite Structures,* vol. 116, pp. 377-387, 2014.

[15] R. Bernstein, D. Derzon and K. T. Gillen, "Nylon 6.6 accelerated aging studies: thermal-oxidative degradation and its interaction with hydrolysis," *Polymer Degradation and Stability,* vol. 88, no. 3, pp. 480-488, June 2005.

[16] E. Dootz, A. 3. Koran and R. Craig, "Physical properties of three maxillofacial materials as a function of accelerated aging.," *The Journal of Prosthetic Dentistry,* vol. 71, no. 4, pp. 379-383, 1994.

[17] M. Frigione and A. Rodríguez-Prieto, "Can Accelerated Aging Procedures Predict the Long Term Behavior of Polymers Exposed to Different Environments?," *Polymers,* vol. 13, no. 16, p. 2688, 2021.

[18] A. Mahmoud, H. Ammar, O. Mukdadi, I. Ray, F. Imani, A. Chen and J. Davalos, "Non-destructive ultrasonic evaluation of CFRP–concrete specimens subjected to accelerated aging conditions," *Ndt & E International,* vol. 43, no. 7, pp. 635-641, 2010.

[19] A. Kumar, R. Singh and B. Sarwade, "Degradability of composites, prepared from ethylene–propylene copolymer and jute fiber under accelerated aging and biotic environments," *Materials chemistry and physics,* vol. 92, no. 2-3, pp. 458-469, 2005.

[20] M. Madhkhan and P. Saeidian, "Mechanical Properties of Ultra-high Performance Concrete Reinforced by Glass Fibers under Accelerated Aging," *International Journal of Engineering,* vol. 34, no. 5, pp. 1074-1084, 2021.

[21] F. Micelli and A. Nanni, "Durability of FRP rods for concrete structures," *Construction and Building materials,* vol. 18, no. 7, pp. 491-503, 2004.

[22] A. Tuncdemir and F. Aykent, "Effects of fibers on the color change and stability of resin composites after accelerated aging," *Dental Materials Journal,* vol. 31, no. 5, p. 872–878, 2012.

[23] Fisher Scientific, "Circulating Baths," Fisher Scientific, [Online]. Available:

https://www.fishersci.ca/ca/en/browse/90088140/circulating-baths. [Accessed 2 12 2022].

[24] Omega, "Immersion Heaters," Omega, [Online]. Available: https://www.omega.co.uk/section/immersion-heaters.html. [Accessed 1 1 2023].

[25] Fisher Scientific, "General Purpose Water Baths," Fisher Scientific, [Online]. Available: https://www.fishersci.ca/ca/en/browse/90088124/general-purpose-water-baths. [Accessed 2 12 2022].

[26] ASTM, G154 Standard Practice for operating fluorecent light apparatus for UV exposure of nonmetallic materials, West Conshohocken, PA, USA: Library of Congress, 2006.

[27] Omico Plastics Inc, "PLASTICS VS. POLYMERS: WHAT'S THE DIFFERENCE?," [Online]. Available: https://omicoplastics.com/blog/plastics-polymers-difference/#:~:text=Polymers%20can%20exist%20organically%20or,not%20all%20polymers%20are%20plastics.. [Accessed 29 06 2023].

[28] H. Webb, J. Arnott, R. Crawford and E. Ivanova, "Plastic Degradation and Its Environmental Implications with Special Reference to Poly(ethylene terephthalate)," *Polymers,* vol. 5, no. 1, pp. 1-18, 2013.

[29] R. C. Thompson, C. J. Moore, F. S. v. Saal and S. H. Swan, "Plastics, the environment and human health: current consensus and future trends," *Philos Trans R Soc Lond B Biol Sci.,* vol. 364, no. 1526, pp. 2153-2166, 2009.

[30] C. David, "Thermal Degradation of Polymers," *Comprehensive Chemical Kinetics,* vol. 14, pp. 1-173, 1975.

[31] S. Kliem, M. Kreutzbruck and C. Bonten, "A review on degradation of polymeric material in the environment," *Materials,* vol. 13, no. 20, p. 4586, 2020.

[32] W. White, "Theory of Corrosion of Glass and Ceramics," in *Corrosion of glass, ceramics and ceramic superconductors*, Norwich NY, Noyes Publications, 1992.

[33] J. Tu, H. Xie and K. Gao, "Prediction of the Long-Term Performance and Durability of GFRP Bars under the Combined Effect of a Sustained Load and Severe Environments," *Materials,* vol. 13, no. 10, p. 2341, 2020.

[34] M. Buijs, "Erosion of Glass as Modeled by indentation Theory," *Journal of the American Ceramic Society,* vol. 77, no. 6, pp. 1676-1678, 1994.

[35] P. Frugier, Y. Minet, N. Rajmohan, N. Godon and S. Gin, "Modeling glass corrosion with GRAAL," *npj Materials Degradation,* vol. 2, no. 35, 2018.

[36] J. Thomason, U. Nagel, L. Yang and E. Sáez, "Regenerating the strength of thermally recycled glass fibres using hot sodium hydroxide," *Composites Part A: Applied Science and Manufacturing,* vol. 87, no. August, pp. 220-227, 2016.

[37] M. Kolli, M. Hamidouche, N. Bouaouadja and G. Fantozzi, "HF etching effect on sandblasted soda-lime glass properties," *Journal of the European Ceramic Society,* vol. 29, no. 13, pp. 2697-2704, 2009.

[38] S. Arrhenius, "Über die Dissociationswärme und den Einfluss der Temperatur auf den Dissociationsgrad der Elektrolyte," *Zeitschrift für Physikalische Chemie,* vol. 4, pp. 96-116, 1889.

[39] ASTM, D2256 Standard Test Method for Tensile Properties of Yarns by the Single-Strand Method, New York: ASTM, 2021.

[40] F. Ellyin and C. Rohrbacher, "Effect of Aqueous Environment and Temperature on Glass Fibre Epoxy Resin Composites," *Journal of Reinforced Plastics and Composites,* vol. 19, no. 17, pp. 1405-1423, 2000.

[41] F. Ellyin and C. Rohrbacher, "The influence of aqueous environment, temperature and cyclic loading on glass-fiber/epoxy composite laminates," *Journal of Reinforced Plastics and Composites,* vol. 22, no. 7, pp. 615-622, 2003.

[42] X. Zhang and Z. Deng, "Effects of Seawater Environment on the Degradation of GFRP Composites by Molecular Dynamics Method," *Polymers,* vol. 14, no. 14, p. 2804, 2022.

[43] ABSA, "AB-525 Overpressure Protection Requirements," 13 12 2021. [Online]. Available: https://www.absa.ca/media/1212/ab-525_opp_requirements_for_pv_and_pp.pdf. [Accessed 4 12 2022].

[44] Canadian Standards Association, CSA B51:19. Boiler, pressure vessel, and pressure piping code, Mississauga, Ontario: Canadian Standards Association, 2019.

[45] American Petroleum Institute, Damage Mechanisms Affecting Fixed Equipment in the Refining Industry, 200 Massachusetts Avenue, NW, Suite 1100, Washington, DC 20001.: API Publishing Services, 2020.

[46] MetalMiner, "Carbon Steel Prices," [Online]. Available: https://agmetalminer.com/metal-prices/carbon-steel/. [Accessed 10 07 2023].

[47] MetalMiner, "Stainless Steel Prices," [Online]. Available: https://agmetalminer.com/metal-prices/stainless-steel/. [Accessed 10 07 2023].

[48] A. Rustandi, N. M. Faisal Rendi and S. Setiawan, "The Use of Cyclic Polarization Method for Corrosion Resistance Evaluation of Austenitic Stainless Steel 304L and 316L in Aqueous Sodium Chloride Solution," *International Journal of Mechanical Engineering and Robotics Research,* vol. 6, no. 6, pp. 512-518, November 2017.

[49] ASTM, Handbook of Comparative World Steel Standards ASTM DS67B, West Conshohocken, PA, USA: Library of Congress, 2004.

[50] American Society of Mechanical Engineers, ASME Boiler & Pressure Vessel Code Sec II Part D, New York, NY: The American Society of Mechanical Engineers, 2017.

[51] C. P. Dillon, Materials Selection for the Chemical Process Industries, Second Edition, Materials Technology Institute, 2004.

[52] A. International, "General information and Physical Properties of Plexiglas," Altuglas International.

[53] L.-F. Wu and M.-J. Tsai, "Effect of laser plasma on Nd:YAG laser drilling of acrylic plate with high optical density," *Optics & Laser Technology,* vol. 149, no. May, 2022.

[54] McMaster-Carr, "Clear Scratch- and UV-Resistant Cast Acrylic Tubes," McMaster-Carr, [Online]. Available: https://www.mcmaster.com/pipe/material~acrylic-plastic/. [Accessed 6 12 2022].

[55] J. Carter and S. Cramer, "Corrosion Resistance of Some Commercially Available Metals and Alloys to Geothermal Brines.," in *Corrosion*

Problems in Energy Conversion and Generation, Pennington, NJ, The Electrochemical Society, 1974, pp. 240-250.

[56] ABSA, "AB-516 PESR User Guide 3rd Edition Rev 0," 2020.

[57] Trendhim, "4 questions to ask before buying a skeleton watch," [Online]. Available: https://www.trendhim.ca/articles/403/4-questions-to-ask-before-buying-a-skeleton-watch?th_source_locale=en-US. [Accessed 15 07 2023].

[58] Holland Watch Group, "Skeleton Watches," [Online]. Available: https://www.hollandwatchgroup.com/skeleton-watches/. [Accessed 15 07 2023].

[59] V. Dimbleby, "GLASS FOR PHARMACEUTICAL PURPOSES," *Journal of Pharmacy and Pharmacology,* vol. 5, no. 1, pp. 1-1064, 1953.

[60] C-Therm, "The Thermal Conductivity of Unfilled Plastics," C-Therm, Fredericton, 2019.

[61] Dow Chemical Canada ULC, "STYROFOAM™ Brand SM Extruded Polystyrene Foam Insulation," Dow Chemical Canada ULC, Calgary.

[62] Electronic Temperature Instruments LTD, "Emissivity Table," Electronic Temperature Instruments LTD, Worthing.

[63] Y. A. Çengel, Heat Transfer: A Practical Approach 2nd Edition, New York: McGraw Hill, 2002.

[64] Omega, "Thermocouple K-Type," Omega, [Online]. Available: https://assets.omega.com/pdf/tables_and_graphs/thermocouple-type-k-celsius.pdf. [Accessed 01 07 2023].

[65] E. Education. [Online]. Available: https://energyeducation.ca/encyclopedia/Specific_heat_capacity. [Accessed 3 12 2022].

[66] D. Systems, "Smartcells Enabling Fast and Accurate CFD," Solidworks, 2018.

Appendix A – Concept Drawings for Fiber Fixtures

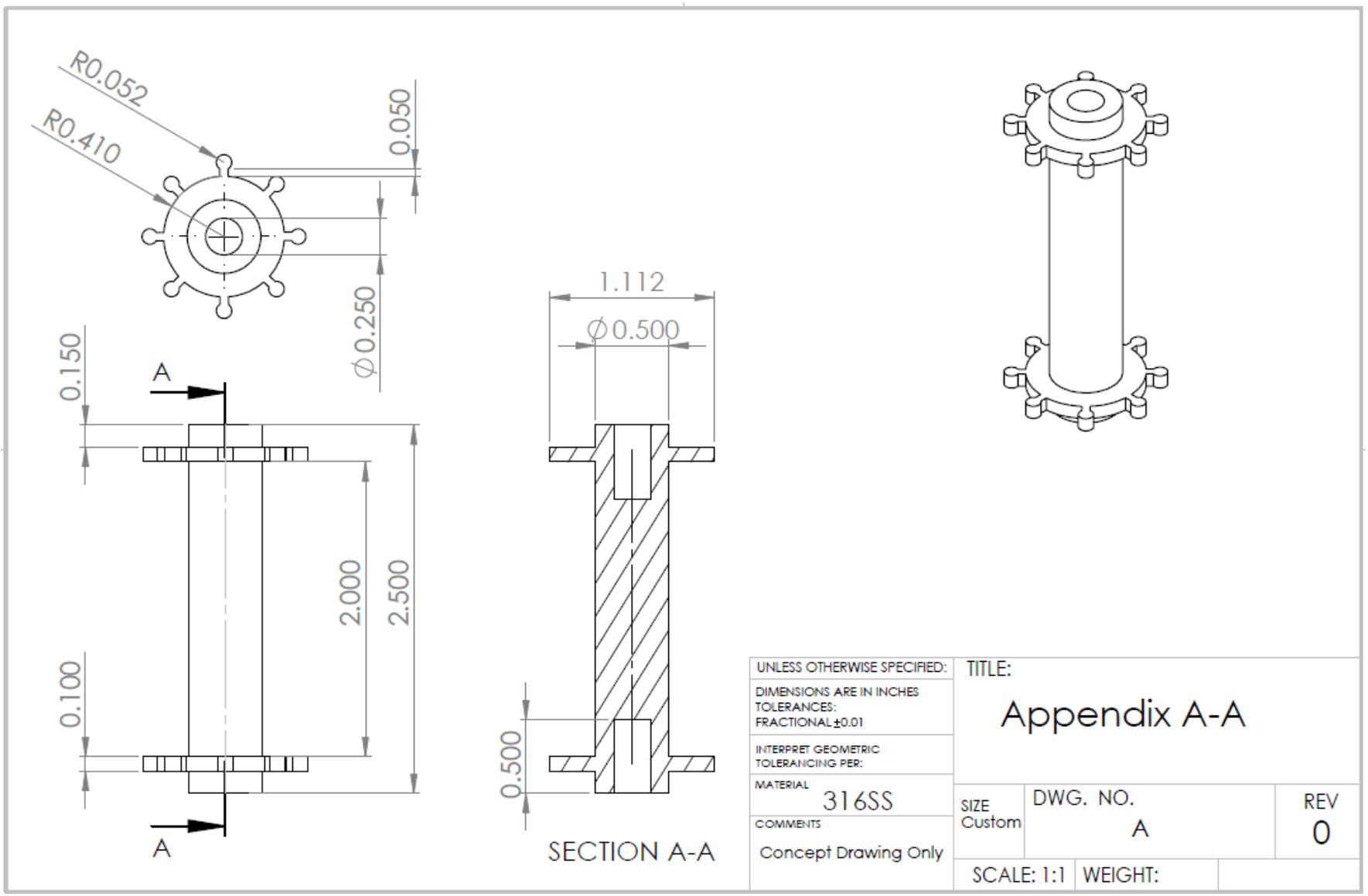
R0.052
R0.410
0.050
⌀0.250
0.150
A
2.000
2.500
0.100
A
1.112
⌀0.500
0.500
SECTION A-A
UNLESS OTHERWISE SPECIFIED:
DIMENSIONS ARE IN INCHES
TOLERANCES:
FRACTIONAL ±0.01
INTERPRET GEOMETRIC TOLERANCING PER:
MATERIAL
316SS
COMMENTS
Concept Drawing Only
TITLE:
Appendix A-A
SIZE
Custom
DWG. NO.
A
REV
0
SCALE: 1:1
WEIGHT:

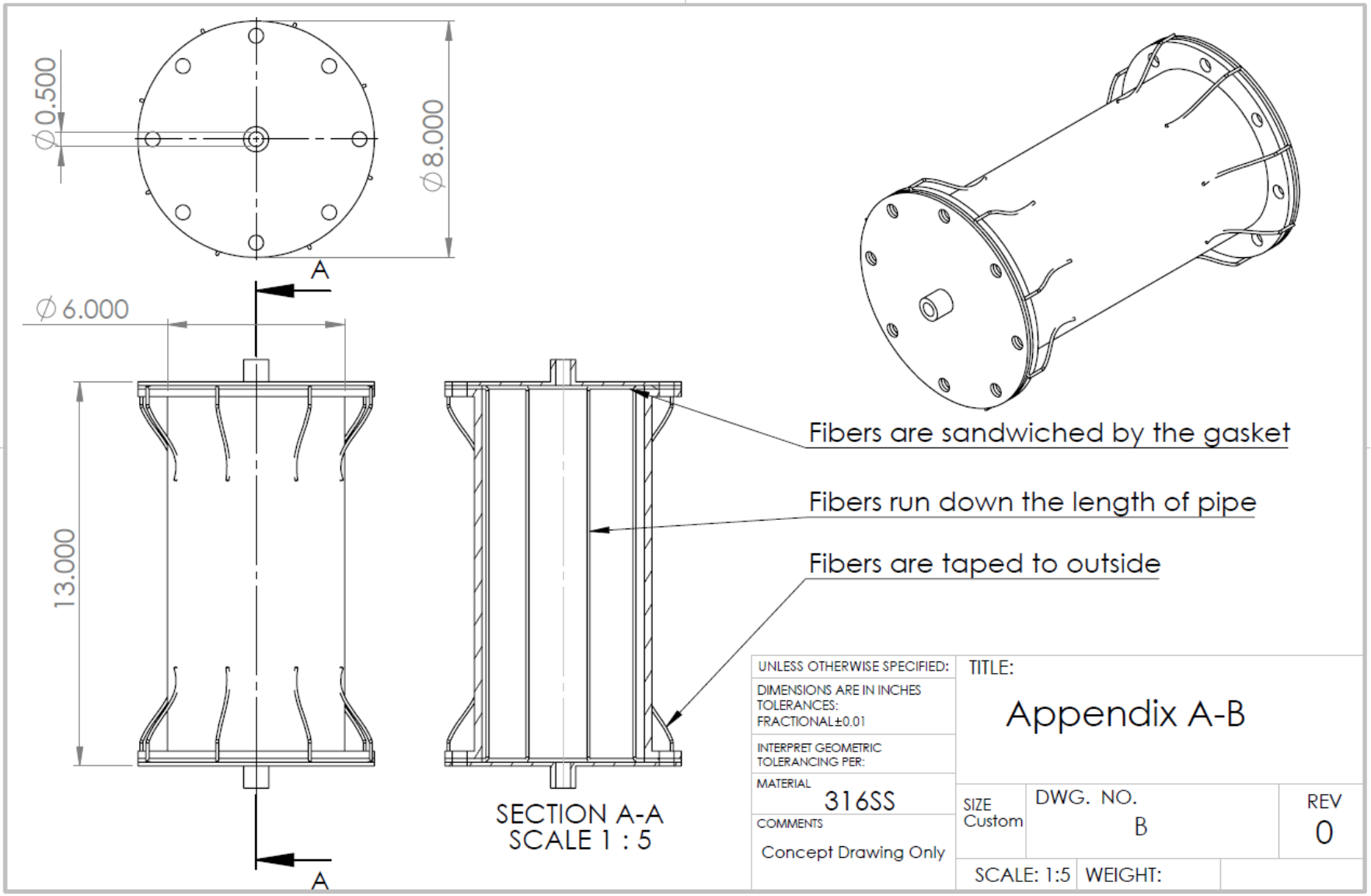
∅0.500
∅8.000
A
∅6.000
13.000
A
SECTION A-A
SCALE 1 : 5
Fibers are sandwiched by the gasket
Fibers run down the length of pipe
Fibers are taped to outside
UNLESS OTHERWISE SPECIFIED:
DIMENSIONS ARE IN INCHES
TOLERANCES:
FRACTIONAL±0.01
INTERPRET GEOMETRIC TOLERANCING PER:
MATERIAL
316SS
COMMENTS
Concept Drawing Only
TITLE:
Appendix A-B
SIZE
Custom
DWG. NO.
B
REV
0
SCALE: 1:5
WEIGHT:

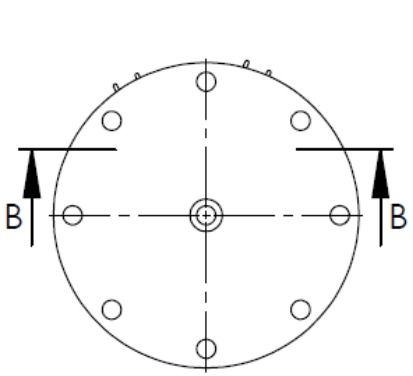

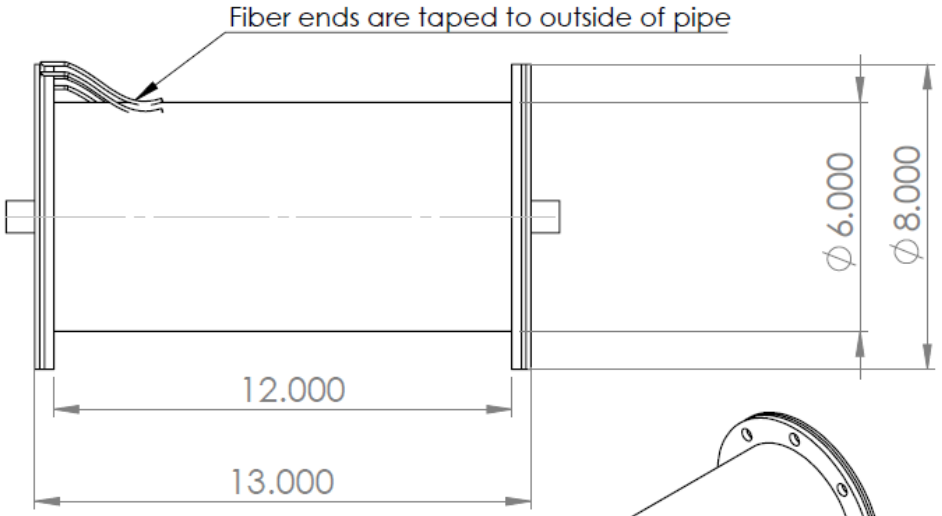

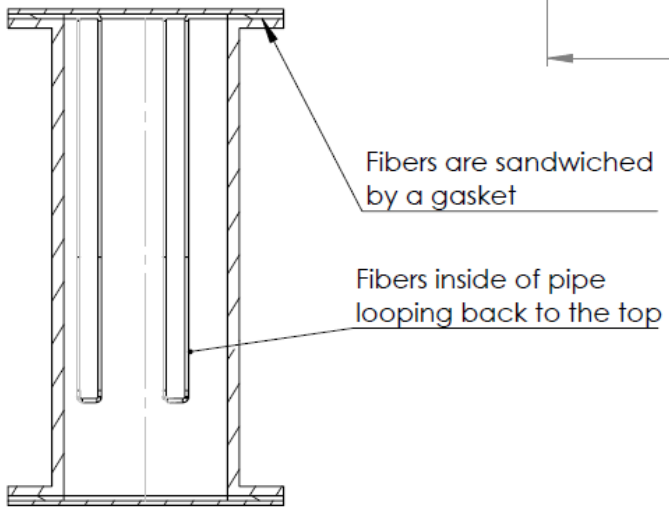

SECTION B-B

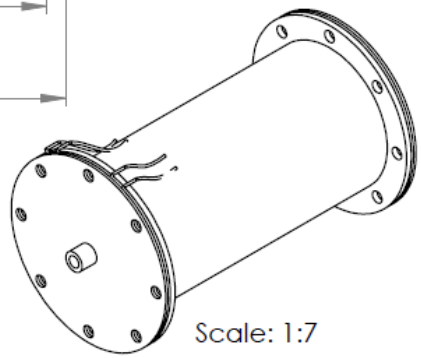

Scale: 1:7

UNLESS OTHERWISE SPECIFIED:	TITLE: Appendix A-C
DIMENSIONS ARE IN INCHES TOLERANCES: FRACTIONAL ±0.01	
INTERPRET GEOMETRIC TOLERANCING PER:	
MATERIAL 316SS	SIZE Custom / DWG. NO. C / REV 0
COMMENTS Concept Drawing Only	SCALE: 1:5 / WEIGHT:

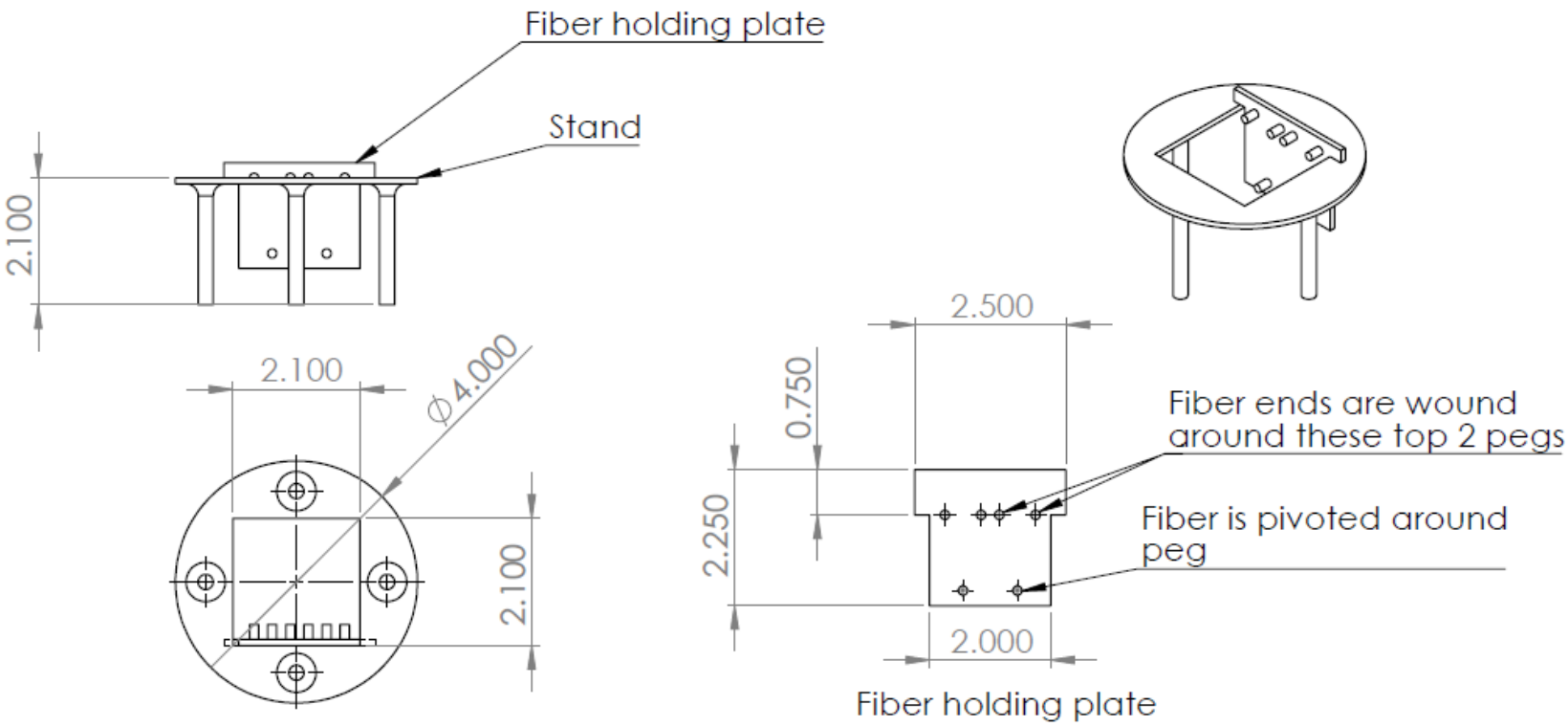

Note: model was scaled for 3D printing as a small palm sized concept model

UNLESS OTHERWISE SPECIFIED:	TITLE: Appendix A-D
DIMENSIONS ARE IN INCHES TOLERANCES: FRACTIONAL ±0.01	
INTERPRET GEOMETRIC TOLERANCING PER:	
MATERIAL: PLA	SIZE: Custom / DWG. NO.: D / REV: 0
COMMENTS: Concept Drawing Only	SCALE: 1:3 / WEIGHT:

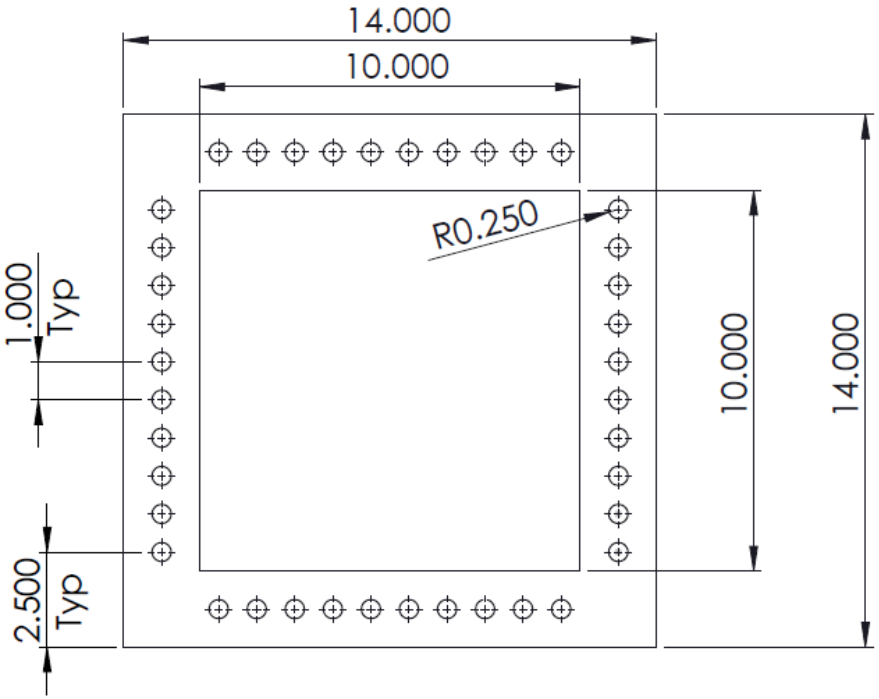

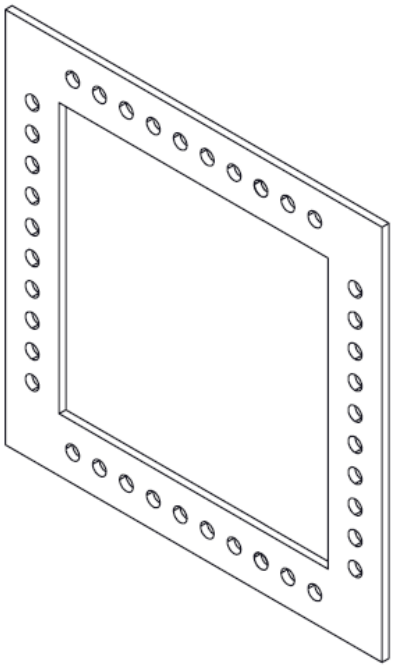

UNLESS OTHERWISE SPECIFIED:	TITLE: Appendix A-E
DIMENSIONS ARE IN INCHES TOLERANCES: FRACTIONAL±0.01	
INTERPRET GEOMETRIC TOLERANCING PER:	
MATERIAL 316SS	SIZE Custom / DWG. NO. E / REV 0
COMMENTS Concept Drawing Only	SCALE: 1:5 / WEIGHT:

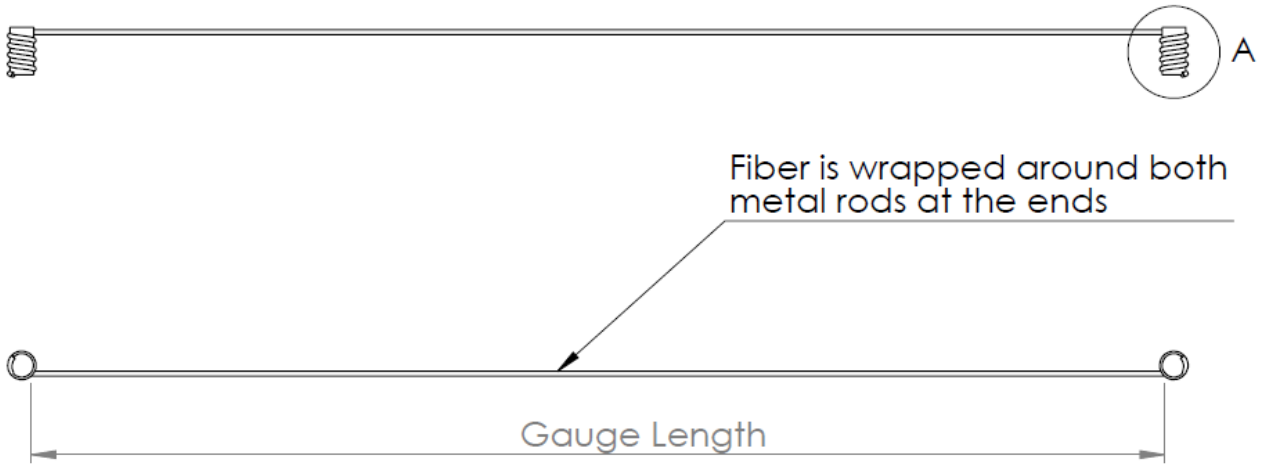

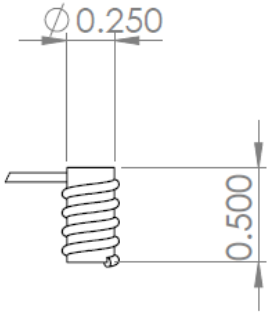

DETAIL A
SCALE 1 : 1

UNLESS OTHERWISE SPECIFIED:	TITLE: Appendix A-F
DIMENSIONS ARE IN INCHES TOLERANCES: FRACTIONAL ±0.01	
INTERPRET GEOMETRIC TOLERANCING PER:	
MATERIAL 316SS	SIZE Custom / DWG. NO. F / REV 0
COMMENTS Concept Drawing Only	SCALE: 1:2 / WEIGHT:

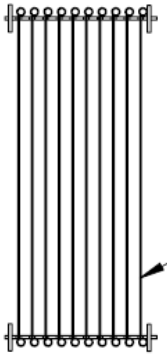

Each fiber is placed onto shelf's slots

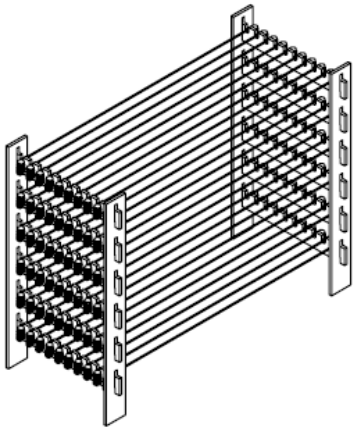

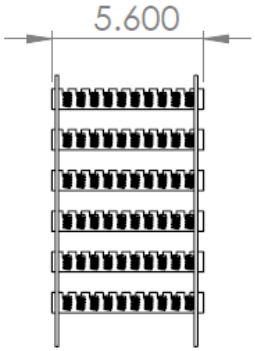

Shelf's legs will be secured, not in current concept

UNLESS OTHERWISE SPECIFIED:	TITLE: Appendix A-F2
DIMENSIONS ARE IN INCHES TOLERANCES: FRACTIONAL±0.01	
INTERPRET GEOMETRIC TOLERANCING PER:	
MATERIAL 316SS	SIZE Custom / DWG. NO. F2 / REV 0
COMMENTS Concept Drawing Only	SCALE: 1:7 / WEIGHT:

ITEM NO.	DESCRIPTION	QTY
1	Top plate - G3	2
2	Mid plate - G2	1
3	SS bolt - 0.250" x 0.625" - 20 TPI	2
4	SS bolt - 0.5" x 2" - 20 TPI	2
5	SS nut - 0.5" - 20 TPI	2

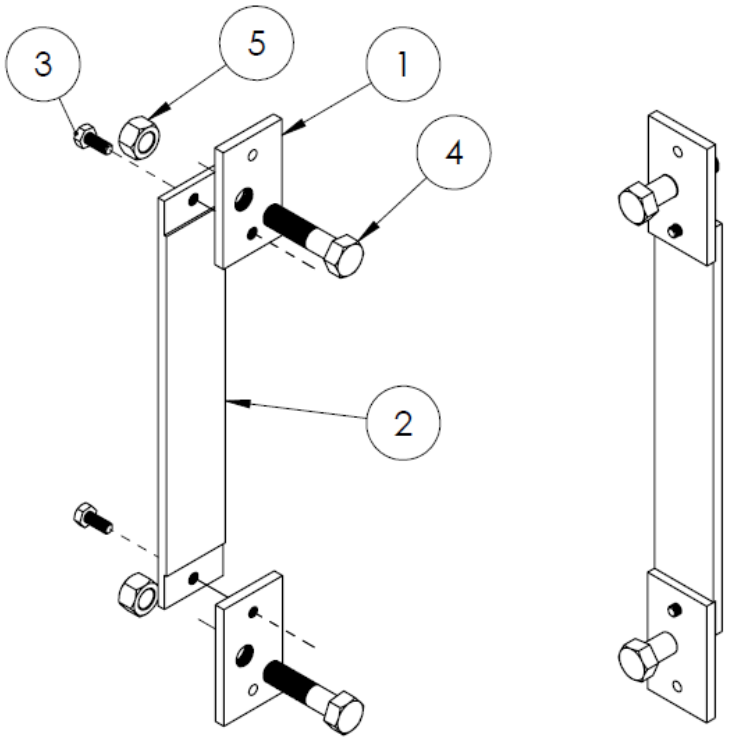

UNLESS OTHERWISE SPECIFIED:	TITLE: Appendix A-G - General Assembly
DIMENSIONS ARE IN INCHES TOLERANCES: FRACTIONAL ±0.01	
INTERPRET GEOMETRIC TOLERANCING PER:	
MATERIAL: 316SS	SIZE: Custom / DWG. NO.: G / REV: 0
COMMENTS: Concept Drawing Only	SCALE: 1:4 / WEIGHT:

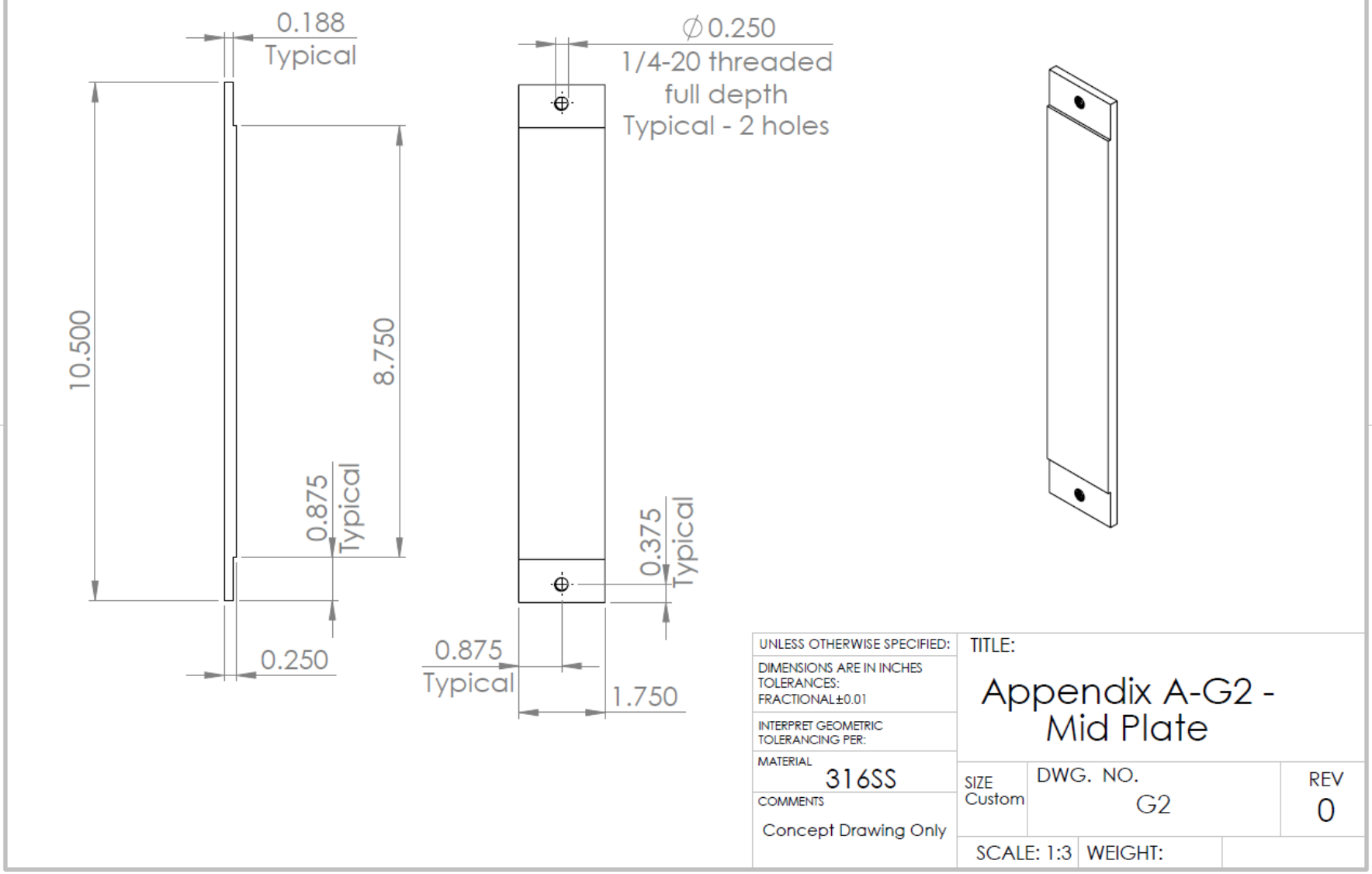
0.188
Typical
∅0.250
1/4-20 threaded
full depth
Typical - 2 holes
10.500
8.750
0.875
Typical
0.375
Typical
0.250
0.875
Typical
1.750
UNLESS OTHERWISE SPECIFIED:
DIMENSIONS ARE IN INCHES
TOLERANCES:
FRACTIONAL±0.01
INTERPRET GEOMETRIC
TOLERANCING PER:
MATERIAL
316SS
COMMENTS
Concept Drawing Only
TITLE:
Appendix A-G2 -
Mid Plate
SIZE
Custom
DWG. NO.
G2
REV
0
SCALE: 1:3
WEIGHT:

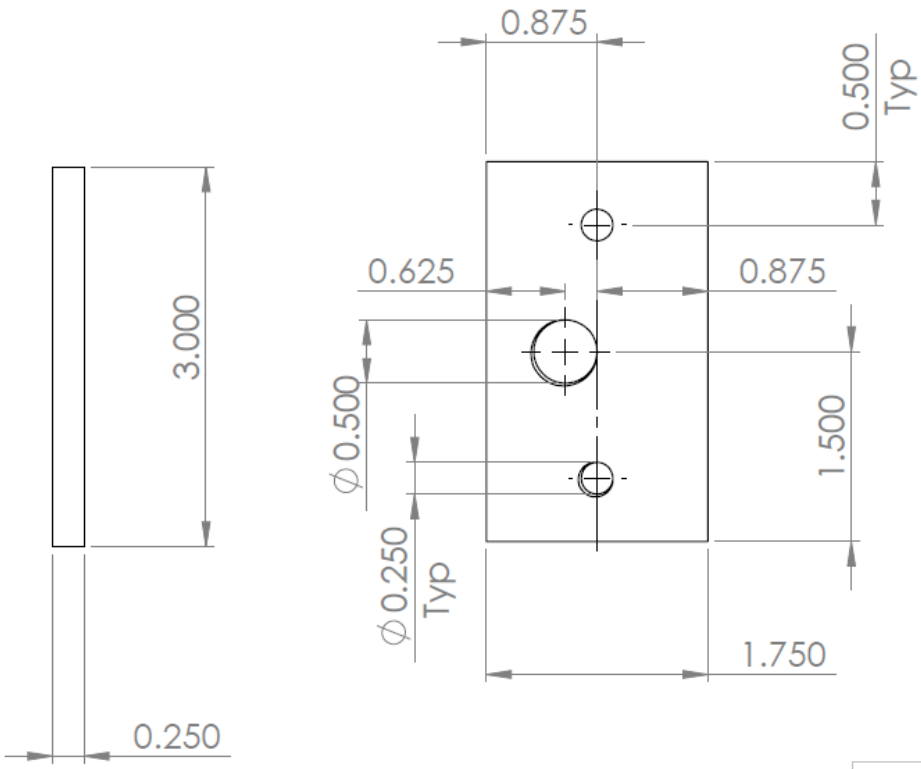

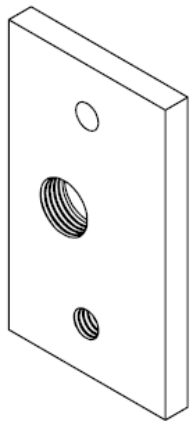

Note: all holes are threaded
full depth 20 TPI

UNLESS OTHERWISE SPECIFIED:	TITLE: Appendix A-G3 - Top plate
DIMENSIONS ARE IN INCHES TOLERANCES: FRACTIONAL±0.01	
INTERPRET GEOMETRIC TOLERANCING PER:	
MATERIAL 316SS	SIZE Custom / DWG. NO. G3 / REV 0
COMMENTS Concept Drawing Only	SCALE: 1:1.5 / WEIGHT:

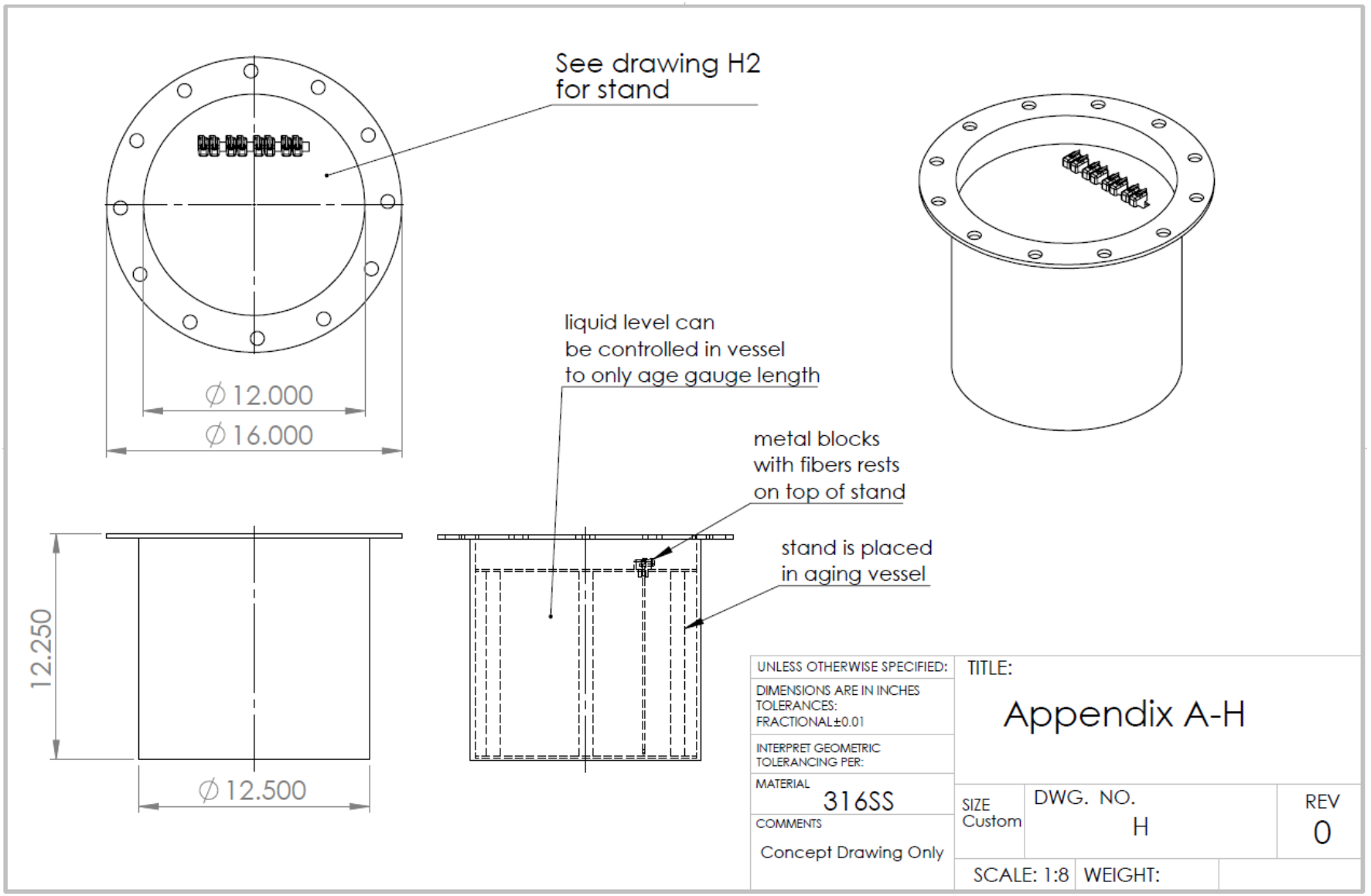
See drawing H2
for stand
liquid level can
be controlled in vessel
to only age gauge length
metal blocks
with fibers rests
on top of stand
stand is placed
in aging vessel
∅ 12.000
∅ 16.000
12.250
∅ 12.500
UNLESS OTHERWISE SPECIFIED:
DIMENSIONS ARE IN INCHES
TOLERANCES:
FRACTIONAL±0.01
INTERPRET GEOMETRIC
TOLERANCING PER:
MATERIAL
316SS
COMMENTS
Concept Drawing Only
TITLE:
Appendix A-H
SIZE
Custom
DWG. NO.
H
REV
0
SCALE: 1:8
WEIGHT:

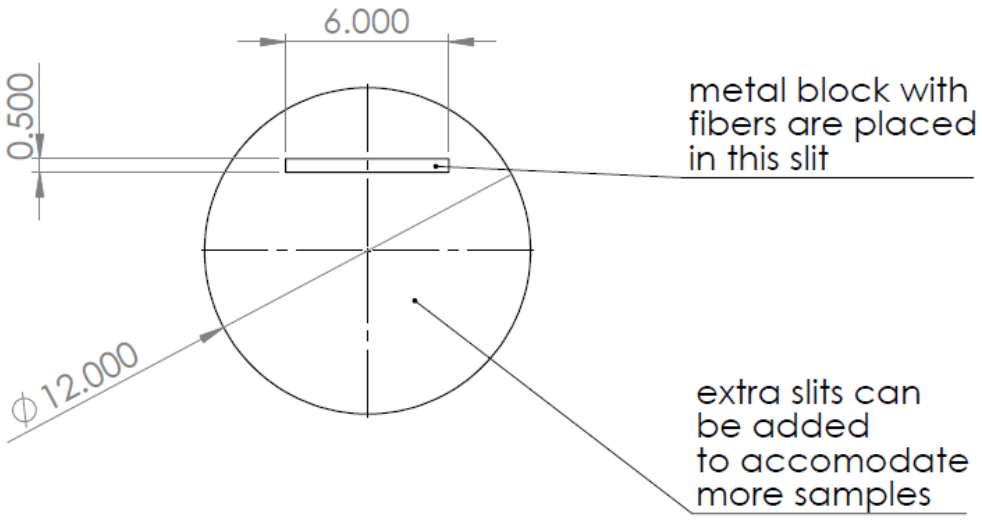

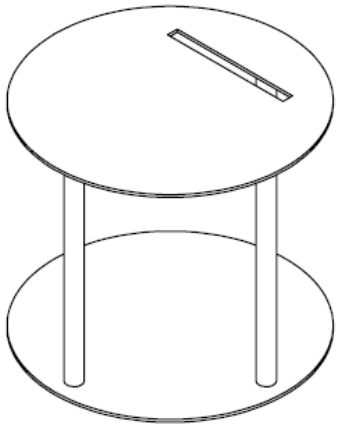

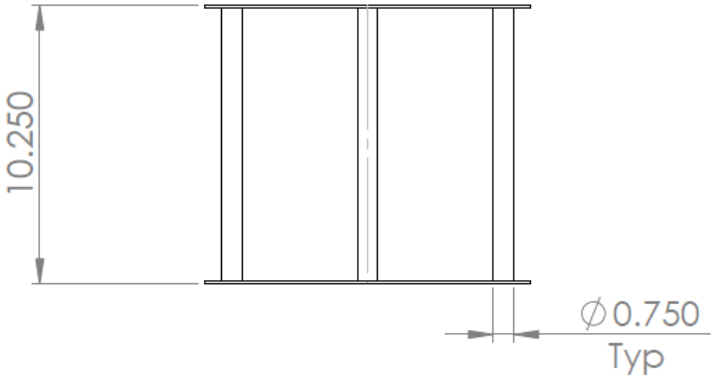

UNLESS OTHERWISE SPECIFIED:	TITLE: Appendix A-H2
DIMENSIONS ARE IN INCHES TOLERANCES: FRACTIONAL ±0.01	
INTERPRET GEOMETRIC TOLERANCING PER:	
MATERIAL 316SS	SIZE Custom / DWG. NO. H2 / REV 0
COMMENTS Concept Drawing Only	SCALE: 1:7 / WEIGHT:

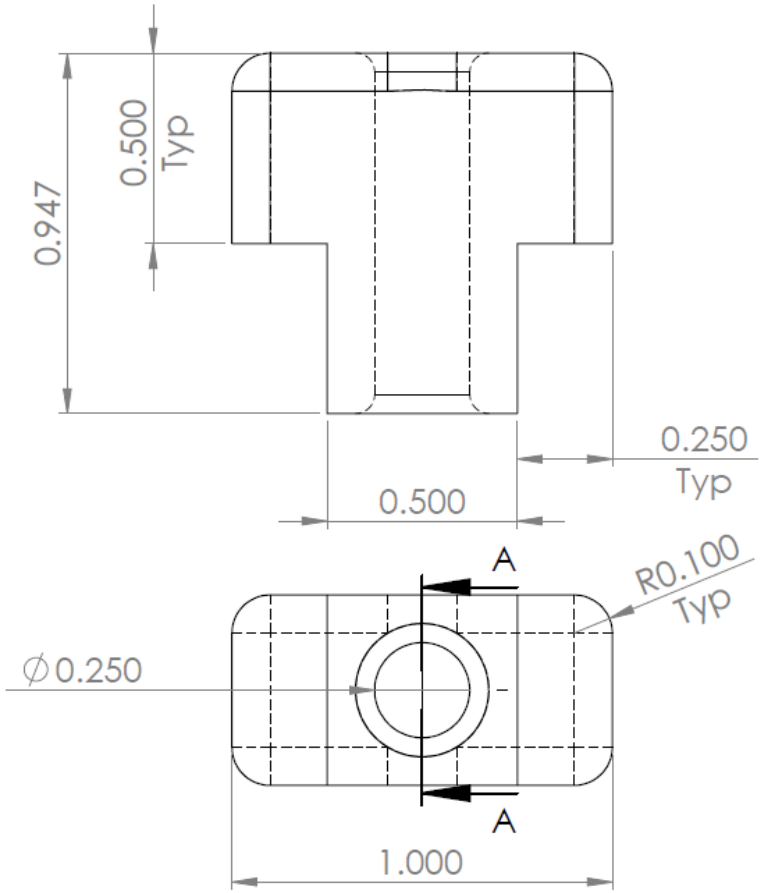

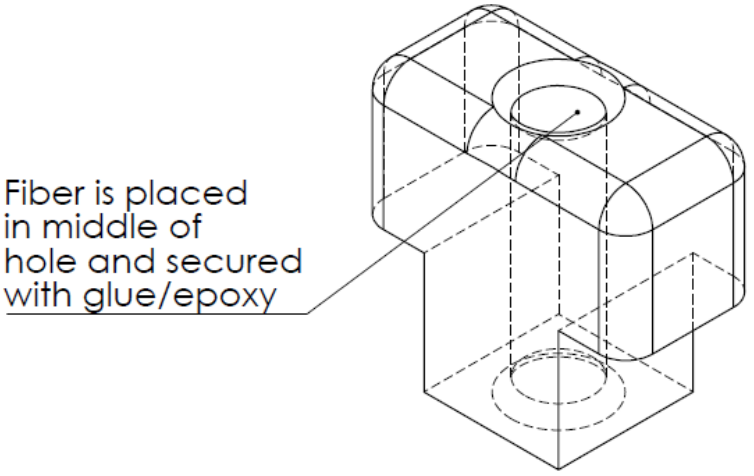

SECTION A-A

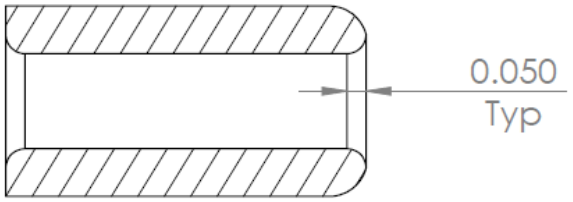

UNLESS OTHERWISE SPECIFIED:	TITLE:
DIMENSIONS ARE IN INCHES TOLERANCES: FRACTIONAL±0.01	Appendix A-H3
INTERPRET GEOMETRIC TOLERANCING PER:	
MATERIAL 316SS	SIZE Custom / DWG. NO. H3 / REV 0
COMMENTS Concept Drawing Only	SCALE: 2:1 / WEIGHT:

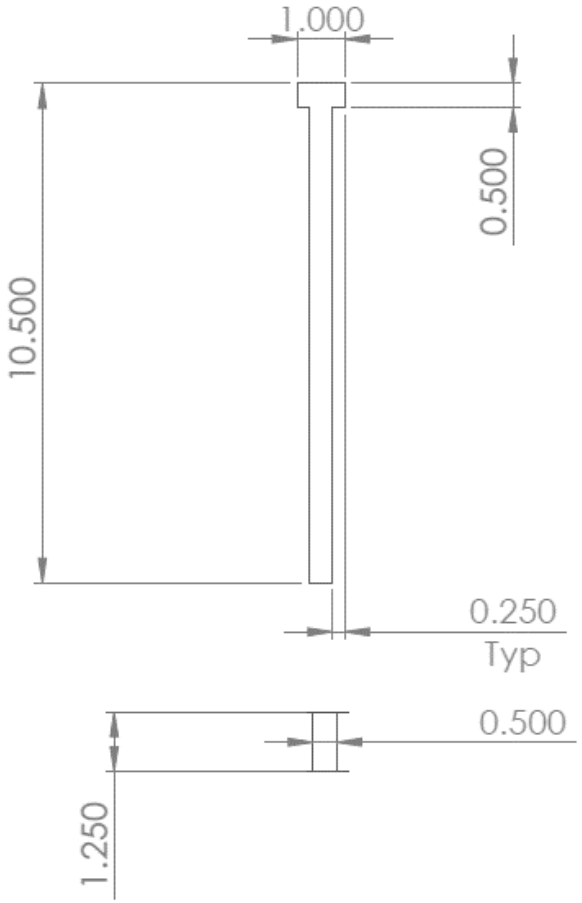

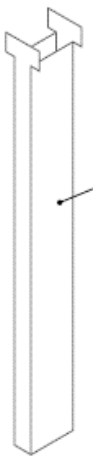

these baskets help separate the fibers from one another

Made of SS mesh, from one piece of mesh folded into basket design

UNLESS OTHERWISE SPECIFIED:	TITLE: Appendix A-H4
DIMENSIONS ARE IN INCHES TOLERANCES: FRACTIONAL ±0.01	
INTERPRET GEOMETRIC TOLERANCING PER:	
MATERIAL 316SS	SIZE Custom / DWG. NO. H4 / REV 0
COMMENTS Concept Drawing Only	SCALE: 1:4 / WEIGHT:

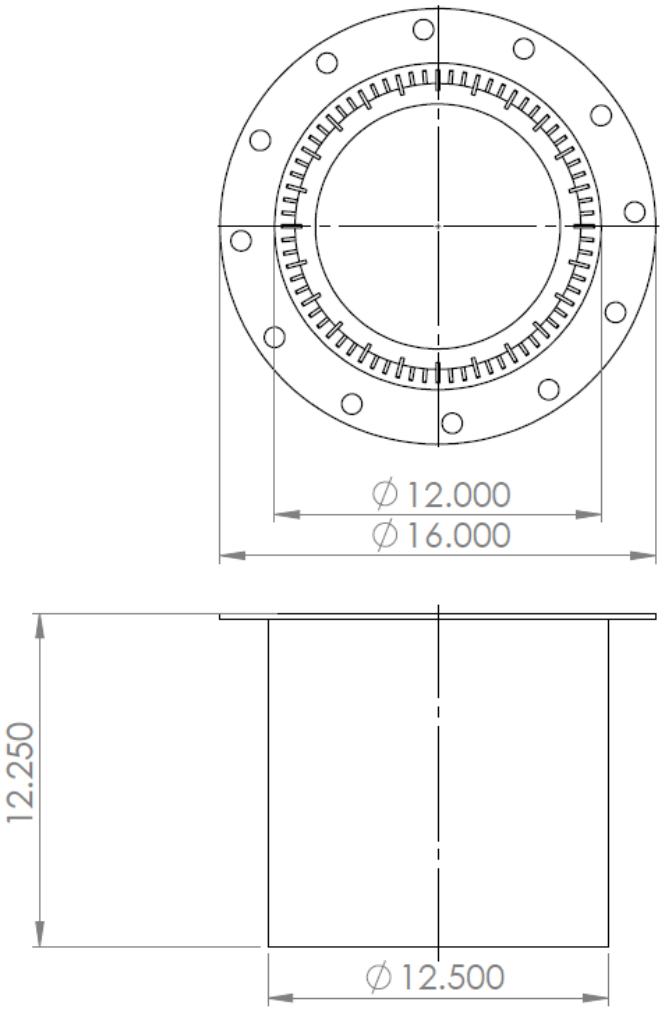

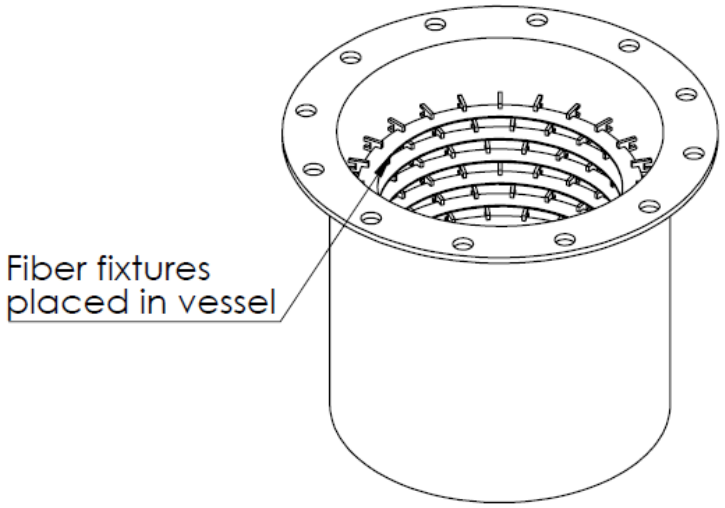

UNLESS OTHERWISE SPECIFIED:	TITLE: Appendix A-I		
DIMENSIONS ARE IN INCHES TOLERANCES: FRACTIONAL±0.01			
INTERPRET GEOMETRIC TOLERANCING PER:			
MATERIAL 316SS	SIZE Custom	DWG. NO. I	REV 0
COMMENTS Concept Drawing Only	SCALE: 1:7	WEIGHT:	

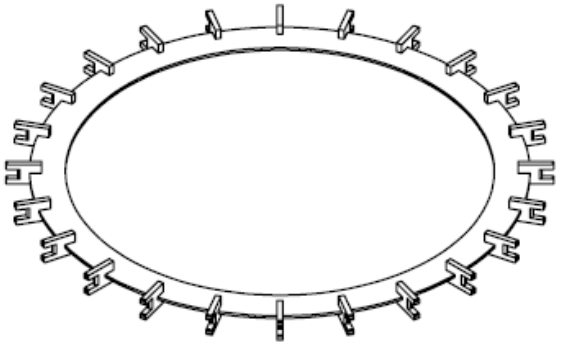

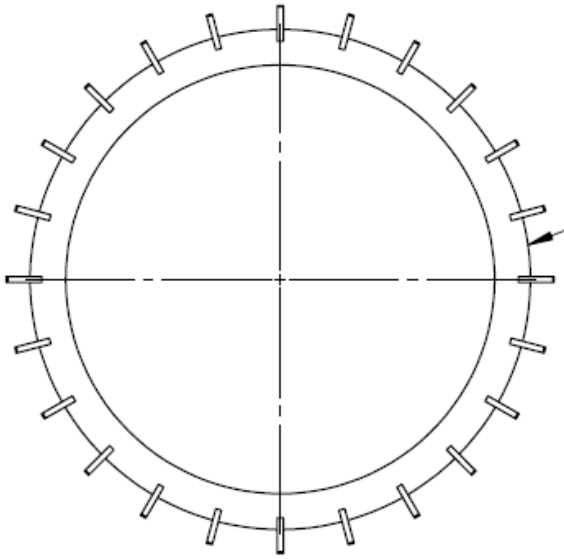

See drawing I3 and I4
Assemble ring from those
2 types of pieces (glue or weld)

UNLESS OTHERWISE SPECIFIED: DIMENSIONS ARE IN INCHES TOLERANCES: FRACTIONAL ±0.01 INTERPRET GEOMETRIC TOLERANCING PER: MATERIAL 316SS COMMENTS Concept Drawing Only	TITLE: Appendix A-I2		
	SIZE Custom	DWG. NO. I2	REV 0
	SCALE: 1:4	WEIGHT:	

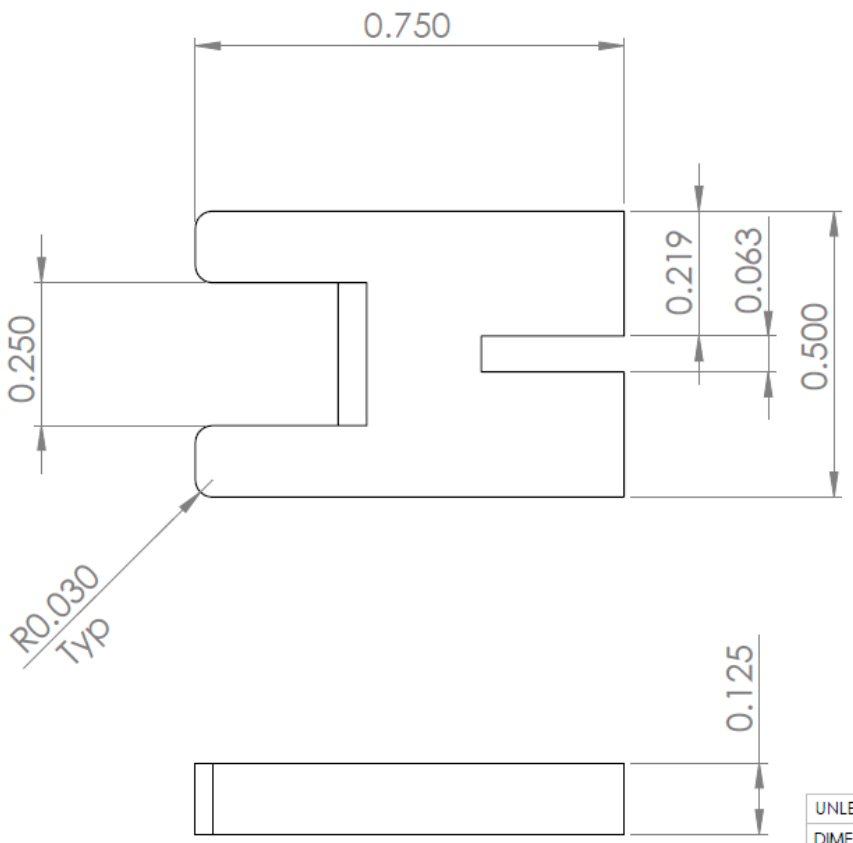

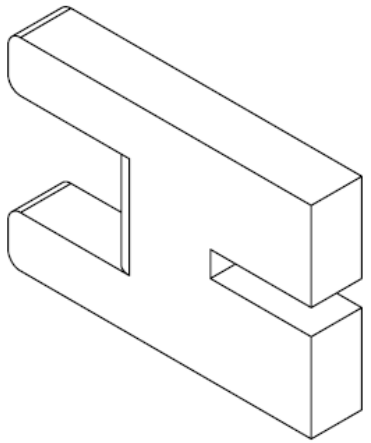

UNLESS OTHERWISE SPECIFIED:	TITLE: Appendix A-I3
DIMENSIONS ARE IN INCHES TOLERANCES: FRACTIONAL±0.01	
INTERPRET GEOMETRIC TOLERANCING PER:	
MATERIAL 316SS	SIZE Custom / DWG. NO. I3 / REV 0
COMMENTS Concept Drawing Only	SCALE: 3:1 / WEIGHT:

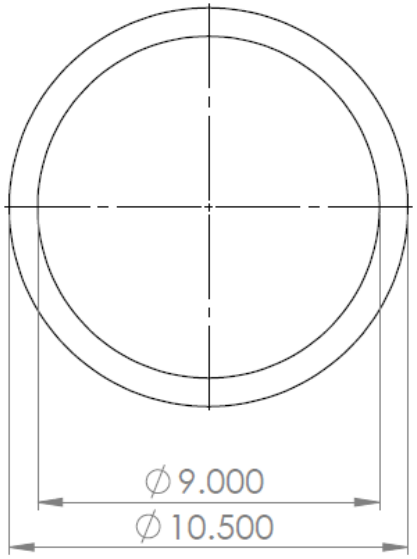

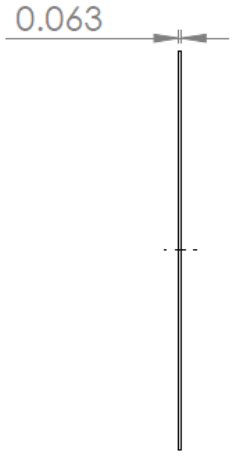

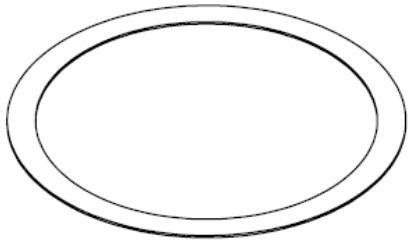

UNLESS OTHERWISE SPECIFIED:	TITLE: Appendix A-I4
DIMENSIONS ARE IN INCHES TOLERANCES: FRACTIONAL±0.01	
INTERPRET GEOMETRIC TOLERANCING PER:	
MATERIAL 316SS	SIZE Custom / DWG. NO. I4 / REV 0
COMMENTS Concept Drawing Only	SCALE: 1:5 / WEIGHT:

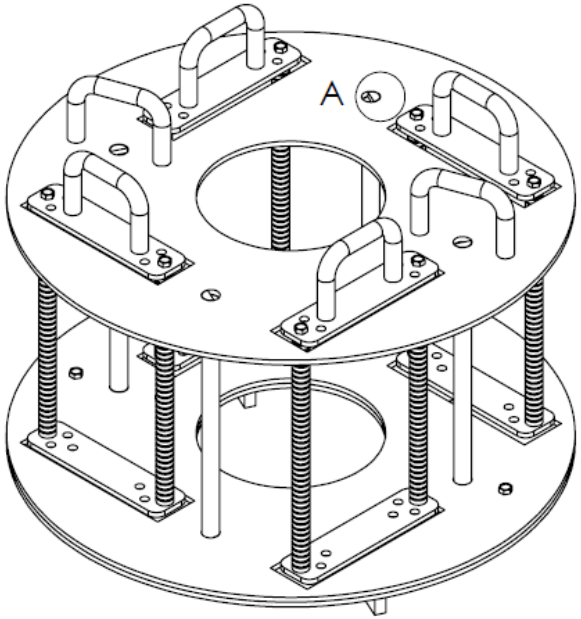

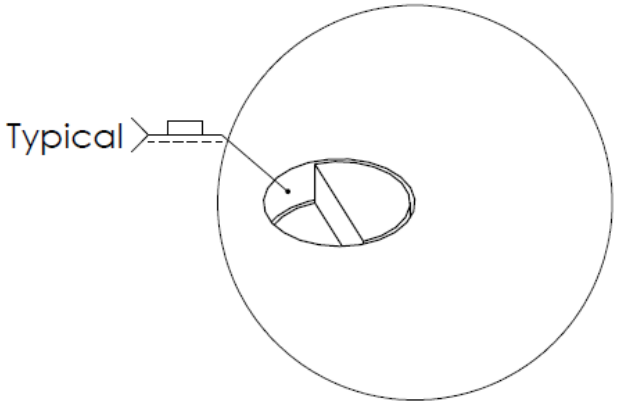

DETAIL A
SCALE 2 : 1

UNLESS OTHERWISE SPECIFIED:	TITLE: Appendix A-J
DIMENSIONS ARE IN INCHES TOLERANCES: FRACTIONAL±0.01	
INTERPRET GEOMETRIC TOLERANCING PER:	
MATERIAL 316SS	SIZE Custom / DWG. NO. J / REV 0
COMMENTS Concept Drawing Only	SCALE: 1:4 / WEIGHT:

ITEM NO.	DESCRIPTION	QTY
1	Top/Bottom Sub Plate - J4	2
2	Grooved Rod - J6	2
3	Handle	1
4	Bolt - #8 x 32 TPI - 1/4" Long	6

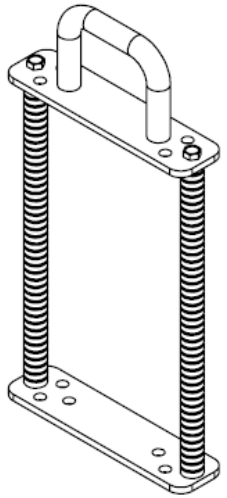

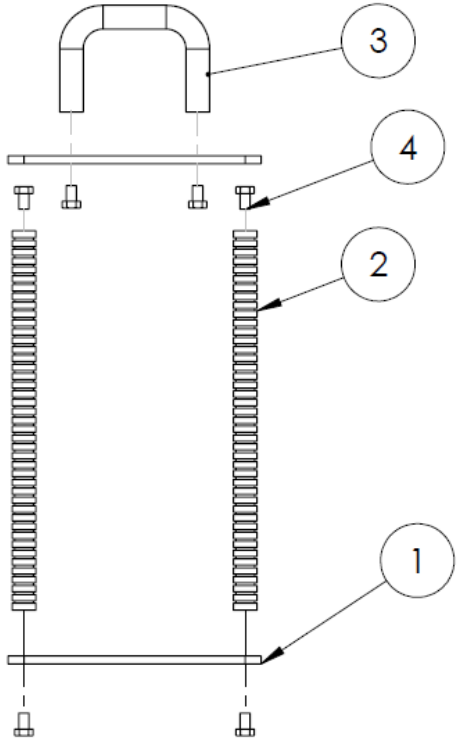

UNLESS OTHERWISE SPECIFIED:	TITLE: Appendix A-J2
DIMENSIONS ARE IN INCHES TOLERANCES: FRACTIONAL ±0.01	
INTERPRET GEOMETRIC TOLERANCING PER:	
MATERIAL 316SS	SIZE Custom / DWG. NO. J2 / REV 0
COMMENTS Concept Drawing Only	SCALE: 1:3 / WEIGHT:

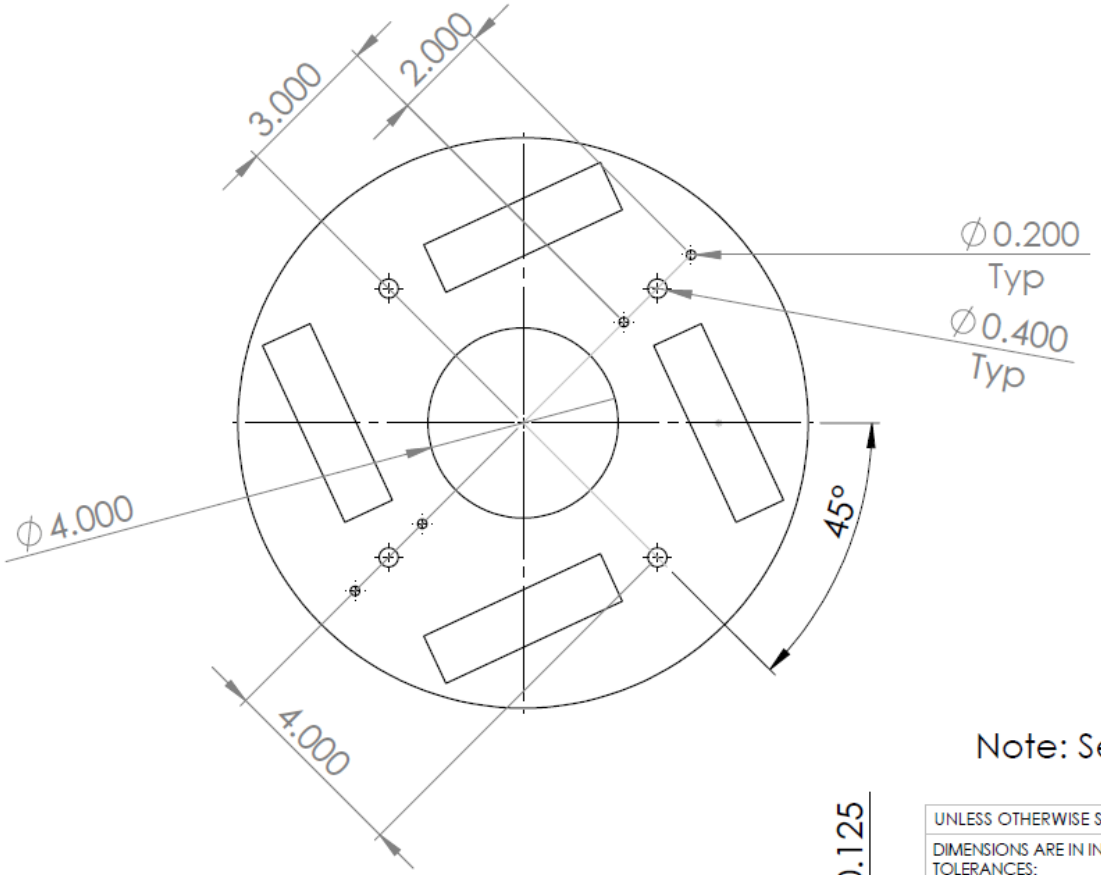

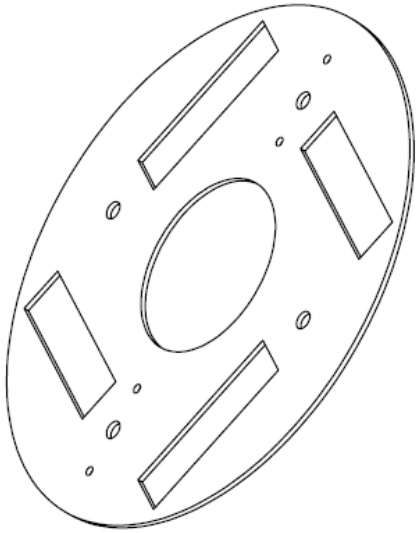

Note: See J3-1 for rectangular slit details

UNLESS OTHERWISE SPECIFIED:	TITLE: Appendix A-J3
DIMENSIONS ARE IN INCHES TOLERANCES: FRACTIONAL±0.01	
INTERPRET GEOMETRIC TOLERANCING PER:	
MATERIAL 316SS	SIZE Custom / DWG. NO. J3 / REV 0
COMMENTS Concept Drawing Only	SCALE: 1:4 / WEIGHT:

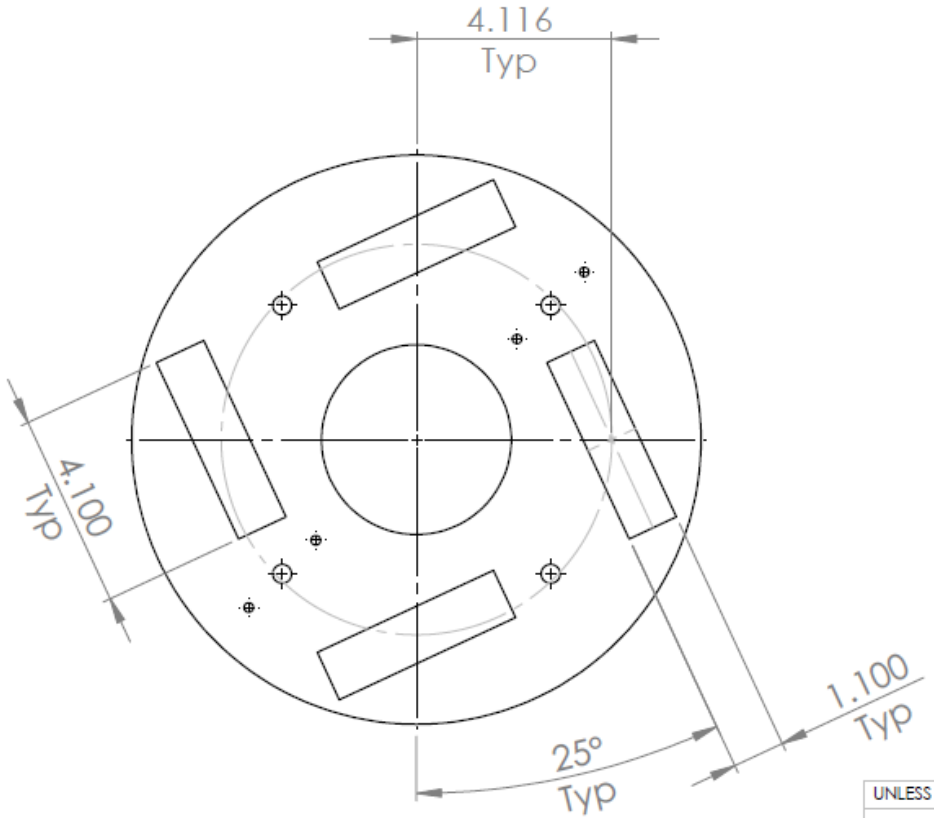

UNLESS OTHERWISE SPECIFIED:	TITLE: Appendix A-J3-1
DIMENSIONS ARE IN INCHES TOLERANCES: FRACTIONAL ±0.01	
INTERPRET GEOMETRIC TOLERANCING PER:	
MATERIAL 316SS	SIZE Custom / DWG. NO. J3-1 / REV 0
COMMENTS Concept Drawing Only	SCALE: 1:4 / WEIGHT:

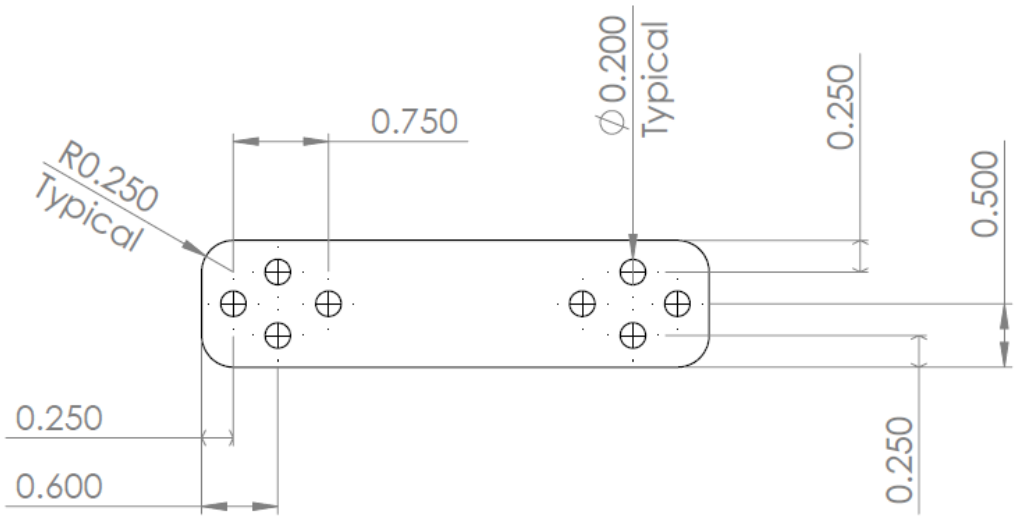

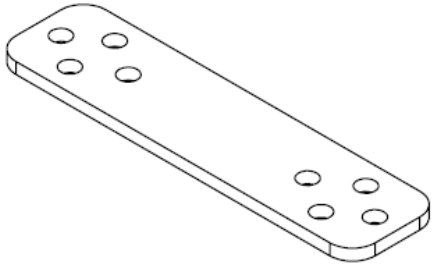

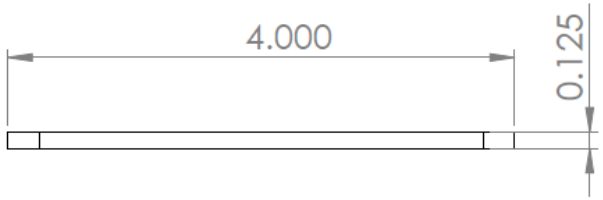

UNLESS OTHERWISE SPECIFIED:	TITLE: Appendix A-J4
DIMENSIONS ARE IN INCHES TOLERANCES: FRACTIONAL ±0.01	
INTERPRET GEOMETRIC TOLERANCING PER:	
MATERIAL 316SS	SIZE Custom / DWG. NO. J4 / REV 0
COMMENTS Concept Drawing Only	SCALE: 1:1.5 / WEIGHT:

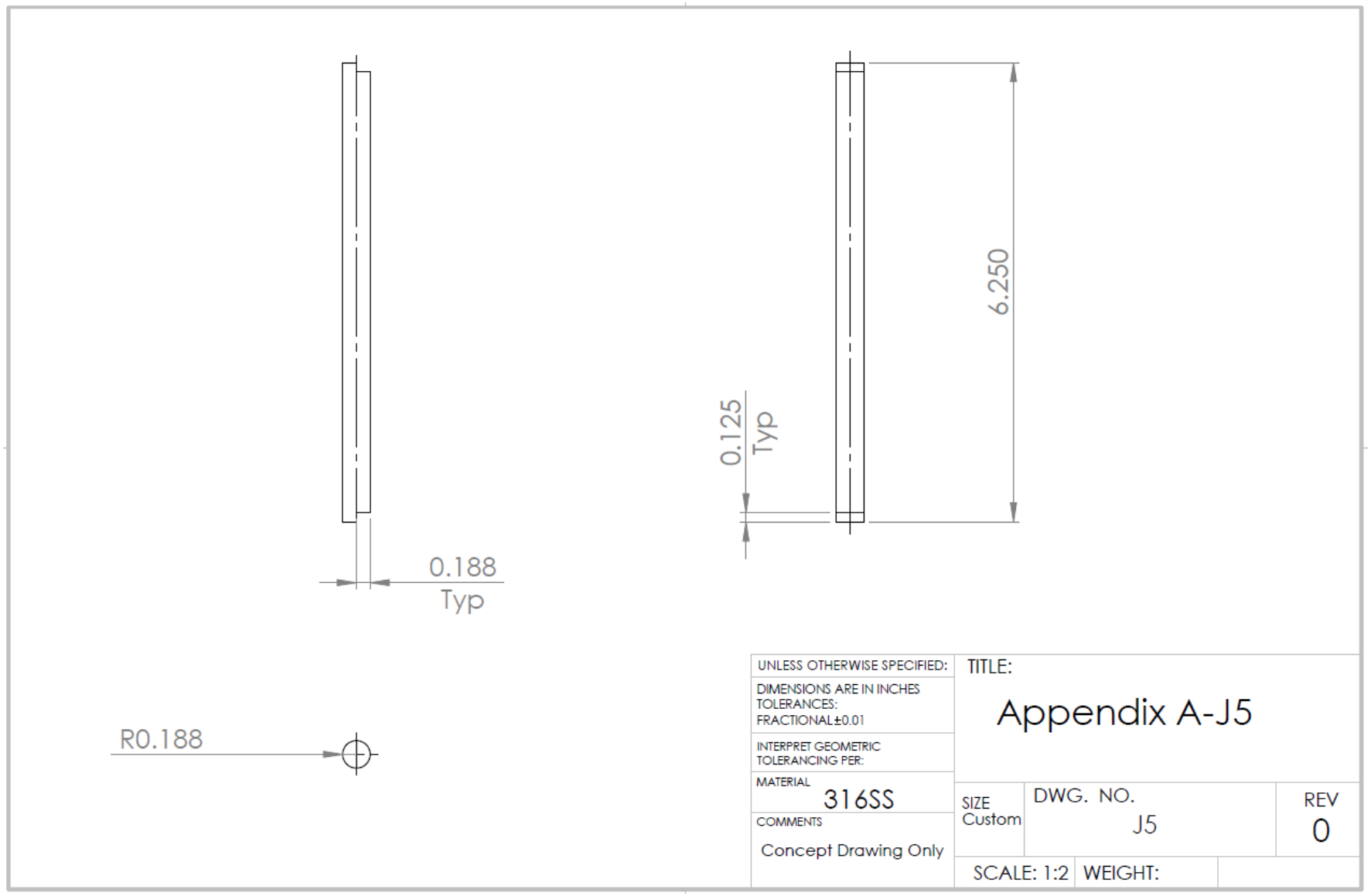
0.188
Typ
0.125
Typ
6.250
R0.188
UNLESS OTHERWISE SPECIFIED:
DIMENSIONS ARE IN INCHES
TOLERANCES:
FRACTIONAL ±0.01
INTERPRET GEOMETRIC TOLERANCING PER:
MATERIAL
316SS
COMMENTS
Concept Drawing Only
TITLE:
Appendix A-J5
SIZE
Custom
DWG. NO.
J5
REV
0
SCALE: 1:2
WEIGHT:

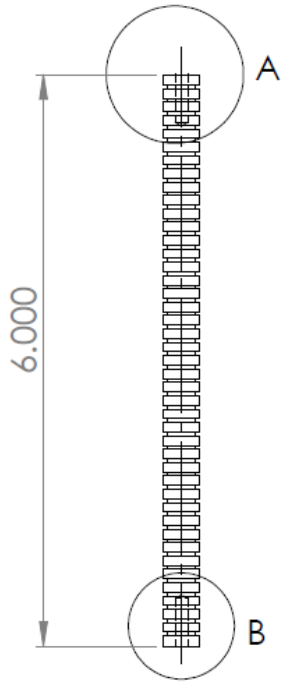

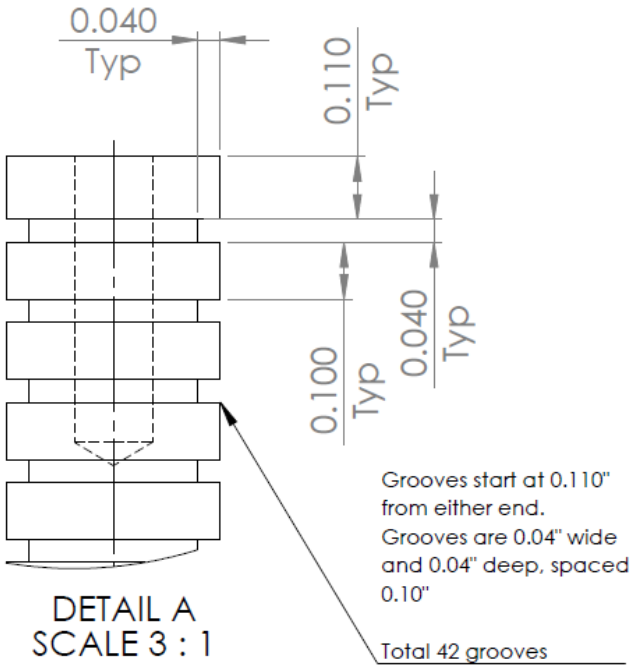

DETAIL A
SCALE 3 : 1

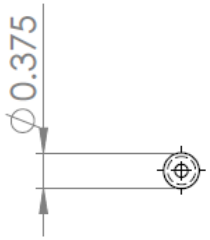

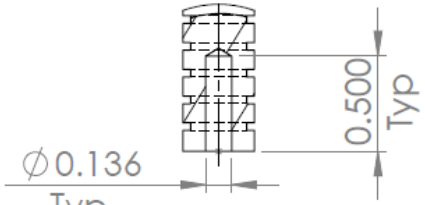

DETAIL B
SCALE 1 : 1

UNLESS OTHERWISE SPECIFIED:	TITLE: Appendix A-J6
DIMENSIONS ARE IN INCHES TOLERANCES: FRACTIONAL ±0.01	
INTERPRET GEOMETRIC TOLERANCING PER:	
MATERIAL 316SS	SIZE Custom / DWG. NO. J6 / REV 0
COMMENTS Concept Drawing Only	SCALE: 1:2 / WEIGHT:

ITEM NO.	DESCRIPTION	QTY
1	Nut - #8 x 32 TPI	4
2	Bolt - #8 x 32 TPI - 1/2" Long	8
3	Handles	2
4	Support Bar - J5	4
5	Top/Bottom Plate - J3	2
6	Base	1
7	Sub Assembly - J2	4

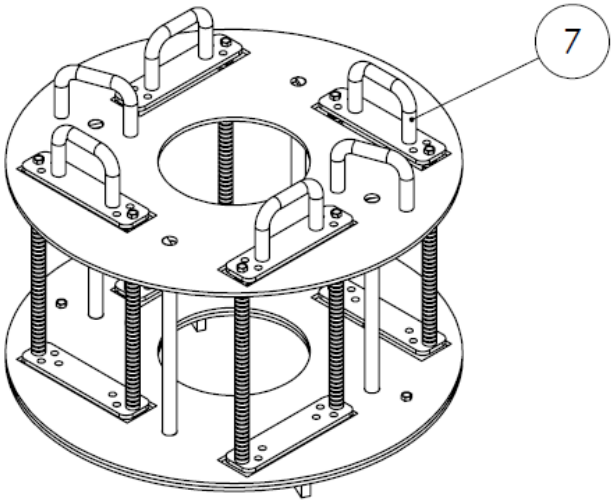

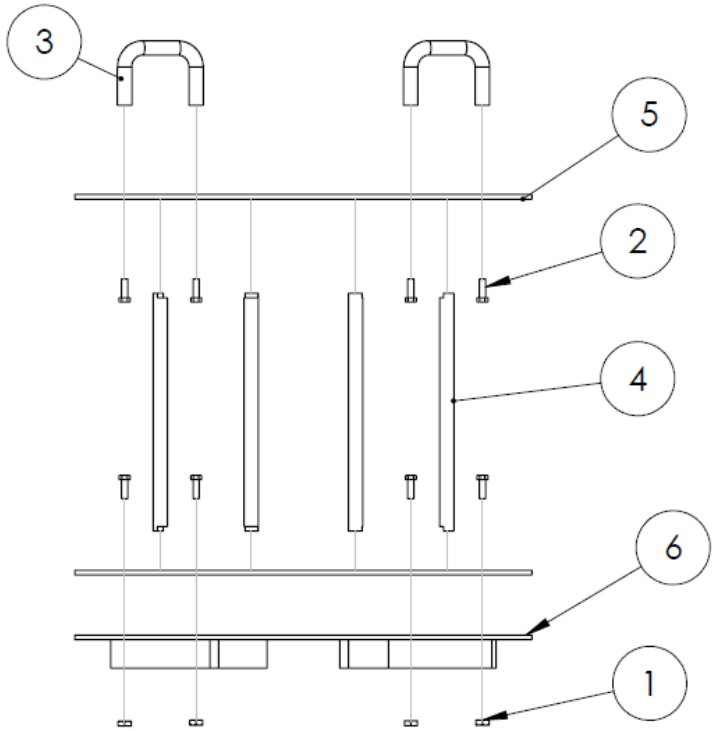

UNLESS OTHERWISE SPECIFIED: DIMENSIONS ARE IN INCHES TOLERANCES: FRACTIONAL±0.01	TITLE: Appendix A-J7
INTERPRET GEOMETRIC TOLERANCING PER:	
MATERIAL 316SS	SIZE Custom / DWG. NO. J7 / REV 0
COMMENTS Concept Drawing Only	SCALE: 1:5 / WEIGHT:

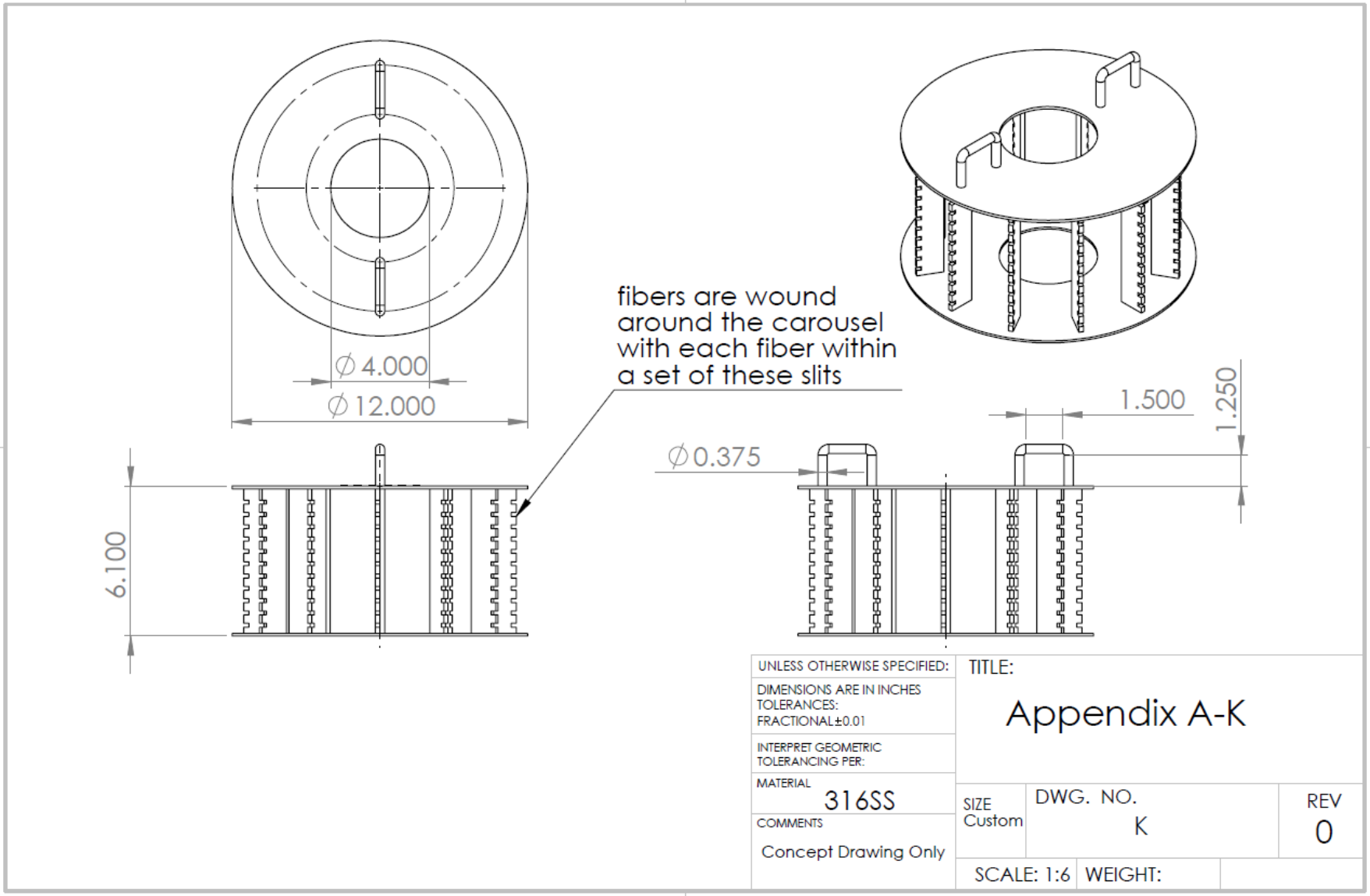
fibers are wound around the carousel with each fiber within a set of these slits
∅4.000
∅12.000
6.100
∅0.375
1.500
1.250
UNLESS OTHERWISE SPECIFIED:
DIMENSIONS ARE IN INCHES
TOLERANCES:
FRACTIONAL±0.01
INTERPRET GEOMETRIC TOLERANCING PER:
MATERIAL
316SS
COMMENTS
Concept Drawing Only
TITLE:
Appendix A-K
SIZE
Custom
DWG. NO.
K
REV
0
SCALE: 1:6
WEIGHT:

Appendix B – Acrylic Aging Vessel

ITEM NO.	DESCRIPTION	QTY
1	Top Disk - 1/4" thick x ⌀14"	1
2	Shell - 1/8" thick x 12" Long	1
3	Bottom Disk - 1/4" thick x ⌀14"	1

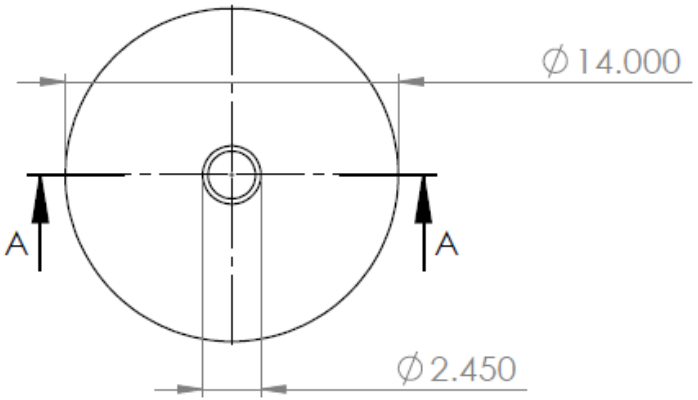

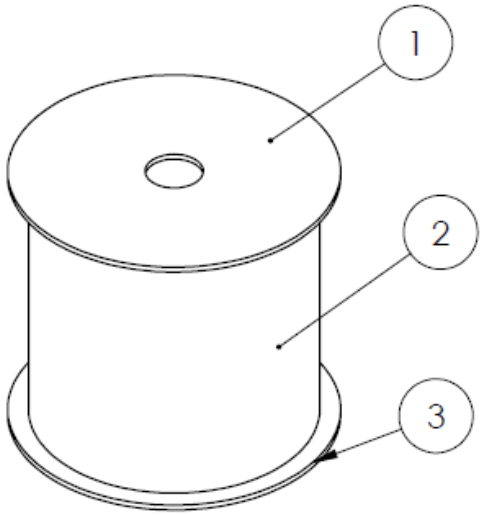

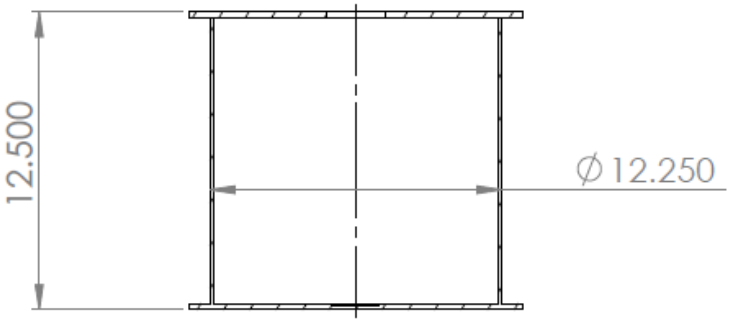

SECTION A-A

UNLESS OTHERWISE SPECIFIED:	TITLE: Appendix B - Acrylic Aging Cell
DIMENSIONS ARE IN INCHES TOLERANCES: FRACTIONAL ±0.01	
INTERPRET GEOMETRIC TOLERANCING PER:	
MATERIAL: Acrylic	SIZE: Custom / DWG. NO.: BA / REV: 0
COMMENTS: Concept Drawing Only	SCALE: 1:8 / WEIGHT:

Appendix C – Acrylic Carousel

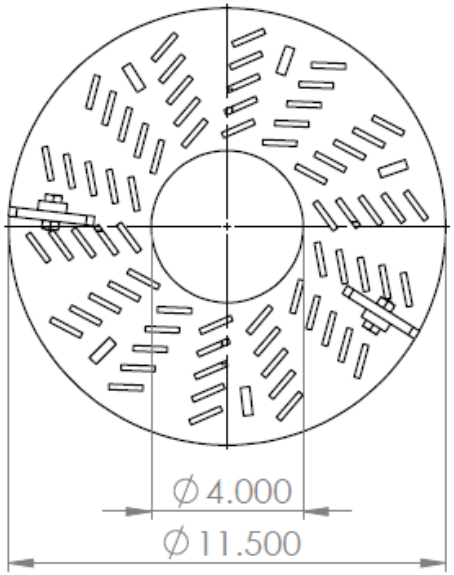

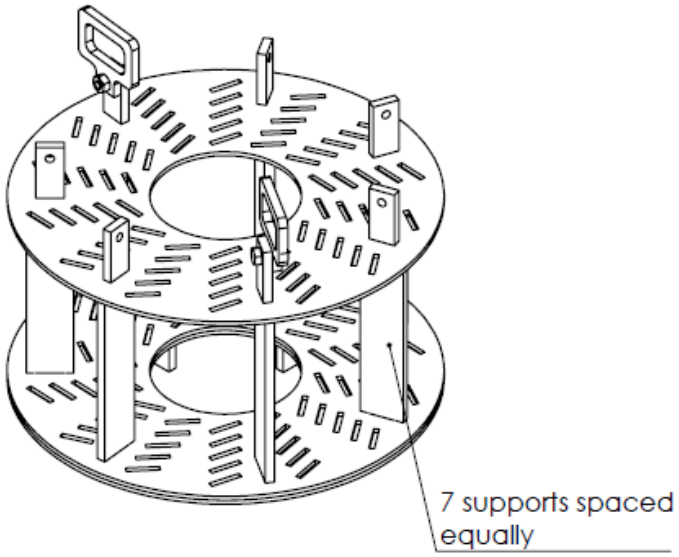

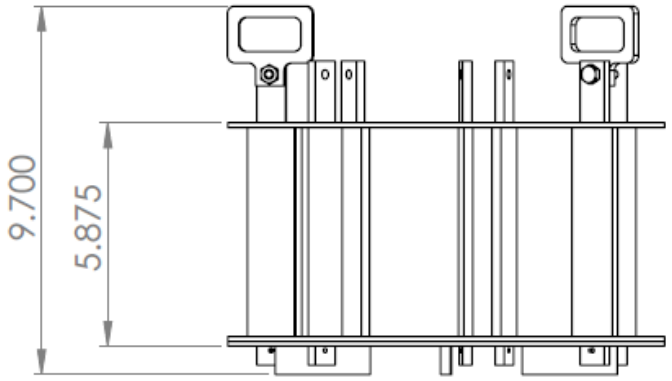

UNLESS OTHERWISE SPECIFIED:	TITLE: Appendix C - Acrylic Carousel
DIMENSIONS ARE IN INCHES TOLERANCES: FRACTIONAL ±0.01	
INTERPRET GEOMETRIC TOLERANCING PER:	
MATERIAL: Acrylic	SIZE: Custom / DWG. NO.: CA / REV: 0
COMMENTS: Concept Drawing Only	SCALE: 1:5 / WEIGHT:

Appendix D – Metal Aging Vessel

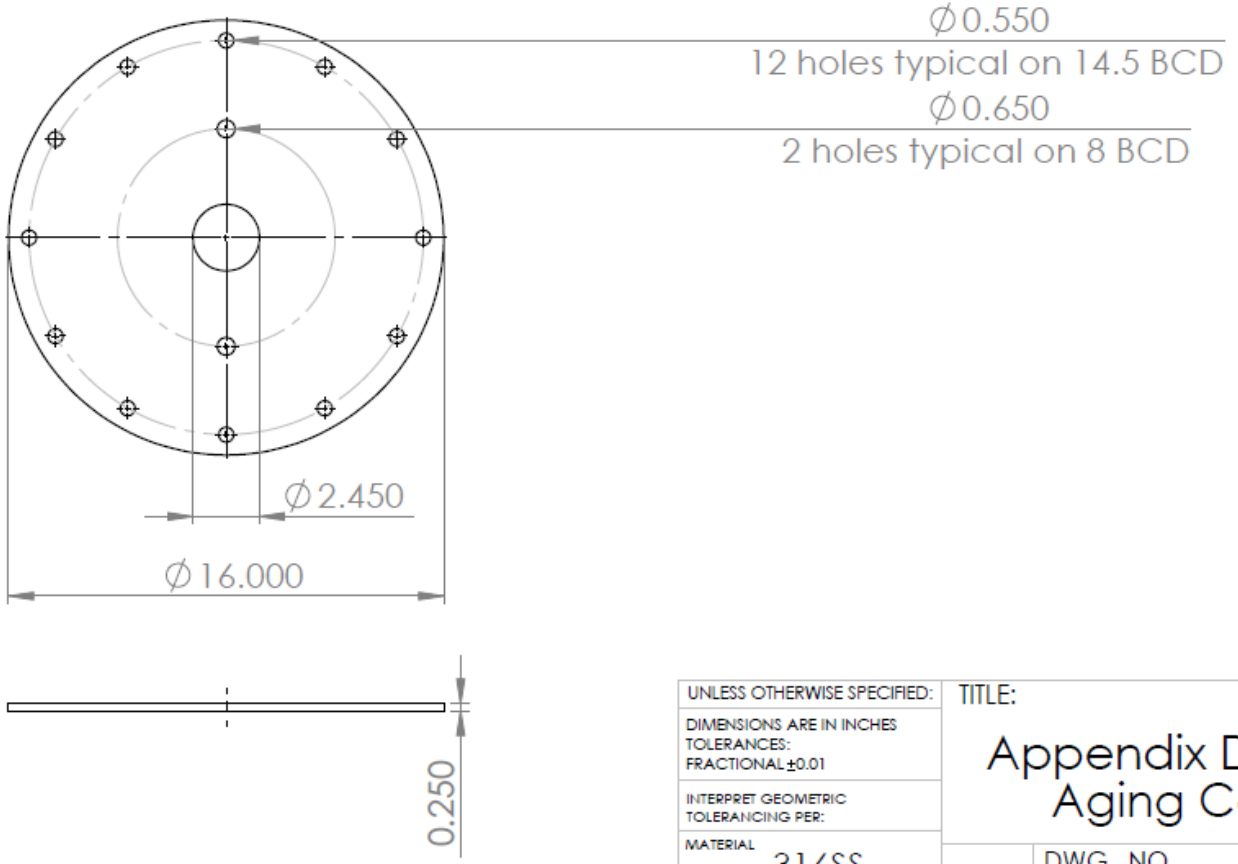

UNLESS OTHERWISE SPECIFIED:	TITLE: Appendix D - Metal Aging Cell Lid
DIMENSIONS ARE IN INCHES TOLERANCES: FRACTIONAL ±0.01	
INTERPRET GEOMETRIC TOLERANCING PER:	
MATERIAL: 316SS	SIZE: Custom / DWG. NO.: DA / REV: 0
COMMENTS: Concept Drawing Only	SCALE: 1:7 / WEIGHT:

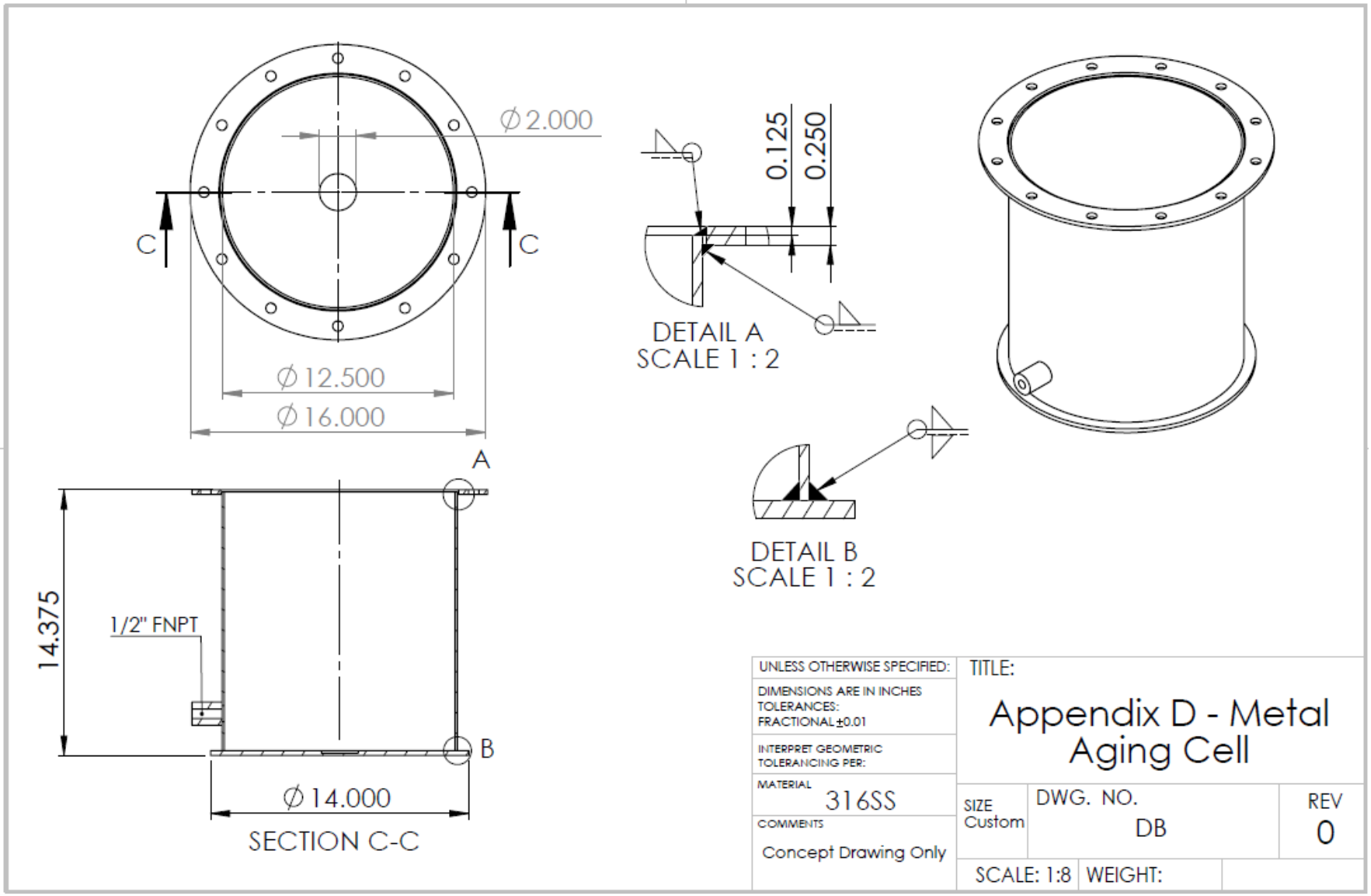
∅2.000
C
C
∅12.500
∅16.000
0.125
0.250
DETAIL A
SCALE 1 : 2
DETAIL B
SCALE 1 : 2
A
B
14.375
1/2" FNPT
∅14.000
SECTION C-C
UNLESS OTHERWISE SPECIFIED:
DIMENSIONS ARE IN INCHES
TOLERANCES:
FRACTIONAL ±0.01
INTERPRET GEOMETRIC TOLERANCING PER:
MATERIAL
316SS
COMMENTS
Concept Drawing Only
TITLE:
Appendix D - Metal Aging Cell
SIZE
Custom
DWG. NO.
DB
REV
0
SCALE: 1:8
WEIGHT:

Appendix E – Metal Carousel

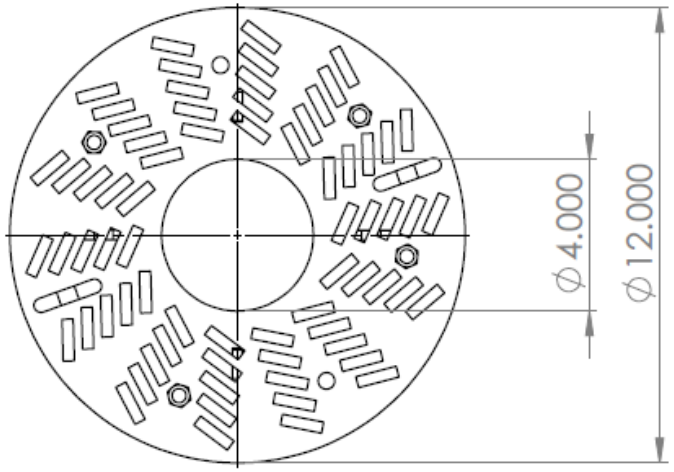

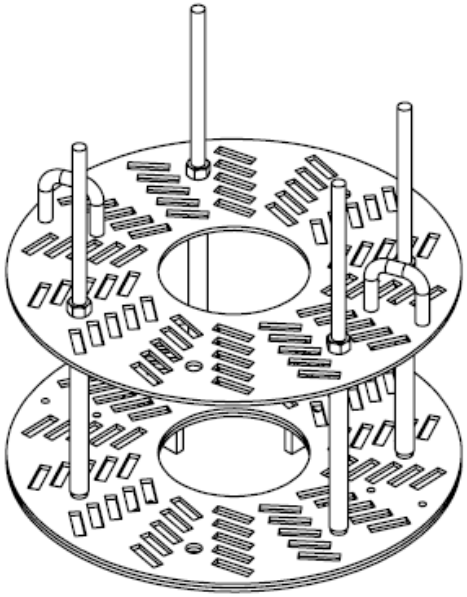

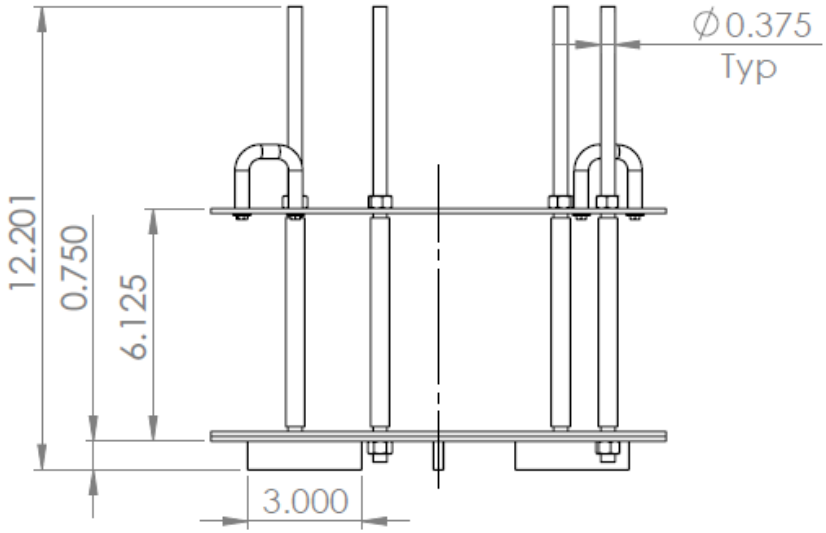

UNLESS OTHERWISE SPECIFIED:	TITLE: Appendix E - Metal Carousel
DIMENSIONS ARE IN INCHES TOLERANCES: FRACTIONAL ±0.01	
INTERPRET GEOMETRIC TOLERANCING PER:	
MATERIAL 316SS	SIZE Custom / DWG. NO. EA / REV 0
COMMENTS Concept Drawing Only	SCALE: 1:5 / WEIGHT:

Appendix F – Tensile Test Coupon

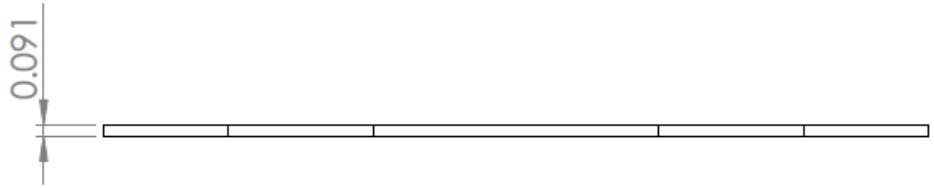

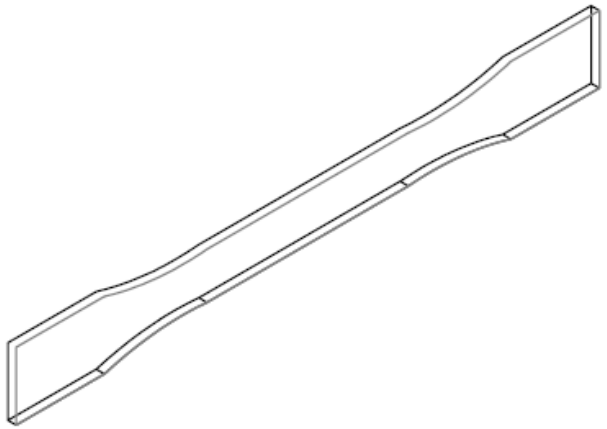

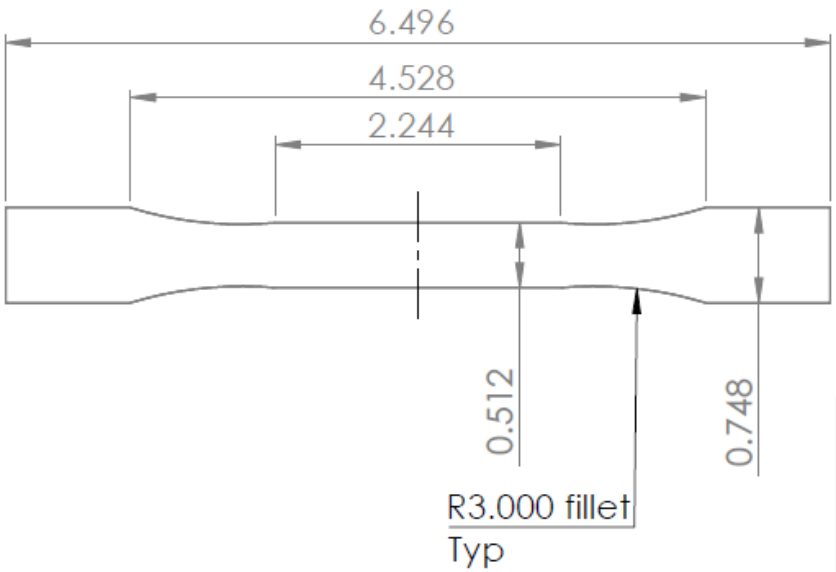

UNLESS OTHERWISE SPECIFIED:	TITLE: Appendix F - Dogbone
DIMENSIONS ARE IN INCHES TOLERANCES: FRACTIONAL ±0.01	
INTERPRET GEOMETRIC TOLERANCING PER:	
MATERIAL: Misc	SIZE: Custom / DWG. NO.: FA / REV: 0
COMMENTS: Concept Drawing Only	SCALE: 1:1.5 / WEIGHT:

Appendix G – Middle Plate Designs

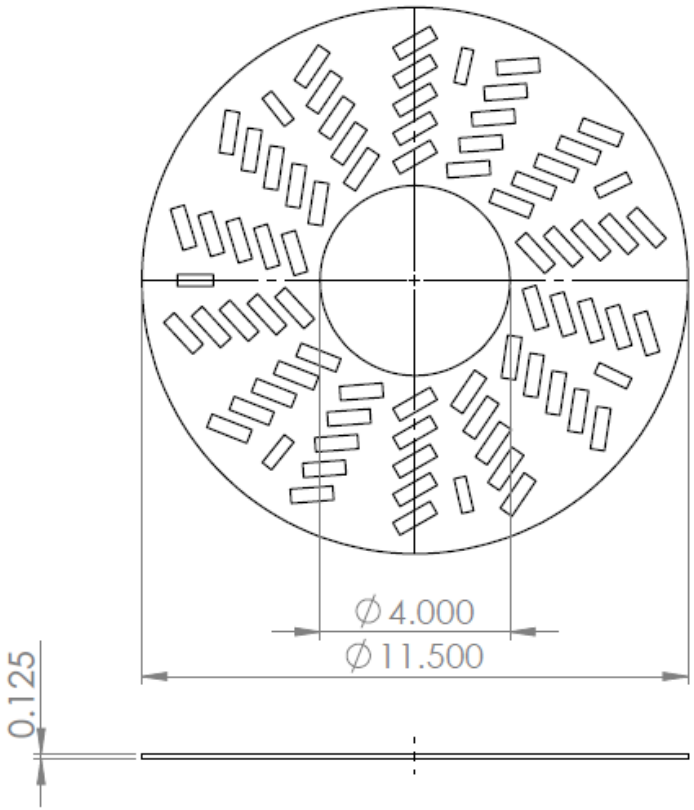

UNLESS OTHERWISE SPECIFIED:	TITLE: Appendix G - Full Top Plate
DIMENSIONS ARE IN INCHES TOLERANCES: FRACTIONAL ±0.01	
INTERPRET GEOMETRIC TOLERANCING PER:	
MATERIAL: Acrylic	SIZE: Custom / DWG. NO.: GA / REV: 0
COMMENTS: Concept Drawing Only	SCALE: 1:4 / WEIGHT:

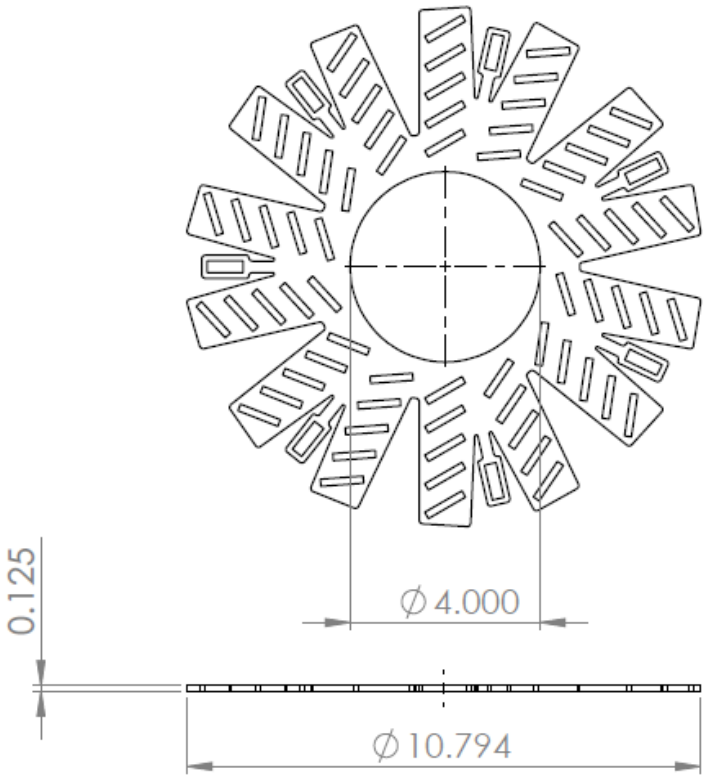

UNLESS OTHERWISE SPECIFIED:	TITLE: Appendix G - Skeletonized Plate
DIMENSIONS ARE IN INCHES TOLERANCES: FRACTIONAL ±0.01	
INTERPRET GEOMETRIC TOLERANCING PER:	
MATERIAL: Acrylic	SIZE: Custom / DWG. NO.: GB / REV: 0
COMMENTS: Concept Drawing Only	SCALE: 1:4 / WEIGHT:

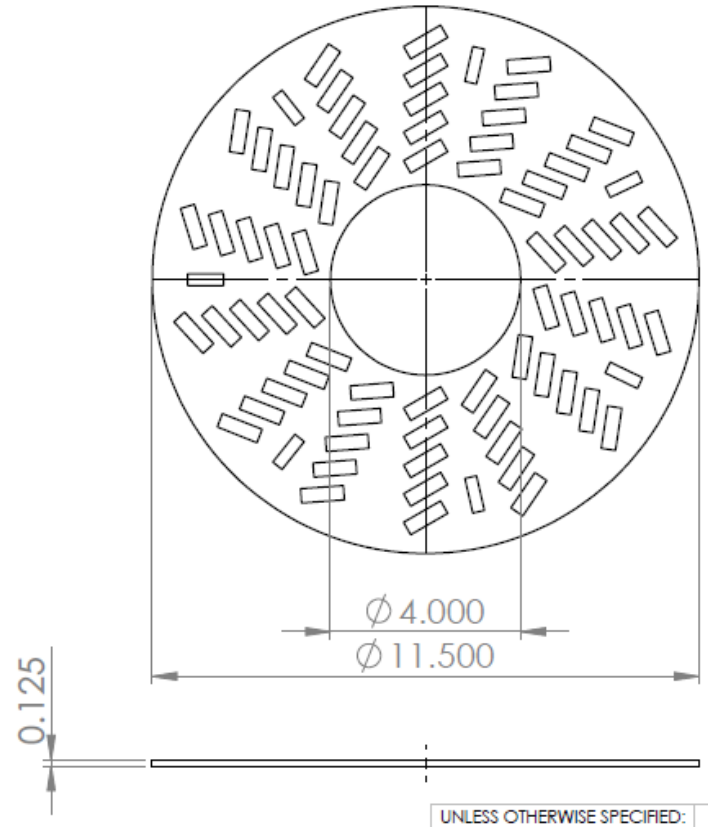

Made of 316SS perforated plate
With 0.125" perforations staggered
by 0.188" center to center

UNLESS OTHERWISE SPECIFIED:	TITLE: Appendix G - Perforated Plate
DIMENSIONS ARE IN INCHES TOLERANCES: FRACTIONAL ±0.01	
INTERPRET GEOMETRIC TOLERANCING PER:	
MATERIAL: 316SS	SIZE: Custom / DWG. NO.: GC / REV: 0
COMMENTS: Concept Drawing Only	SCALE: 1:4 / WEIGHT: